ROBUST MULTISENSOR-BASED FRAMEWORK FOR EFFICIENT ROAD INFORMATION SERVICES

by

AMR EL-WAKEEL

A thesis submitted to the

Department of Electrical and Computer Engineering

In conformity with the requirements for

the degree of Doctor of Philosophy

Queen's University

Kingston, Ontario, Canada

January 2020

Abstract

Next-generation intelligent transportation systems of future road traffic monitoring will be required to provide reports of road conditions. Monitoring road surface conditions benefits drivers and the community. Road surface anomalies contribute to increased risk of traffic accidents, reduced driver comfort and increased wear of vehicles. Municipalities usually inspect the road surface quality through manual eye inspection that is inefficient, exhausting and consumes resources.

Motivated by the growing demand for efficient road information services for connected and automated vehicles, this thesis proposes a comprehensive framework for monitoring road surface conditions. An intelligent and robust road surface monitoring system integrating vehicular and smart devices' inertial sensors and GNSS receivers within and amongst vehicles is designed and developed in this research.

To ensure rich data collections, land vehicles of different types are used in the road tests. A wavelet packet analysis was applied to the sensor measurements to separate the road anomalies' signatures from both the vehicle motion dynamics and the sensor noise. Various feature extraction techniques were used to identify several types of road anomalies. The constructed features were utilized in building datasets of these road anomalies. The datasets were leveraged to build and assess the performance of a support vector machine classifier to detect and categorize multiple road anomalies of different severity levels.

In order to overcome the GNSS receivers' challenges in geo-referencing the monitored anomalies,. In this framework, the vehicles' onboard motion sensors are integrated with GNSS receivers to provide accurate, continuous, and adaptive resolution geo-referencing to the monitored anomalies. The road anomaly information is then utilized to provide assessment for the average quality of the road segments using a fuzzy inference system. The developed road segment quality database was then used by another fuzzy classifier that can be utilized in route planning to evaluate all possible routes and suggest the one of highest road quality.

The future deployment of the system developed in this research will contribute to reducing congestion and accidents along the roads, enabling road labelling based on accessibility and conditions, providing personalized alerts and route recommendations, and improving road safety for all drivers.

Co-Authorship

- **Journal Papers:**

1. A. S. El-Wakeel, J. Li, A. Noureldin, H. S. Hassanein, and N. Zorba "Towards a Practical Crowdsensing System for Road Surface Conditions Monitoring", *IEEE Internet of Things Journal*, Dec. 2018.

2. A. S. El-Wakeel, A. Osman, N. Zorba, A. Noureldin, and H. S. Hassanein "Robust Positioning for Road Information Services in Challenging Environments", *IEEE Sensors Journal*, Dec. 2019.

3. A. Abdelrahman*, **A. S. El-Wakeel***, A. Noureldin and H. S. Hassanein "Crowdsensing-based Personalized Dynamic Route Planning for Smart Vehicles", *IEEE Network*, Jan. 2020.

* Authors contributed equally to this work and they are first co-authors.

- **Conference Papers:**

4. A. S. El-Wakeel, J. Li, M. T. Rahman, A. Noureldin and H. S. Hassanein, "Monitoring Road Surface Anomalies Towards Dynamic Road Mapping for Future Smart Cities", *5th IEEE Global Conference on Signal and Information Processing (GlobalSIP)*, Montreal, CA, Nov. 2017.

5. A. S. El-Wakeel, A. Osman, A. Noureldin and H. S. Hassanein, "Road Test Experiments and Statistical Analysis for Real-Time Monitoring of Road Surface

Conditions", *GLOBECOM 2017 - 2017 IEEE Global Communications Conference*, Singapore, SG, Dec. 2017.

6. A. S. El-Wakeel, A. Noureldin and H. S. Hassanein and N. Zorba "Utilization of Wavelet Packet Sensor De-noising for Accurate Positioning in Intelligent Road Services", *14th International Wireless Communications and Mobile Computing Conference (IWCMC)*, Limassol, CY, Jun. 2018. **"Best Paper Award"**

7. A. S. El-Wakeel, A. Noureldin, H. S. Hassanein and N. Zorba "iDriveSense: Dynamic Route Planning Involving Roads Quality Information", *GLOBECOM 2018 - 2018 IEEE Global Communications Conference,* Abu-Dhabi, UAE, Dec. 2018.

8. A. S. El-Wakeel, A. Noureldin, N. Zorba, H. S. Hassanein "A Framework for Adaptive Resolution Geo-Referencing in Intelligent Vehicular Services", *2019 IEEE 90th Vehicular Technology Conference (VTC 2019-Fall),* Honolulu, HI, USA, Sept. 2019.

- **Competitions:**

9. A. S. El-Wakeel, A. Noureldin, and H. S. Hassanein "iDriveSense: Towards Efficient Road Information Services", IEEE Communications Society Student Competition "*Communications Technology Changing the World*", 2018. "**Second Prize**"

Acknowledgements

First and foremost, all praises and thanks to my God "Allah" for his blessings and for giving me the ability to learn, conduct research, and write this thesis. It is only with His guidance and help that this work was accomplished.

I would like to express my appreciation and gratitude to my supervisor Prof. Aboelmagd Noureldin. Throughout my Ph.D., his limitless guidance, support and patience helped and enabled me to complete my research work and thesis. Also, I would like to extend my gratitude and appreciation to my co-supervisor Prof. Hossam Hassanein for his valuable suggestions and motivations during my Ph.D..

I want to thank all my previous and current colleagues in NavINST and TRL research labs. I will always remember your personal and professional support, and your nice attitude.

To my parents, Fatma and Saad, words can never describe my sincere and deep appreciation, and gratitude to all your efforts throughout my whole life. You have been always the main source of love and support and you have always believed in, and guided me. I owe you everything I achieved and will achieve.

To my wife, Manar, your true love, sincere friendship and pure soul have enlightened my life. I really appreciate your endless care and support. You have always believed in me, and helped me to pass any challenge. Manar, without you, I would not be writing these lines now.

To my brothers, Ahmed and Hossam, I have enjoyed every single moment of our life together. Your care, support and love have been always appreciated.

Last but not least, to my sons, Eyad and Yousef, you are the whole world to me and the most precious gift from Allah. May Allah protect and guide you, always.

Contents

List of Figures

List of Tables

List of Abbreviations

AAA	American Automobile Association
AV	Allan Variance
KF	Kalman Filter
EKF	Extended Kalman Filter
FFT	Fast Fourier Transform
FIS	Fuzzy Inference System
FOG	Fiber Optic Gyroscopes
GNSS	Global Navigation Satellite Systems
GPS	Global Positioning Systems
ICT	Information and Communication Technologies
IMU	Inertial Measurement Unit
INS	Inertial Navigation Systems
IoT	Internet of Things
ITS	Intelligent Transportation Systems
KNN	K-Nearest Neighbor
LBS	Location-Based Services
MEMS	Micro-Electro-Mechanical Systems
MPF	Mixture Particle Filter

RMS	Root mean Square
PF	Particle Filter
PASER	Pavement Surface Evaluation and Rating
PRN	Pseudo-Random Noise
QI	Quality Indicator
RIS	Road Information Services
RISS	Reduced Inertial Sensor System
SIR	Sampling/Importance Re-sampling
STFT	Short-Time Fourier Transform
SVM	Support Vector Machine
UAV	Unmanned Aerial Vehicle
USDOT	United States Department of Transportation
WDFT	Windowed Discrete Fourier Transform
WMRA	Wavelet Multi-Resolution Analysis

Chapter 1

Introduction

1.1 Background

The Internet of Things (IoT) is a network of devices with embedded technology that can collect, analyze, interact, and communicate data within itself or its environment through the internet [1]. According to the analyst firm Gartner Inc. [2], it was estimated that, in 2017, 8.4 billion devices were connected to the internet, and the end of 2020 will deploy 20.4 billion IoT devices. Consequently, in this ever-changing technological era, the IoT introduces endless opportunities and connections to enhance the efficiency of existing solutions leading to the global expansion of technological networks. IoT applications are commonly associated with smart homes, wearables, smart cities, and intelligent vehicles [3]. These applications create an environment where every device communicates with other related devices to automate the home and industry and provides data to interested users [4].

The evolution of smart cities continues to improve efficiency, safety, and living standards. Smart city services range from healthcare and waste management to traffic and pedestrian monitoring in hopes of creating a sustainable, intelligent system [5]. Specifically, intelligent transportation applies sensing, analysis, control, and communication to ground transportation through the IoT to increase safety and mobility [6].

Accordingly, location-based services (LBS) could be used to augment the quality of intelligent transportation. Crowdsensing as an aspect of crowdsourcing could benefit LBS, as sensed data can be transmitted with user participation or in an opportunistic form where no specific involvement of users is required [7]. Additionally, Micro-Electro-Mechanical Systems (MEMS) are sensors embedded in smart devices, vehicle motion sensors, and global positioning systems (GPS) receivers that contribute heavily to crowdsensing LBS [8]. Consequently, various intelligent transportation applications such as Road Information Services, traffic congestion monitoring, real-time route planning, driver behavioural pattern systems, and road surface monitoring could be efficiently implemented, utilized, and assessed [9].

Intelligent transportation systems (ITS) are a significant component of information and communication technologies (ICT). The evolution of computers, sensors, control, communications, and electronic devices can lead to ITS solutions that save lives, time, money, energy, and the environment. Modern computers and communication systems technologies are being developed in a manner to improve transportation worldwide. The integration of such systems provides several forms of interactive links between travellers, vehicles, and infrastructures to eliminate the challenges in transportation [10]. Considering the ITS market size, Grand View Research stated that the market was valued at $20.94 billion in 2015. The market size is expected to reach $66.5 billion by 2024. The share of the North American ITS industry is predicted to be more than $26 Billion [11]. As a result of the governments' increasing demand for drivers and pedestrian safety, roadway ITS is predicted to have the most significant share of the market [12].

Next-generation ITS, specifically those involved in road traffic monitoring, will be required to provide reports about traffic congestion, road conditions, and driver behaviour. Road surface anomalies are one of the road conditions indicators, contribute to increased risk of traffic accidents, reduced driver comfort, and increased wear on vehicles. As in both cases of either attending an anomaly or trying to avoid it, that could introduce a lower level of driver control on the vehicle and might lead to an accident or cause damage. According to the American Automobile Association (AAA), two-thirds of U.S drivers are worried about road surface anomalies; AAA reports that approximately $3 billion a year is spent on car repairs due to road surface anomalies [13]. Also, 33 % of the 2M+ accidents reported by Transport Canada between 2001 and 2011 were attributed to weather or road conditions [14].

Consequently, various countries, through their ITS organizations and societies, are monitoring and analyzing road surface conditions as a part of their frameworks towards efficient ITS. The United States Department of Transportation (USDOT) has set a strategic plan for ITS research for 2015-2019. In their plan, USDOT stated the importance of monitoring road surface conditions. Field test data collected from onboard vehicle sensors are used to assess the road surface condition [15]. Also, ITS Canada society highlighted the importance of monitoring road conditions in their strategic plan, specifically in winter [16]. In Europe, the European Commission set an ICT infrastructure for ITS services. They monitor road conditions using sensors, cameras or induction loops through police cars or road users. Sensed data are then processed in traffic control centres to identify the quality of the roads [17]. Further, ITS Australia, in their report at the ITS

world congress, suggested that land vehicles could collect information about the road's health through the vehicle's sensors, which is useful for data road operators [18].

1.2 Motivation

Smart cities have raised expectations regarding efficient functioning and management as a result of the rapid growth in the ICT sectors. Specifically, the road information services (RIS) systems as they affect the residents and almost all their essential daily activities. The primary purpose of an adequate RIS system is to provide residents with updated about various aspects of the roads taken daily. This information enables dynamic and comfortable trip planning while considering the residents' preferences and priorities that draw their perspectives in having timely, comfortable and safe trips [19].

Nevertheless, RIS systems operated by city authorities provide residents with information regarding traffic status, scheduled or unplanned road construction or maintenance, weather conditions that would hinder safe driving such as ice, snow or sandstorms. This information is afforded on city operation websites or can be broadcast on TV and radio channels. In some situations, road signs are leveraged to communicate updated traffic messages or to inform about road maintenance or road closures [20]. On the other hand, route planning applications such as Google Maps, Apple Maps Connect, and Waze provide their users with vital information regarding their potential routes in an offhand manner. Likewise, the information includes already known traffic patterns in specific route portions at distinct time windows. Also, Google Maps services include online changes to route recommendations based on unexpected jams or construction work.

Conversely, corwdsensed-based trip-planning application Waze relies on lively sensed traffic situations that are shared by the users [21].

However, road quality information is neither collected and analyzed nor provided or considered in route planning recommendations. As mentioned earlier, road anomalies such as cracks, potholes, and utility holes cause dangerous driving scenarios and can induce vehicle damages and pricey repairs [22]. There are some attempts at monitoring road surface conditions. Nevertheless, most of them depend on third-party sensing infrastructure with limited information. Road information services monitored by authorities mostly rely on specific software simulation integrated with specialized instrumentation and in some cases, conditions are reported manually [15, 23]. In the current literature, most of the available road surface monitoring systems lack full insight into the required aspects that formulate robust monitoring of anomalies. These systems either presented a few types of anomalies [24] or just focused on details of one type of anomaly [25]. Respectively, the absence of adequate detection and classification of road types and anomalies introduces inaccurate information regarding the road surface condition, which in turn leads to ambiguous road segment assessments. This shortcoming prevents the authorities' efforts from affording timely and appropriate road surface maintenance.

Furthermore, some solutions that detect and classify road anomalies lack adequate geo-referencing of the detected events as they rely only on GPS. Generally, in urban areas and downtown cores, the localization accuracy dramatically deteriorates due to GPS satellite signal blockage and multipath [26, 27]. Moreover, complete GPS outages also occur while driving under bridges or in tunnels. To mitigate these challenges, inertial navigation

systems (INS) are integrated with GPS receivers to provide accurate and continuous positioning [26]. The low-cost MEMS-based inertial sensors (accelerometers and gyroscopes) that are embedded in INS systems in land vehicles and ubiquitous smart devices are not susceptible to the same challenges of GPS. Stand-Alone INS solutions are liable to long-term position drifts and errors due to inertial sensors' biases and noises. Uncertain and erroneous geo-referencing of the monitored anomalies again will distract the efforts required for road maintenance.

Most of the current trip planning applications are enabling their trip planning recommendations relying on shortest paths and fastest routes [21]. Although, such route suggestions may discount drivers' preferences concerning safe and comfortable trips. Road quality information is the crucial aspect that enables drivers a safe and comfortable trip but was not considered in most of the route planning systems [22]. Many factors exacerbate a driver's frustration and stress, deteriorated road surface conditions can lead to vehicle damage, and dangerous driving scenarios are but only a couple. Thus, dynamic route planning involving road quality assessment information facilitates safe and comfortable daily trips for smart city drivers.

1.3 Problem Statement

To develop a RIS system that considers the assessment of road surface conditions and provides effective route planning based on the road quality information that is assessed by the system. Many factors may impact the performance of RIS systems:

- **Sensors:** many of the land vehicles are equipped with motion sensors such as accelerometers and gyroscopes that are good candidates for capturing road anomalies. Most likely, ubiquitous smart devices of the drivers are embedded with inertial sensors such as accelerometers and gyroscopes. These sensors can also be utilized in road surface conditions detection. Withall, both sets of sensors (vehicles, smartphones) are usually MEMS-based sensors that experience high noises. Subsequently, these sensor measurements must be de-noised to efficiently capture the road anomalies' effects on these measurements, while considering separating the irregularities effects from land vehicle motion dynamics. Also, where a driver places the smart device in the land vehicle may introduce undesirable and misleading measurements that confuse anomaly detection algorithms. Lastly, sensor measurements need to be collected at a high data rate to enable a detailed description of the anomaly behaviour on these measurements.

- **Data Validity:** for a reliable RIS system, the data sets describe road surface anomalies and lead to a fair assessment of road qualities that need to be carefully considered. Consequently, data sets have to be frequently collected. Various land vehicles with numerous specifications equipped with various motion and inertial sensors at different orientations along with diverse driving styles and approaches of anomalies attendance for sure lead to multiple signatures of the same road anomaly on the sensed data.

- **Anomaly Detection:** regarding the efficient detection of road surface types and conditions, RIS systems have to adopt sufficient feature extraction techniques that assure capturing the distinct, descriptive signature of each type of road anomaly. Subsequently, RIS systems have to use adequate classification techniques to correctly categorize the sensed anomalies to enable efficient reporting for authorities or relevant services providers.

- **Robust Geo-referencing:** considering a careful road surface monitoring, continuous and accurate localization of the monitored events is highly required. Both standalone GPS receivers and the ones embedded in the smart devices are vulnerable to partial or complete outages under many different driving scenarios. Integrated GPS/INS solutions need to seriously overcome the INS geo-referencing drifts and errors during the absence of reliable and adequate GPS positioning solutions. Moreover, most standalone GPS receivers or integrated positioning systems operate at 1 Hz, while at high speeds, high-resolution geo-referencing is needed to localize the detected road anomalies precisely.

- **Route Planning:** frequent assessments of the road segments quality based on the sensed anomalies open the door towards dynamic and efficient vehicle routing. For enabling safe and comfortable trips, knowing the road segments quality information can suggest the smoother routes among the ones suggested by route planning applications or service providers. On the other hand, in further levels, route quality information can introduce alternative routes that may align with

drivers' preferences and provide more insights towards dynamic traffic management.

1.4 Research Objectives

The ultimate objective of this research is to:

"Utilize the sensors available in land vehicles and passengers' smart devices to develop an Intelligent RIS system capable of adequately detecting, categorizing and geo-referencing road surface types and anomalies and enables efficient dynamic route planning involving road information quality"

The specific goals of this research are to:

1- Utilize different types and grades of accelerometers and gyroscopes from both land vehicles and smart devices to enable a rich collection of data for different road types and anomalies therein.

2- Explore the effects of multiple common road types and irregularities on the vehicle motion to understand their effect on the vehicle and driver behaviour.

3- Enhance the quality of measurement in low-cost sensors to ensure reliable performance while collecting the road types and anomalies data.

4- Process the measurements by feature extraction techniques to extract plentiful and distinguishable features for each road anomaly type facilitating its categorization.

5- Categorize the road anomalies and types to provide the municipalities with this information required for road maintenance and enable road quality assessments, utilizing a multi-level Support Vector Machine (SVM) classifier that can detect

and classify various road anomaly types and irregularities with different levels of severity.

6- Provide continuous, accurate and reliable positioning information at a high data rate available in all environments to provide geo-referencing of the detected anomalies and navigation solution for route planning. Integrated positioning through adopting de-noised-based reduced inertial sensor system (RISS)/GNSS while enabling the operation of the RISS independently over long periods without GPS measurements, both in downtown areas and other GPS denied environments.

7- Introduce dynamic route planning involving road quality information to enable safe and comfortable trips.

1.5 Contributions

The main contributions of this thesis research are listed below:

1- The experimental work of this research was based on numerous real road experiments by adopting different car models that span multiple types, sizes and model year. These experiments provided a comprehensive collection of a variety of driving scenarios. With the utilization of both onboard vehicle and smart devices sensors; the signature of multiple road anomalies has been successfully identified on the measurements collected from accelerometers and gyroscopes.

2- An inertial sensor de-noising method based on wavelet packet analysis was developed in this research to enhance the quality of the data sensed by low-cost MEMS sensors, and to separate the vehicle motion dynamics and the effects of the road anomalies from other measurement noises and disturbances.

3- Several feature extraction techniques such as statistical, time, frequency and others were utilized to capture unique features describing the monitored road anomalies to enable efficient categorization of them.

4- A multi-level SVM classifier that can detect and classify various road anomaly types and irregularities with different levels of severity was developed in this research.

5- The utilization of the de-noised inertial sensors to provide accurate RISS was explored and developed in this research. When integrated with GPS receivers, the RISS/GPS provided accurate and continuous high-resolution positioning solutions for both localizing the detected anomalies and navigating the drivers during their trips.

6- A fuzzy inference system (FIS) is utilized to assess the average quality of road segments based on different criteria such as the segment length, the number of, nature and the level of severity of the anomalies. Also, an additional FIS was used to provide route recommendations based on metrics corresponding to the average quality of the route's road segments, trip time and length.

1.6 Thesis Outline

The thesis is organized as follows. In Chapter, a comprehensive literature review and current state of the major components of the monitoring road conditions systems, as well as route planning metrics, were provided. This chapter is followed by Chapter 3, where the system architecture and the road surface anomalies and types are identified, detected and categorized. In Chapter 4, an adaptive resolution geolocation framework is presented

and discussed to enable efficient and continuous localization for the monitored anomalies. A dynamic route planning system that involves the average route road quality is presented in Chapter 5. In Chapter 6, the thesis contributions and findings are summarized as well as an insight into the potential future work motivated by this thesis's conclusions.

Chapter 2

Background and Literature Review

2.1 Road Surface Condition and Quality Monitoring and Assessment

Environmental attributes such as weather, ageing, sun, water, ...etc., are one of the significant causes of road pavement distress. Besides, according to pavement surface evaluation and rating (PASER) manual introduced by transportation and information center at the University of Wisconsin-Madison [28], heavy and repeated loads can lead to structural deficiencies for the road pavement. Municipalities and government agencies are always considering the utilization of public funds for enabling safe, convenient and cost-effective road surfaces that demand priorities stabilizing and taking challenging decisions regarding pavement management. Accordingly, a comprehensive pavement management system mainly collects data to estimate multiple road characteristics such as roughness (ride), surface distress (condition) and structure (pavement strength and deflection) [28].

Road surface condition is the most crucial element in the pavement management system for both the vehicle and driver safety [28]. PASER helps the staff in categorizing the road condition quality into four main classes: surface deflects, surface deformation, cracks, and patches and potholes. However, PASER ratings, which are recommended to be updated every two years, have some drawbacks. In challenging environments, such in North America, in two years, road surface conditions may dramatically deteriorate. Also, the

stuff manual reporting does not measure the effects of the road conditions and their corresponding severity level on the vehicle motion. The limitations of the municipalities' current pavement management systems have triggered the need for a periodic reporting of the road conditions utilizing new systems and including additional perspectives.

To enhance the road conditions monitoring process, some cities like Boston, Massachusetts, USA launched a crowdsensing-based system to monitor road conditions [56]. In this system, which was named "Street Bump" the city residents leveraged the accelerometers and the GPS on their smartphones to collect information about the city's road quality. The city accordingly updated its maps with the information of the road anomalies and classified them into actionable and non-actionable classes. Street bump application helped the city of Boston in identifying the significant anomaly that disturbed the cars, and this was the manhole covers. In addition, the United States Department of Transportation (USDOT), leveraged the on-board vehicle sensors to monitor the road conditions rather than the regular manual reporting process [33]. The testbed included inertial sensors, GPS receivers and Laser senor. The findings of the road experiments included recommendations on the importance of using the on-board sensors regularly to monitor the road surface conditions.

2.2 Current State of the Art for Monitoring Road Surface Conditions

This section presents the literature regarding RIS systems that monitor road surface types and irregularities as long as the systems took into consideration drivers' comfort and safety

while providing route recommendations. Eventually, these systems were built on experimentation bases or in simulated environments. Experimental based systems have adopted different types of sensors, either in vehicles or within smart devices. Also, there were numerous feature extraction techniques utilized to capture the road anomaly behaviour on the sensed data. For categorization and classification of the detected irregularities, many techniques were applied, spanning threshold-based techniques and machine learning approaches. Over and above, most of the literature has used GPS receivers for localizing the road anomalies. Many systems and service providers have considered drivers' preferences in route recommendations for trip planning.

2.2.1 Sensors used in Detecting Road Surface Anomalies

In literature, the developed road condition monitoring systems have mainly considered the detection of the road anomalies and the localization of the detected road irregularities. There are many sensors adopted in sensing road irregularities. Inertial sensors, namely accelerometers and gyroscopes, are the most utilized sensors for road condition monitoring [22]. Accelerometers are the devices that can measure the linear accelerations or specific forces in three orthogonal axes: x-axis, y-axis and z-axis [26].

On the other hand, gyroscopes are the devices that can measure the angular rotation around three orthogonal axes: x-axis, y-axis and z-axis. The accelerometers and gyroscopes can be separate or combined in an inertial measurement unit (IMU) that contains three axes of accelerometers and three axes of gyroscopes. The IMUs are usually categorized

based on the technologies and the specifications of the accelerometers and gyroscopes, and their target applications. In general, IMUS are classified into the following classes [26, 29]:

- Commercial-grade: that contains MEMS accelerometers and gyroscopes. The cost of these IMUs is in the range of several US dollars. The commercial-grade IMUs are used in various applications such as smartphones, tablets, airbags and portable navigation. The accelerometers have bias error in the range of 100-1000 µg while the gyroscopes have a drift around 0.1 degrees per second.

- Tactical grade: These IMUs cost ranges between 5,000 to 20,000 US dollars. They contain solid-state accelerometers and fibre optic gyroscopes (FOG). The bias error of the accelerometer is between 1-5 mg, and the gyroscope drift is between 1 to 10 degrees per hour. These IMUs can be used in unmanned air vehicles (UAVs) and guided weapons.

The other two categories are navigation grade and strategic grade IMUs. These IMUs have relatively high prices, and they are used in applications such as mapping, high precision geo-referencing and submarines. Commercial grade inertial sensors and IMUs are the ones that are usually used in monitoring road condition systems.

Initially, the three-axis accelerometers that measure the forward, transverse and vertical linear accelerations were commonly used [30]. Where they were mounted in land vehicles for experimentation activities, the results of some, all or combinations of their measurements were used in event detection. In [30], the data of the three-axis external unit accelerometers were collected. Independent accelerometer measurement and the

combination of the vertical and transversal accelerations were used. Likely, in [31], the three-axis accelerometers data were collected while the root mean square (RMS) of both transversal and vertical accelerations were used to indicate the presence of an anomaly. The full IMU contains three-axis accelerometers, and three-axis gyroscopes were also used for sensing road anomalies. Speed bumps were sensed in [32] using the measurement from transversal acceleration and the angular rotation around both forward and transversal axis.

USDOT has collected the data of a full IMU mounted on land vehicles with three-axis accelerometers and three gyroscopes measurements to sense road irregularities. In their initial analysis, they adopted only the longitudinal and vertical acceleration measurements, although they recommend the usage of gyroscope data for adequate anomaly detection [33]. Otherwise, measurements from vehicles embedded accelerometers were gathered at a different data rate and used in pothole detection [34]. Google [35] have leveraged vertical acceleration sensor to collect data to assess roads quality. The mentioned works have utilized inertial sensors that are embedded with the vehicles or were intentionally mounted for experimentation and data collection purposes.

Inertial sensors embedded in smart devices such as smartphones and tablets were widely used for sensing and collecting data related to road surface anomalies [9]. The smart devices are equipped with various sensors that span accelerometers, gyroscopes, compasses and barometers. Inertial sensors like accelerometers and gyroscopes are the potential players in leveraging smart devices for road condition monitoring. In particular, accelerometers were widely adopted in sensing road anomalies. Generally, one or more axis of the three-

axis accelerometers embedded in the smart devices is used for sensing uneven roads [24]. As in some systems, the anomalies are sensed using the vertical acceleration [24, 36], a combination of the vertical and horizontal accelerometers axis [37], or a combination of the longitudinal, transversal and vertical acceleration measurements [25, 38]. Also, in addition to the utilization of the accelerometers, other systems adopted gyroscopes measurements to sense some road irregularities [39-40]. A combination of one or more gyroscopes is used in the case in [39], while the three-axis gyroscopes are all used in [40, 41].

Despite the extensive usage of the commercial-grade inertial sensors in monitoring the road surface anomalies, these sensors are liable to biases, noises and errors that can lead to inadequate monitoring of the road conditions. Some of these errors are deterministic and can be compensated, utilizing laboratory calibration [26, 42]. Examples of some inertial sensors deterministic errors are shown in figure 2.1 and figure 2.2.

- **Scale factor:** is the error because of the manufacturing imperfection or ageing. This error appears in the form of deviation of the input-output gradient from unity.
- **Bias:** appears in the form of the nonzero constant output reading in the case of zero input.
- **Nonlinearity:** appears in the form of the nonlinear relation between the input and the output.

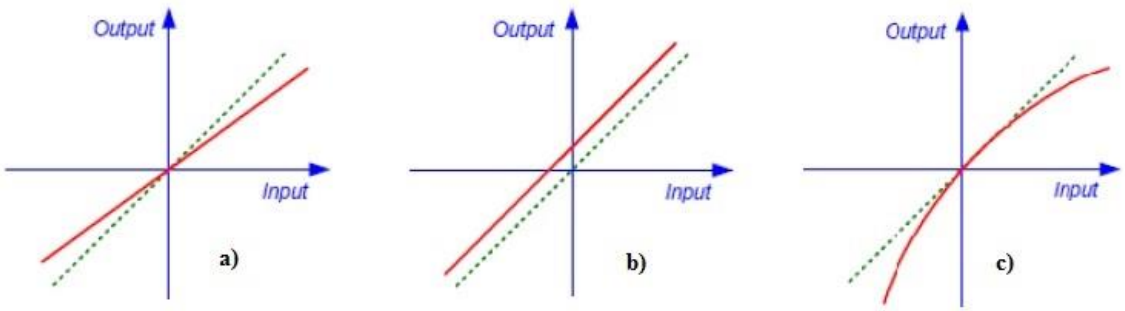

Figure 2-1 Inertial sensor errors: a) scale factor, b) bias and c) nonlinearity (adapted and modified with permission of [26])

- **Quantization:** it is the error that appears in digital systems when converting the analog input into digital values.
- **Scale factor sign asymmetry:** mismatched push-pull amplifiers introduce a difference in the input-output gradient for positive and negative values of input.
- **Dead zone:** the range where the output is absent although there is an input value

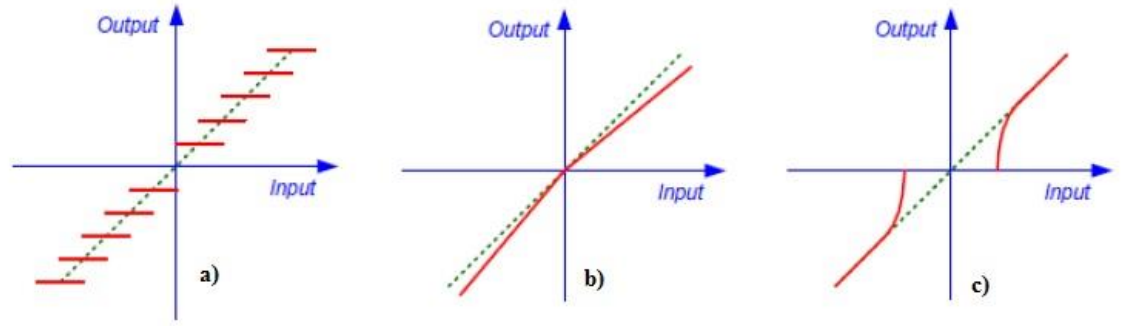

Figure 2-2 Inertial sensors errors: a) quantization, b) asymmetry and c) dead zone (adapted and modified with permission of [26])

There are also some random and stochastic errors and noises that are more challenging to estimate [26, 42].

- **Bias drift:** temperature changes can introduce random variance in the bias at different time instances.
- **Scale factor instability:** appears in the form of random change of the scale factor.
- **Electronic noise:** is also called white sensor noise that is caused by power supplies, digitization's quantization errors or by the intrinsic semiconductor devices noise.
- **Exponentially correlated noise:** it is a temperature-sensitive noise. It appears due to the variations in heat distribution and the internal and external temperatures. It is a time-varying additive noise that affects sensor bias.

In order to assure reliable monitoring of road conditions, the mentioned above biases, errors and sensors need to be removed either by compensation, offline processing, de-noising or through a combination of the processes.

2.2.2 Features Extraction Techniques

Road surface types and anomalies lead to unusual vibrations in the land vehicle. Subsequently, these vibrations introduce significant effects on the inertial sensors measurements. Different road anomalies have multiple signatures on the sensed measurements. To capture these signatures, various feature extraction techniques are used to detect the road irregularities and to distinguish their types [9]. Fundamentally, feature extraction techniques can be grouped into statistical, time and frequency domain features.

Statistical features usually describe the statistical distribution of a windowed signal or within a given time frame. The statistical features can measure the central tendency in a signal like the mode, which is the most frequent value of a signal in a time window. Also, the mean value of the signal over a window segment is considered as a feature:

$$mean(u) = \overline{u[n]} = \frac{\sum_{n=1}^{N} u[n]}{N} \tag{2.1}$$

On the other hand, there are statistical features that measure the dispersion to figure out the spread of the data values. For example, the variance $var(u)$ is an indicator of how much a signal is dispersed around its mean [43]. It is equivalent to the mean of the squares of the differences between the signal values and their mean. While the square root of the variance is the standard deviation $std(u)$ [44]:

$$var(u) = \sigma_u^2 = \overline{(u - \bar{u})^2} \tag{2.2}$$

$$std(u) = \sigma_u = \sqrt{\overline{(u - \bar{u})^2}} \tag{2.3}$$

Time-domain features mainly describe the change in the signal values with respect to time such as zero-crossing rate and threshold crossing rate. Zero crossing rate measures

the number of times the signal value changes its sign from positive to negative and vice versa, and it is relevant only with the signals that change their values signs.

$$zcr(u) = \frac{1}{N-1}\sum_{n=1}^{N-1} \mathrm{I}\{u[n]u[n-1] < 0\} \tag{2.4}$$

$$\mathrm{I}\{cond\} = \begin{cases} 1 \; if \; cond \; is \; TRUE \\ 0 \; if \; cond \; is \; FALSE \end{cases} \tag{2.5}$$

Frequency domain features represent signals according to their frequency components. The Fourier analysis, the well-known frequency analysis, breaks down the signal into a group of sinusoids of multiple frequencies. Thus the time domain signal is transformed into frequency-based components or domain. The major disadvantage of Fourier analysis is that once the signal is transformed into the frequency domain, all the time domain information is lost. Therefore, the transformed signal needs to be localized in the time domain to mitigate the drawbacks of the Fourier analysis. Short-time Fourier transform (STFT), also known as windowed discrete Fourier transform (WDFT), is simply a group of Fourier transforms of a signal across blocks of the signals, which may be interleaved or not [45].

$$STFT[k,m] = \sum_{\forall n} u[n]w[n-m]e^{-j\frac{2\pi kn}{N}} \tag{2.6}$$

$$w[n] = \begin{cases} 1, if\ 0 \leq n-1 \\ 0, otherwise \end{cases} \tag{2.7}$$

In WDFT, a time window is predefined, assuming local signal periodicity. For each window, the WDFT produces a sequence of complex values whose magnitudes are those of the discrete frequencies of the input. A significant drawback of WDFT is that a window with a fixed width always raises the time-frequency trade-off, as narrow window width leads to appropriate time localization, but insufficient frequency resolution is obtained. Also, WDFT can experience phenomena named spectral leakage, as to model a frequency that does not have an integral number of periods in the record length, energy is spread into all the other frequencies [46].

To overcome the challenges of WDFT, Wavelets are proposed and adopted. In wavelets, the analysis grants the use of relatively long time windows where low-frequency components are required [47]. Meanwhile, where high-frequency content is needed, shorter intervals are adopted. Consequently, in the wavelet multi-resolution analysis (WMRA) process, the signal is divided into multiple resolution levels, as shown in figure 2.3. The signal approximation, A, contains the low-frequency component of the signal. The signal detail, D, is the representation of the high-frequency components of the analyzed signal. At each new decomposition level, the signal approximation, A_i, is also decomposed into new pairs of the signal approximations, A_{i+1}, and details, D_{i+1}.

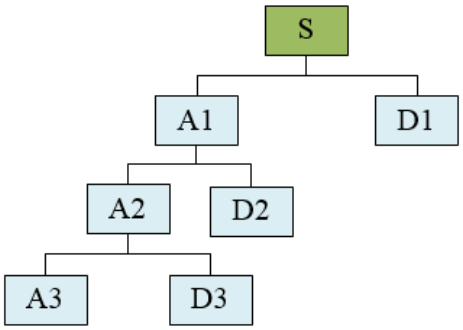

Figure 2-3 Wavelet decomposition tree

In WMRA, a wavelet function, Ψ_t, is used to seek the details in a signal in operation equivalent to high pass filtering where a scaling function, ϕ_t, is designed to smooth the input signal to seek its approximation in a process equivalent to low pass filtering [47]. The wavelet and scaling functions are usually orthonormal functions. There are numerous wavelet functions families such as Daubechies, Haar, Coiflets and Morlet [47].

Moreover, statistical feature extraction techniques, such as amplitude thresholds were used to detect road irregularities[24, 25]. In [24], a vertical accelerometer was used in detecting road anomalies. An amplitude threshold was proposed to detect potholes at low speeds by checking if the value of the vertical acceleration has exceeded the predetermined threshold within a 20 milliseconds time window [24]. Predetermined thresholds were used to detect different sizes of potholes and drain pits in [25]. The thresholds were set and tuned to detect the anomalies with the aid of a vertical accelerometer. Standard deviations were also used in [25] to detect potholes. The algorithm was searching for vertical acceleration consecutive measurements that exceed preset standard deviation levels. In

[34], using simulated pothole data, standard deviations of the forward and vertical acceleration were used to detect potholes. Root mean squares of the three axes accelerometers were used in [48] to detect uneven roads.

Frequency domain techniques such as fast Fourier transform (FFT) was also used in [48] to calculate the frequency components in the acceleration measurements during the road anomalies events. In [40], FFT was used to compute the frequency components of three-axis accelerometers and one gyroscope to detect road anomalies. Wavelet analysis [39] was used to describe the behaviour of the road anomalies on the sensed accelerometer data. A Symlet Wavelet family of four decomposition levels was used to decompose the acceleration signal for capturing the road anomalies features. All the described feature extraction techniques were used in separate or combined to extract features from the linear accelerations and angular rotations measurements to detect the road types and surface conditions.

2.2.3 Road Surface Types and Anomalies Categorization

Road Anomalies classification is required to provide efficient reporting and to assure proper road maintenance. Generally, predetermined thresholds are used to classify different types of road irregularities [25]. The threshold-based classification was mainly used to classify the road conditions into smooth and uneven roads. Also, the threshold-based classification was adopted to categorize different types or sizes of road anomalies. In Nericell system [24], the predetermined amplitude thresholds were adopted to classify speed bumps and potholes. Also, in [25] preset peak to peak, standard deviations thresholds were used to

classify different pothole sizes and drain pits. However, the classification based on the trivial predetermined thresholds can experience various challenges when being tested in cases where the sensors, cars and anomalies are changed.

Machine learning techniques are also used to classify road surface conditions. There are two main categories of machine learning: supervised and unsupervised learning [49]. For monitoring road surface conditions, supervised machine learning classifiers are more convenient than the unsupervised-based classifiers. In general, the supervised learning classification process is utilized to establish the relationship between the inputs and the corresponding outputs in a given system. This process has been named supervised as the learning techniques are mapping the inputs into outputs based on previously labelled inputs. The machine learning model is constructed and trained by the previously labelled inputs in order to be able to classify the new inputs to the most appropriate finite classes that were initially determined in the training process. The supervised learning enhances its predictive performance as it is trained on more labelled data [50].

For SVM, when the data has just two classes, it searches for the best possible hyperplane that identifies and separates the two classes from each other with every class, including all its corresponding data points. For an SVM classifier best hyperplane, it has to have the largest possible margin between the two data classes. The best hyperplane for an SVM means the one with the broadest margin between the two classes. The margin is the maximal width of the slab parallel to the hyperplane that has no interior data points. The data points that are close to or on the boundary of the margin are the support vectors.

For more than two and nonlinearly separable data classes, SVM is in trying to locate most of the data or features, S_m, that fit a class in a sphere. The sphere comes with radius, r, where it can be minimized as follows [51]:

$$\begin{aligned} & min\, r^2 + C \sum_{m=1}^{k} \Gamma_m \\ & Such\ that \quad (\|C - S_m\|)^2 \leq r^2 + \ \Gamma_m \\ & \Gamma_m \geq 0 \end{aligned} \tag{2.8}$$

where C is a parameter for the number of errors and sphere volume trade-off control, Γ_m is a factor that allows some data samples to endure outside a sphere. Consequently, for two data or feature vectors S_m and S_n it can be proven that:

$$\begin{aligned} & max \sum_{m=1}^{k} \gamma_m \langle S_m . S_n \rangle - \sum_{m,n=1}^{k} \gamma_m \gamma_n \langle S_m . S_n \rangle \\ & s.t.\ 0 \leq \gamma_m \leq C \ and \ \sum_{m=1}^{k} \gamma_m = 1 \end{aligned} \tag{2.9}$$

as $\langle S_m . S_n \rangle$ is the feature vectors' inner product, and γ_m and γ_n are Lagrange multipliers.

Furthermore, decision trees are another supervised-based machine learning classification technique. The decision tree classifier is predicting responses to the inputs based on a series of yes or no questions [52]. This approach is downsizing the potential classification classes

until it reaches to the most relevant class corresponding to the classifier input. The downsizing decision process starts from the beginning of the tree (root node) down to the leaf node. For example, a tree that classifies the inputs into two classes starts at the root node. Then according to the features test that includes thresholds comparisons, the tree down to left or right leaf nodes. Accordingly, at the leaf nodes, there is a possibility of additional feature-based threshold comparisons or the tree predicts a decision on which class do the input data belong [52].

In addition, k-nearest neighbour (KNN) is a form of supervised classification, feature vectors are grouped into clusters, during the training phase, each corresponding to a class [53]. KNN is considered as an instance-based classifier. Given an input feature vector, the cluster which is closest to this vector is considered to belong to that class. An arbitrary parameter is set through the training process that indicates classifier noise sensitivity. The classifier is more sensitive to the noise when this parameter is high and also this means that the classes are more distanced [53]. Also, ensemble Meta classifiers adopt classification techniques where multiple classifiers of a different or similar type are being trained over the same or subsets of a training set [54]. Notably, in bagging, a classifier is being trained in leveraging subsets of training sets. The construction of the subsets is a result of random selection from the main training set.

Moreover, supervised-based machine learning classification was adopted in detecting and categorizing road surface conditions. An SVM classifier with one level was used in [36] to classify the road surface into smooth and non-smooth classes. Likewise, in [4], a support vector machine classifier was used to classify road irregularities into two major

types. The first anomaly type spans railroad crossings and small potholes, while the second type contains speed bumps and massive potholes. Also, in [45], road anomalies are classified using a one-class support vector machine into safety-related type (speed bumps) and dangerous type (potholes). In [56], an AdaBoost classification technique was used to classify the uneven roads according to the need for immediate maintenance, as deemed by the authors. The anomalies were classified into two categories, actionable such as bumps and potholes, and non-actionable such as cobblestone roads and speed bumps.

Decision trees classifier was also used in one level classification in [40] to classify the road conditions into smooth or potholed. In [39], two support vector machine-based classification steps are used to classify road anomalies. The first classification step was utilized to classify the anomalous and the regular roads. The second classification step categorized the road anomalies into three categories of severe, mild and span. Each category grouped road anomalies that share the same effects on the vehicle motion and that have the same level of severity.

Accordingly, the proposed road conditions classification systems in researched literature lack some essential aspects. In some systems, there is a generic road anomaly classification in terms of two broad categories, such as smooth road or potholed one. While in other systems, some classes group in one class multiple types of road anomalies that they are different concerning their nature, required maintenance action and even their effects on the vehicle and the possibility of avoidance. Also, most of these systems do not consider the severity level of the monitored anomalies, which is essential when reporting to the authorities to help them in setting their plans and priorities for further actions.

2.2.4 Geo-Referencing Road Anomalies

Municipalities need accurate geo-referencing of the monitored road anomalies to provide timely and proper maintenance and repairs for the deteriorated roads, otherwise, the road irregularities detection efforts will be useless. In General, GPS is the most famous navigation and geo-referencing system. GPS is a satellite navigation system in the space that presents location and time information. This information is available regardless of the weather conditions, anywhere on or near the earth, where there is a line of sight to four or more GPS satellites. The GPS provides globally essential functionalities to military, civil and commercial users. The government of the United States maintain this system and enable GPS services to everyone with access to a GPS receiver without any required or collected fees [57].

The GPS project was developed in 1973 to overcome the limitations of previous navigation systems, integrating ideas from several predecessors, including several detailed engineering design studies from the 1960s. GPS was created and realized by the U.S. Department of Defense (DoD) and was initially run with 24 satellites. It became fully operational in 1995.

Each satellite transmits a radio signal that contains both a pseudo-random noise (PRN) code and a navigation message. The PRN code is used by the receiver to find the transit time, as a preliminary to calculating the range (called pseudo-range ρ) from the satellite to the receiver by multiplying this by the speed of light. It also calculates the satellite's position from the information in the navigation message. With the information from at least three satellites, the receiver can use the process of trilateration to compute its position

in terms of latitude, longitude and altitude, as shown in figure 2.4. The signal from a fourth satellite is needed to cancel the receiver's clock bias, b.

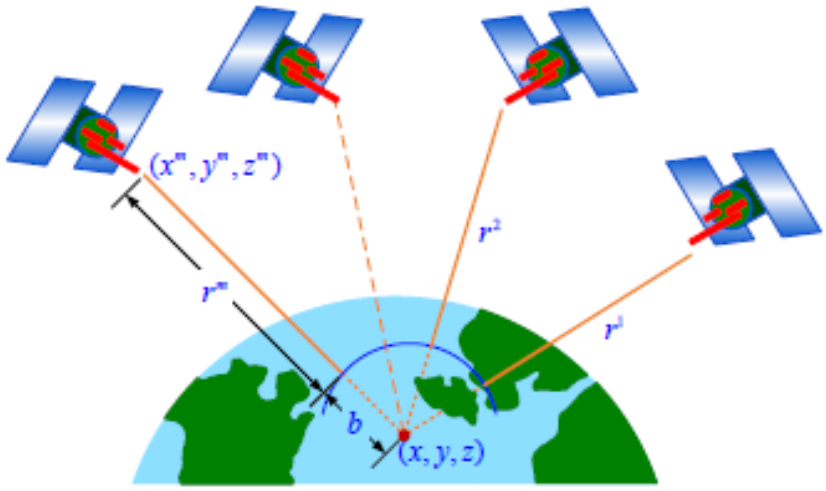

Figure 2-4 Concept of trilateration which enables a GPS receiver to calculate its position (x, y, z) based on the four range measurement (adapted and modified with permission of [26])

Pseudo-ranges are obtained by measuring the time it takes for the GPS signal to propagate from the satellite to the receiver and then multiplying by the speed of light [58]. Since the satellite's and receiver's clocks are not synchronized (mainly due to the clock in the receiver being inexpensive), these pseudo-ranges are biased by an amount equal to the receiver's clock offset. This offset is the fourth unknown in addition to the positional components of latitude, longitude and height. Therefore measurements from at least four satellites are required to solve these equations for four unknowns [26]. The pseudo-range measurement for the mth satellite can be written as [26]

$$\rho^m = r^m + c\ \delta_r + c\ \delta_s + c\ I^m + c\ T^m + \varepsilon_\rho^m \tag{2.10}$$

ρ^m is the measured pseudo-range between the m^{th} satellite and the receiver (meters)

c is the speed of light (meters/second)

r^m is the true range between the receiver's antenna at time t_r and the satellite's antenna at time t_t(meters)

δ_r is the receiver's clock offset (second)

δ_s is the satellite's clock offset (second)

I^m is the ionospheric delay (second)

T^m is the tropospheric delay (second)

ε_ρ^m is the error in range due to various sources such as receiver noise, multipath, satellite clock modelling, and orbit discrepancies (meters)

After correcting the satellite clock bias, ionospheric and tropospheric errors, the corrected pseudo-range is given by

$$\rho^m = r^m + c\ \delta_r + \tilde{\varepsilon_\rho^m} \tag{2.11}$$

Where, $\tilde{\varepsilon_\rho^m}$ represents the total effect of residual errors.

Standalone GPS receivers or the ones embedded in smart devices are the favourite geo-location sources for the detected events [58]. In many systems, standalone GPS receivers are used to localize the anomalies with an update rate of 1 Hz [58, 31, 34, 35]. The other systems used the GPS receivers embedded in the smart devices to locate the anomalies [36] and also with an update rate of 1 Hz. Although, for accurate and high-resolution

road anomalies geo-referencing, a GPS receiver with an update rate of 5 Hz was used in [59].

GPS systems have the advantage of being available in any open-sky location on the globe on the condition of the presence of a suitable receiver. GPS receivers may reach a precision of 3-10 meters in the open sky [57]. However, the drawbacks of GPS positioning are the absence of GPS signals in urban canyons and, therefore, the absence of a positioning solution in such areas. Also, the multi-path effects [26] on GPS signals in urban areas lead to degradation in positioning accuracies, and the relatively high power consumption [60] of GPS receivers may not allow consumers to use GPS positioning for a long time on their smart devices.

All these challenges limit the usage of the standalone GPS technology while geo-referencing detected road anomalies. In addition, most of the commercial GPS receivers have a position update at 1 Hz, which lacks the appropriate location resolution required for localizing the road anomalies specifically at the high-speed vehicle operation.

2.2.5 Route Planning Metrics

Trip route planning services receive great interest, particularly in big and crowded cities [61, 62]. In general, trip planning applications and service providers afford route recommendations based on relatively shorter paths, less traffic congestion and also with up to date construction work [20]. Consequently, some of the leading players of route planning, like Google, have used live traffic network information to route the users dynamically. For example, Google maps provide online recommendations to re-route

vehicles when the initially selected routes are experiencing instantaneous traffic congestion. Many factors cause traffic congestion, such as untraditional mobility behaviour or accidents.

Crowdsensed based trip planning application Waze [21] relies on lively sensed traffic situations that are shared with the users' intervention. APOLO [63] system was introduced to mitigate the network overload that appeared in many of the traffic management systems as a result of information exchange between vehicles and servers. A comprehensive traffic monitoring system that operates on both online and offline bases was proposed. In the offline stage, real data processing is used to create mobility patterns. While in the online stage, the vehicles are re-routed away from the congested routes. The results showed a reduction in the travel time by 17 % along with a speed increase of 6% compared to contemporary approaches.

Also, in the literature systems provided suggestions to enable shorter and faster routing for land vehicles. In [64], an adaptive routing approach was created using a probabilistic dynamic problem technique to deal with route planning. In the proposed algorithms, the authors looked for minimizing the predicted in route trip time while deeming the broadcasted traffic information, onboard based traffic state measurement, and historical traffic patterns. Also, in [19] a personal behaviour based trip planning was presented to contribute a solution to traffic congestion problems. The authors assumed and discussed that driving preferences change from one driver to another and that these changes could be dealt with in a way to create drivers' profiles that are used in their route planning, contributing toward less traffic congestion. Moreover, in [20], authors have determined

three compelling factors of personal based route planning. These essential considerations are road safety in terms of the presence of snow or black ice, traffic speed and traffic congestion level. The contributions of these factors are evaluated based on the fuzzy inference engine, while the optimization problem enabled the overall optimum routing. In [65], a route planning system was proposed to involve future traffic hazards while routing the vehicle. This system consisted of three components, which are real-time data streamed from the vehicles, data collected by automatic traffic loops sensors and the component that used both data sources to predict future traffic conditions through the Spatio-temporal random field process.

To assure relaxing trips, in [66], a system was introduced to reduce the distances of the routes along with providing suggestions for routes with high-quality scenery. A memetic algorithm was used to enable skyline scenic trip planning while keeping low travel distances. To ensure drivers and travellers' safety, a system was proposed in [67] to provide route planning while avoiding routes that confront a high crime rate. A risk model based on crime data provided by Chicago and Philadelphia was introduced to the city public networks. Still, road quality information is the crucial aspect that enables drivers' safe and comfortable trips was not considered in most of route planning systems in the researched literature. In Table 1, a comprehensive summary is provided for the systems that were proposed to monitor the road conditions. The comparison spans several aspects and components of these systems.

2.3 Summary

In this chapter, a comprehensive background and literature review on the road conditions monitoring and information-based route planning was presented. The municipalities' road management systems were highlighted specifically in the road conditions monitoring, and assessment components and processes were explained. In addition, detailed descriptions of the various components of the current state of the art of the road conditions monitoring systems were provided. Also, this chapter included a discussion on the different perspectives of the route planning applications. The chapter was concluded by a detailed comparison of the system components of multiple existing road condition monitoring systems.

Table 2-1 Comprehensive study of road conditions monitoring systems

Reference	Sensors Used	Feature Extraction Techniques	Classification Techniques	Types of Road Conditions	Geo-Referencing	Feedback
Mohan et al. [27]	Vertical–axis accelerometer & smartphone	Statistical (thresholds)	Threshold classification	Bumps and potholes	GPS (1 Hz) (smartphone)	NA
Mednie et al. [25]	3-axis accelerometers & smartphones	Statistical (thresholds, peaks, standard deviations)	Thresholds classification	Large and small potholes, pothole clusters, gaps, drain pits	GPS (1 Hz) (smartphone)	NA
Eriksson et al. [30]	3-axis accelerometers & GPS	Statistical (peaks), frequency (high pass filter),	Machine learning (technique missing)	Smooth road, potholes, manholes, railroad crossing, joints	GPS (1 Hz)	NA
Jang et al. [31]	3-axis accelerometers & GPS	Statistical (RMS)	Neural Network	Impulse, rough, smooth classes	GPS	NA
Fox et al [34]	Simulated 3-axis accelerometers & GPS	Statistical (means, standard deviations, peaks, products)	SVM	Pothole regions and non pothole regions	GPS	NA

Reference	Sensors Used	Feature Extraction Techniques	Classification Techniques	Types of Road Conditions	Geo-Referencing	Feedback
Harikrishnaan & Gopi [37]	Smartphone vertical and longitudinal accelerometer	Statistical (peaks, absolutes, thresholds	Threshold classification	Potholes, humps	NA	NA
Xue et al. [38]	smartphone 3–axis accelerometers & GPS	Statistical (thresholds), frequency domain (moving averages, Fourier transform, wavelets)	K-mean clustering	Multi depth pothole	GPS (1 Hz) (smartphone)	NA
Seraj et al. [39]	Smartphone 3-axis accelerometers, gyroscopes & GPS	Statistical (thresholds, peaks), frequency domain (moving averages, Fourier transform, wavelets)	SVM	Severe, Mild and Span	GPS (1 Hz) (smartphone)	NA
Allouch et al. [40]	Smartphone 3-axis accelerometers, gyroscopes	Statistical (peaks), frequency l(low pass filter, FFT)	Decision Trees	Smooth road, potholes	GPS (1 Hz)	Driver

Reference	Sensors Used	Feature Extraction Techniques	Classification Techniques	Types of Road Conditions	Geo-Referencing	Feedback
Perttunen et al. [48]	Smartphone 3-axis accelerometers & GPS	Statistical (Multiple), FFT	SVM	Type 1, Type 2	GPS (1 Hz)	Driver
Brisimi et al [56]	Simulated 3-axis accelerometers & GPS	Statistical (average, range, standard deviation, covariance), frequency domain (FFT)	Machine Learning (multiple Techniques)	Actionable, non actionable	GPS	Manucipali -ties
Pont et al. [58]	3-axis accelerometers & GPS	Statistical (average, range)	Thresholds clustering	Road quality indicator	GPS (1-5 Hz)	Driver

Chapter 3

System Architecture, and Road surface Conditions Detection and Categorization

Existing RIS systems lack several factors such as practicality, efficiency, frequent updates and feedback to the drivers. In this chapter, a system architecture is provided. This system's ultimate goal is to detect, categorize, geo-locate and report the road surface conditions and their level of severity. Also, this system provides route evaluations and recommendations based on average route surface quality while considering the route time and length. This chapter included the experiments set up, data collection procedures, sensor de-noising, feature extraction and anomalies classification.

3.1 System Architecture

In this section, an overview of the system architecture and information flow, as shown in Figure 3.1, is presented. The system leveraged a wide variety of IMUs, global navigation satellite systems (GNSS) receivers, integrated navigation systems, smartphones, tablets and cameras. These sensors are mounted in several land vehicles in an open setup or gathered on testbeds to collect data that is crucial in monitoring the road surface conditions. The collected data are then passed to a sensor de-noising component to enhance the inertial measurement quality and to separate the frequencies describes the anomalies signatures from the ones that describe the regular vehicle movement.

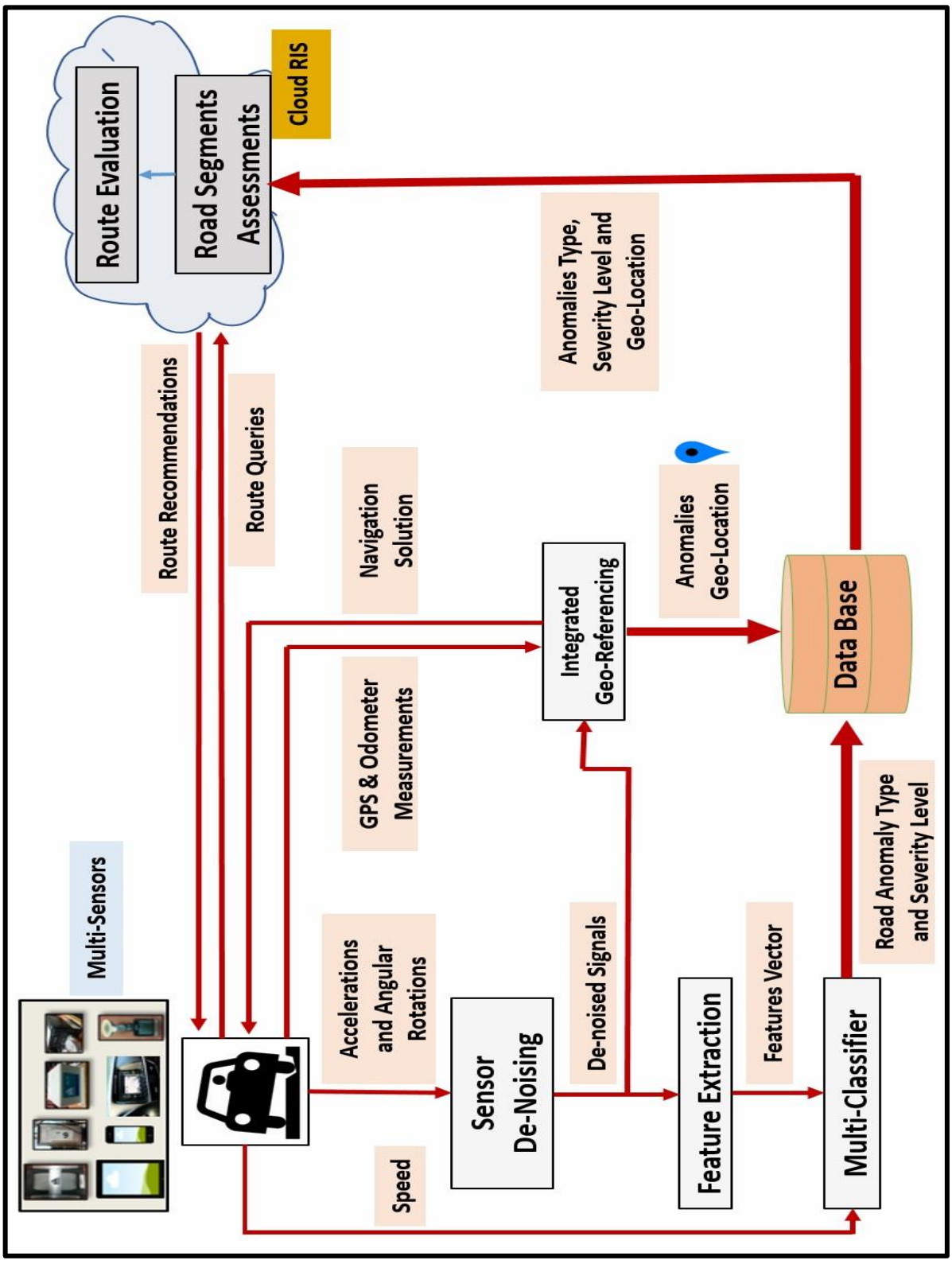

Figure 3-1 System architecture

Afterwards, the cleaned data are processed using the feature extraction component that captures distinct features to distinguish the different road anomalies. Consequently, the extracted features are used to construct data sets that are used in building a multi-level classifier that categorize the road anomalies and their level of severity.

The detected and categorized road anomalies are then geo-located with the aid of the integrated geo-referencing component. The de-noised inertial sensor measurements are integrated with GNSS measurements to provide accurate and continuous localization of the monitored anomalies. The location information is provided at different data rates up to 10 Hz according to the vehicle speed. Nevertheless, the road anomalies and their geo-location are used to create datasets that are transferred to the clouds using any available communication technology. In the cloud, the corwdsensed data sets that are collected from different vehicles are used in the assessment of the road conditions and evaluating the average route quality of the potential routes that are provided to the drivers by both in-vehicle and smart devices navigation applications. In the following sections and chapters, the detailed system components and information flow will be discussed and evaluated.

3.2 Analysis of Road Surface Conditions Types and Effects

As previously discussed, the effects of road surface anomalies and the government's attention in monitoring and repairing affected roads both highlight the importance of addressing irregularities and their effect on multiple common driving styles.

Figure 3-2 Multiple types of road anomalies

Several driving surveys were held in different locations to identify and label the most common road anomalies and define their effects as per the example shown in Figure 3.2. The several driving surveys enabled the identification and categorization of road surface types and anomalies over several road test trajectories. The road distress appears in different forms such as transverse cracks, longitudinal cracks, crocodile cracks, and road

dents. Also, this distress might cause the removal of pavement, introducing various levels of potholes. In addition, road-related infrastructure services such as manholes, speedbumps, drain pits, road and bridge joints, deceleration strips, and railroad crossings may also damage vehicles when they are improperly maintained.

Regarding the effects of the anomalies mentioned above, they affect vehicle motion from different perspectives. According to their nature, a vehicle can either attend the event with single-sided or double-sided wheels. Under certain conditions, the vehicle could attend the event with only one wheel due to swerving. Potholes, manholes and drain pits are examples of single-sided anomalies while transverse cracks, bridge expansion joints, and railroad tracks are examples of double-sided road irregularities. Figure 3.3 shows the effects of the event on the vehicle motion.

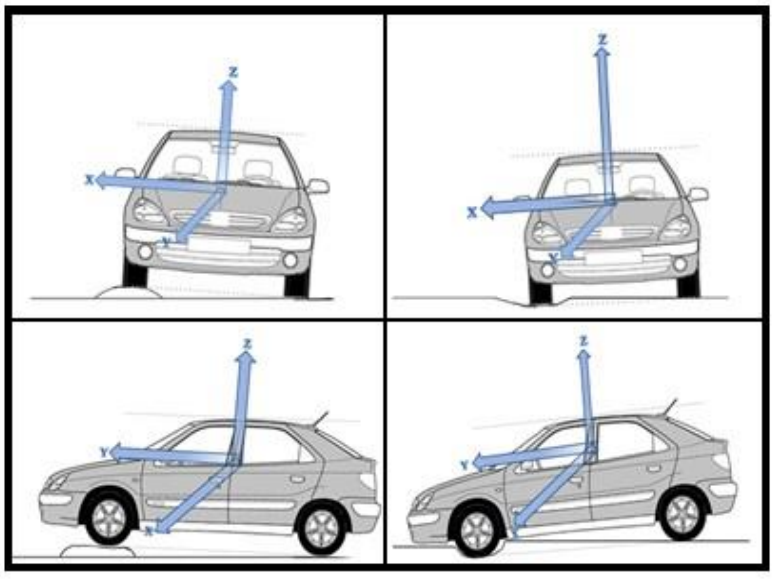

Figure 3-3 Vehicle motion under single and double-sided anomalies

The vehicle motion disturbance varies according to the nature of the anomaly and its severity level. The anomalies can induce vehicle tilt downwards, upwards or either right or left sides. Therefore, there is a growing demand for crowd-based information services to monitor road health conditions and road hazards. The conducted initial surveys enabled the identification of road types and anomalies. These defined anomalies have different effects on the linear accelerations of the accelerometers utilized in these surveys. Figures 3.4 to 3.14 show the collected acceleration measurement at 100 Hz of data rate during driving on various road anomalies. In Figure 3.4, the raw linear acceleration measurements in the direction of (x, y, and z) while the vehicle was stationary for a time window of five seconds. f_x is the transversal acceleration, f_y is the forward acceleration, and f_z is the vertical acceleration.

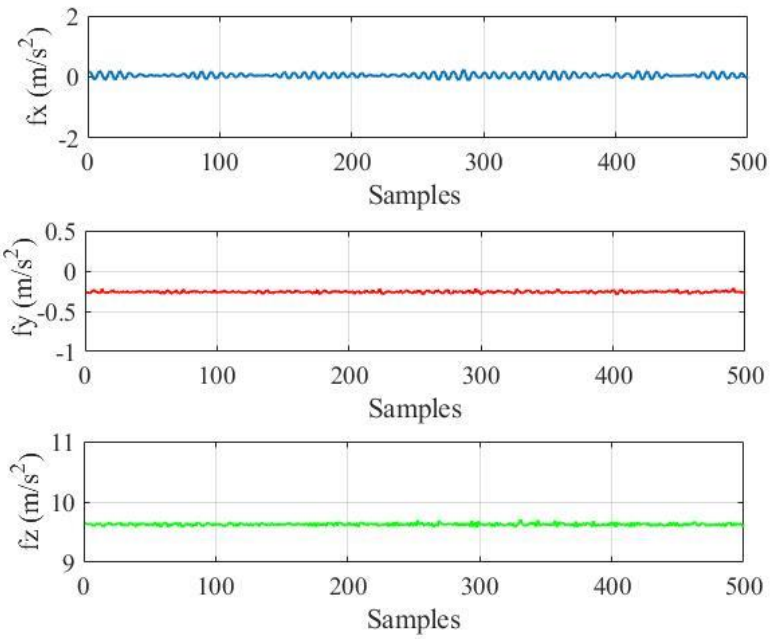

Figure 3-4 Vehicle linear measurements acceleration during (Stationary) road driving

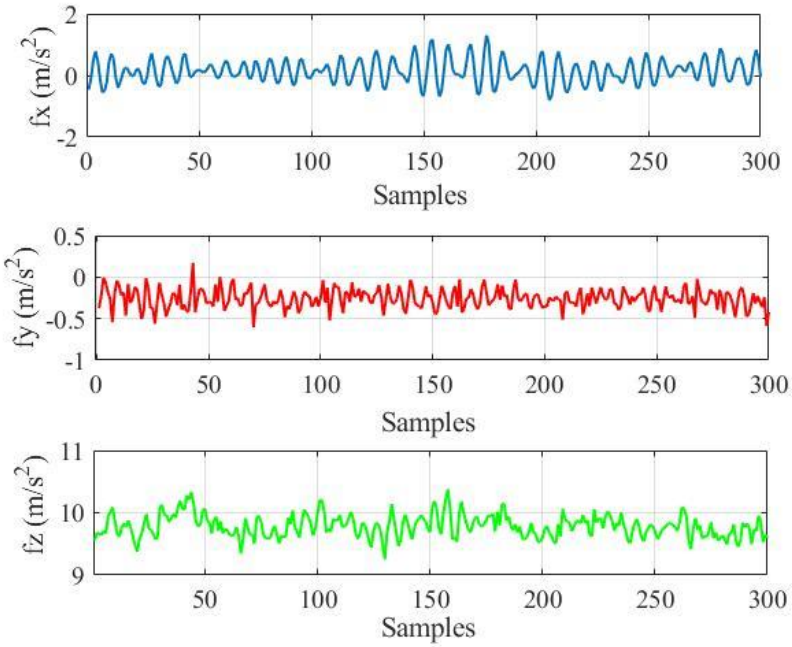

Figure 3-5 Vehicle linear acceleration measurements during (Smooth) road driving

During the stationary periods, the linear acceleration measurements are approximately constant. The linear acceleration measurements of the vehicle during driving on a smooth road is illustrated in Figure 3.5. In the smooth road driving, the linear acceleration measurements started to show some change in the readings. However, the absence of large disturbances proved the road smoothness.

Figures 3.6 to 3.8 shows the performance of the linear acceleration measurement during driving over single-sided road anomalies. Figure 3.6 showed the linear acceleration measurement in a time window of one second when the land vehicle was driven over a pothole. The linear acceleration measurements experienced a significant disturbance approximately between the sample thirty-five to the sample sixty-five.

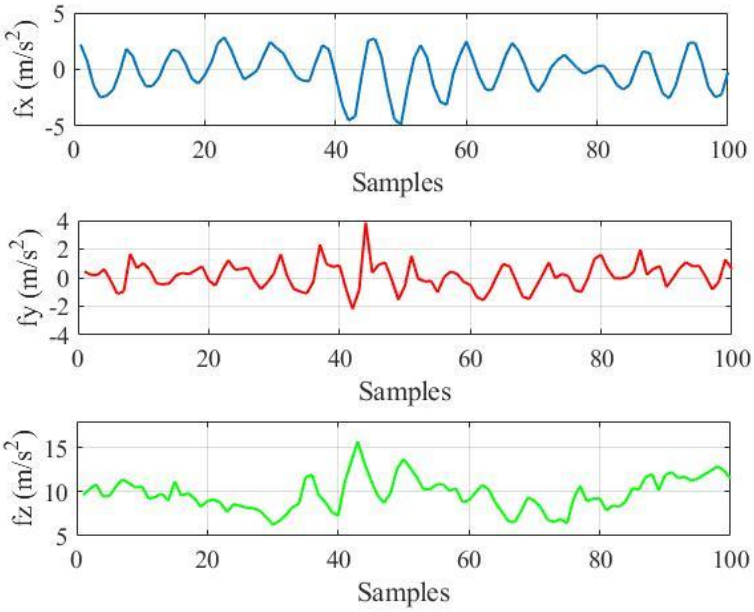

Figure 3-6 Vehicle linear acceleration measurements during driving over a (pothole)

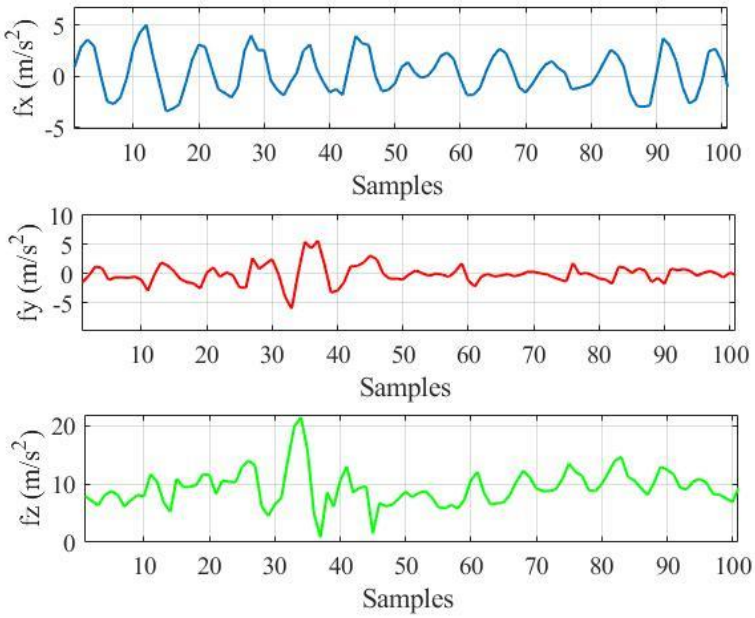

Figure 3-7 Vehicle linear acceleration measurements during driving over a (manhole)

The linear acceleration measurements during driving over a manhole are presented in Figure 3.7. The measurements show a significant change approximately between the sample twenty-five and sample 45. Since potholes and manholes are single-sided anomalies, they induce a similar effect on the acceleration measurements, as depicted from Figures 3.6 and 3.7. The driving over longitudinal carracks is shown in figure 3.8. The acceleration measurements were disturbed during a time window of three seconds and did not show significant change within particular samples.

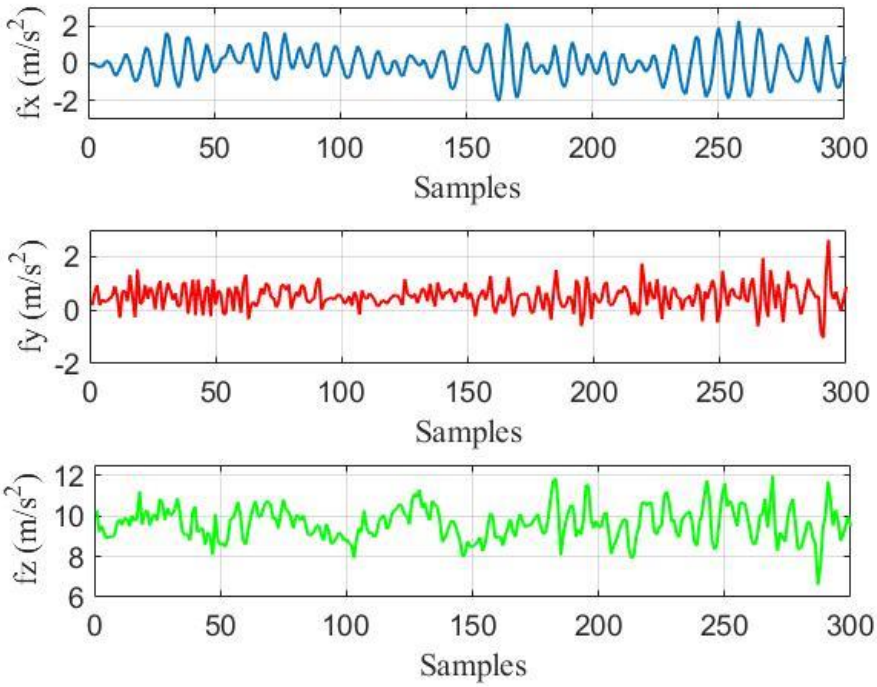

Figure 3-8 Vehicle linear acceleration measurements during driving over (longitudinal cracks)

Figures 3.9-3.12 present the effects of the double-sided anomalies on the linear acceleration measurements. The transverse cracks' effects are provided in figure 3.9. The linear acceleration measurements collected in a time window of two seconds are mainly disturbed between the sample eighty to the sample hundred and ten. Bridge expansion joints transverse the vehicle movements and is also considered a double-sided anomaly. Figure 3.10 demonstrates the acceleration row measurements during a time window of two seconds. The effects of the bridge expansion joints are similar to the transverse cracks. In addition, railroad tracks transverse the vehicle movement and change the vehicle's linear acceleration. Figure 3.11 illustrates the acceleration measurements during a three seconds time window where the significant effects appear between samples hundred and two hundred.

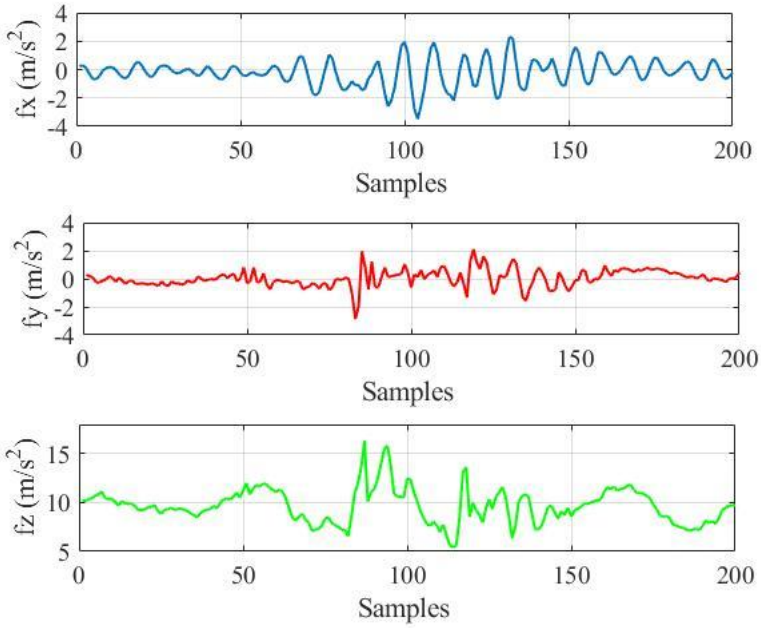

Figure 3-9 Vehicle linear acceleration measurements during driving over (transverse cracks)

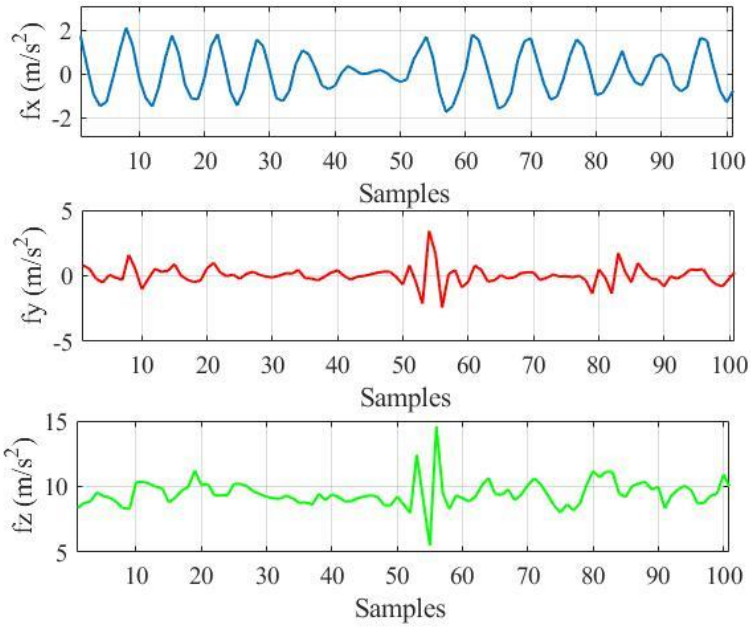

Figure 3-10 Vehicle linear acceleration measurements during driving over (bridge expansion joint)

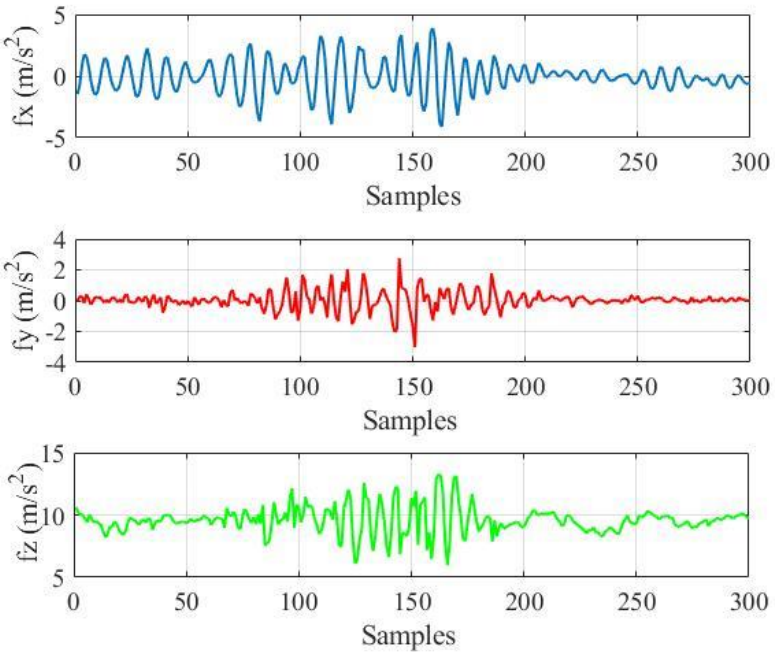

Figure 3-11 Vehicle linear acceleration measurements during (railroad crossing) drive

The speedbump is another type of transverse road. However, the vehicle attending a speedbump tilt upwards first and that is contradicting the other examples of the transverse cracks and the bridge expansion joints where the vehicle tends to tilt downwards when the approach these anomalies. Figure 3.12 demonstrates the change of the acceleration measurement during a speedbump event. Figure 3.13 shows a different type of road (paved stone road) where the vehicle shakes significantly, and the linear acceleration measurement is disturbed over the time window. Figure 3.14 identifies driving over a steel causeway, which is similar to the driving over a paved stone road. However, the disturbances in acceleration measurements in the case of the paved stone road is more significant than the ones induced by the steel causeway drive.

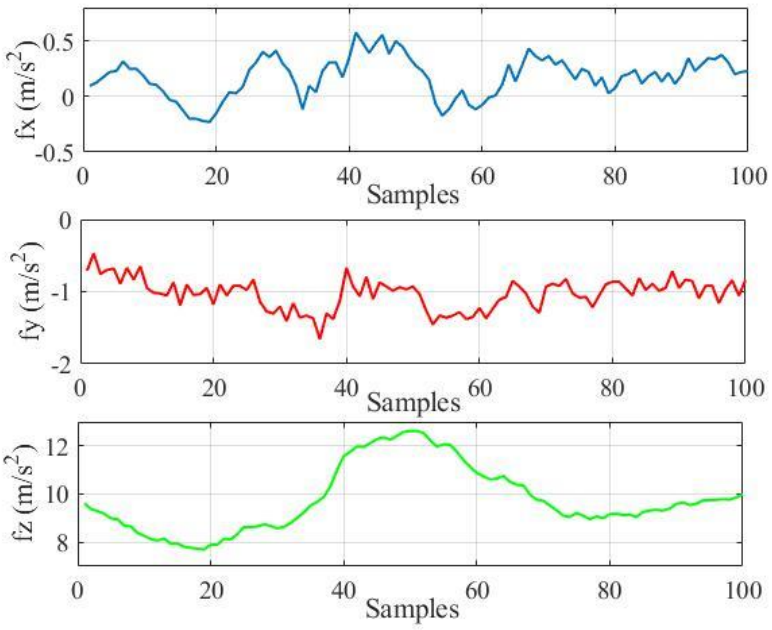

Figure 3-12 Vehicle linear acceleration measurements during driving over a (speedbump)

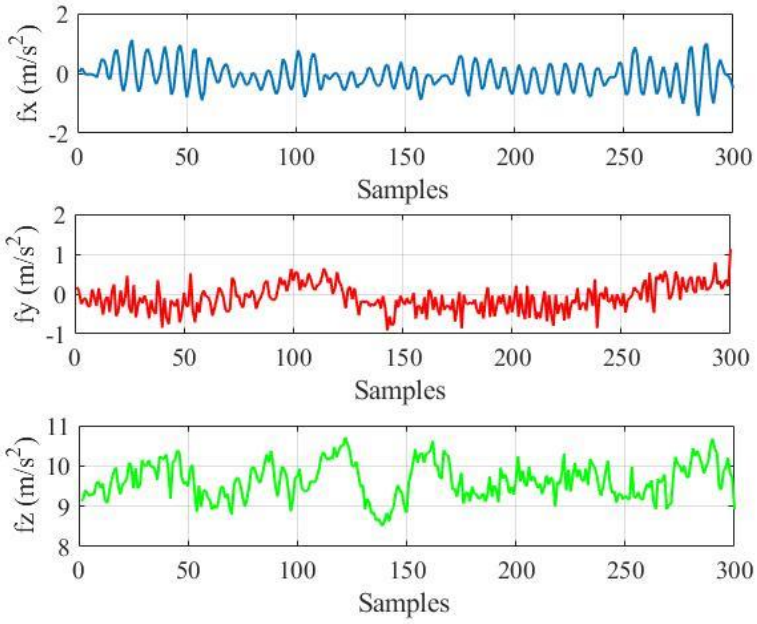

Figure 3-13 Vehicle linear acceleration measurements during driving over (paved stone road)

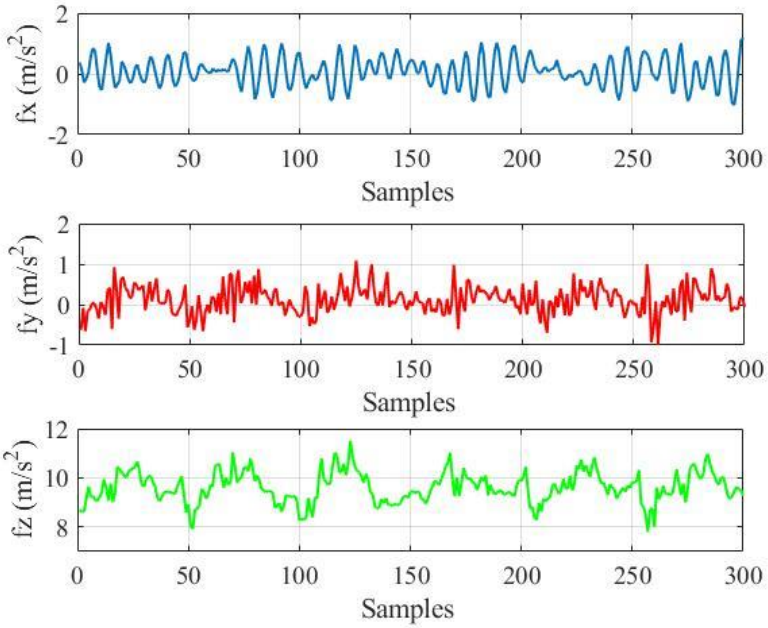

Figure 3-14 Vehicle linear acceleration measurements during driving over (steel causeway)

The conducted road surveys enabled insights on the common types of road anomalies and indicated the importance of providing frequent road monitoring due to the anomalies' significant effects on the vehicle movement and implicitly driver comfort. To provide an efficient road monitoring system, rich data collection of different road anomalies is required

3.3 Rich Data Collection and Database Building

In this section, a rich data collection framework is presented. Data collection methods process both the vehicle and smart devices sensors to recognize the road-related anomalies, such as the existence of potholes, manholes, and other road surface objects. Sensor measurements from both the vehicle and the driver's smartphone are first synchronized and time-tagged to the GPS time.

Multiple trajectories of varying lengths were developed and used in anomaly identification, and system training and testing purposes. For the trajectories, multiple IMUs, GPS receivers, and integrated positioning units were utilized. Three smart devices, two smartphones (Nexus 5, Samsung Galaxy S4) and one tablet (Samsung GT-N8010) were used. These devices are embedded with six degrees of freedom IMUs and GPS receivers. In addition, a low-cost MEMS grade six degrees of freedom IMU (Crossbow), and two integrated positioning units (VTI and Novatel) were leveraged. The VTI includes a MEMS grade IMU and an OEM GNSS receiver. The Novatel Span integrated solution includes a tactical grade span-CPT IMU with MEMS accelerometers, fibre-optic gyros, and the OEM GNSS receiver. A MiVue 388 Dash Cam was also for recording the trajectories. The utilized sensors are listed in Table 3.1. The utilized inertial sensors and

IMUs have different grades, data rates and specifications. They are categorized as commercial-grade (smart devices inertial sensors, and IMU Xbow) and tactical grade IMU-CPT. These sensors are gathered on a testbed or in an open setup and then mounted on multiple vehicles as shown in Figure 3.15

Table 3-1 Sensors and Systems Utilized in Road types and Anomalies Data Collection

Utilized Sensors & Systems
Nexus 5, Samsung Galaxy S4 (Smartphones) Samsung GT-N8010 (Tablet)
NovAtel Span integrated navigation system KVH CPT Inertial Measurement Unit (IMU) OEM4 (GNSS receiver)
VTI integrated navigation system MEMS grade IMU U-blox LEA-60 (GNSS receiver)
Crossbow IMU CC-300
CarChip Pro OBDII
MiVue 388 (Dash Cam)

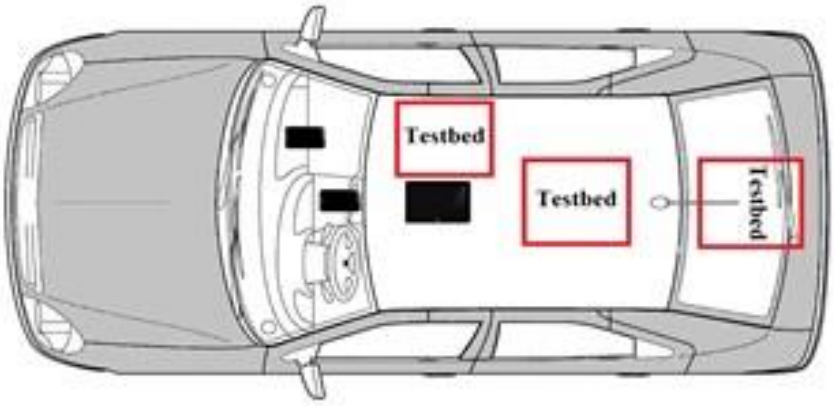

Figure 3-15 Testbed and smart devices locations in the vehicle

Eight land vehicles: two vans, two sedans, two crossovers, one mini-van, and one hatchback were utilized in the trajectories. They were intentionally chosen to span multiple sizes, vendors, wheel sizes, quality of suspensions, model, and make, which provides a broad range of real-driving scenarios. The testbeds and open setup are positioned and oriented differently in the vehicles, as shown in Figures 3.15 and 3.16. The positions of the testbed range from the front passenger seat, middle backseats (minivan and van), and trunk (crossover and hatchback). In an open setup, smartphones and tablets are secured on the armrest, windshield, dashboard, front passenger seats, and cup holder. Multiple trajectories were held using the mentioned forms of the experimental setup, as shown in Figure 3.17. These trajectories spanned different road types and anomalies in the downtown core, residential neighbourhoods, and urban streets.

The experimental setup handled different events using various vehicles, sensor grades, driving behaviours, and speeds. This leads to a rich collection of different data sets that describe every single event by driving over them with different driving styles and speeds. In order to obtain highly descriptive data, all sensors were logged at their maximum and relevant data rates. For smart devices, the accelerometers measurements were logged at approximately 100 Hz, the gyroscopes measurements were logged at approximately 200 Hz, and the GPS measurements at 1 Hz. In regards to the external IMUs, Crossbow (Xbow), and IMU CPT, they were logged at 100 Hz for both accelerometers and gyroscopes while the VTI full IMU was logged at 20 Hz. Additionally, the VTI and Novatel OEM GPS receivers were logged at 1 Hz. Similarly, the integrated positioning solutions provided by both units (VTI and Novatel Span integrated solution) were obtained at 1 Hz.

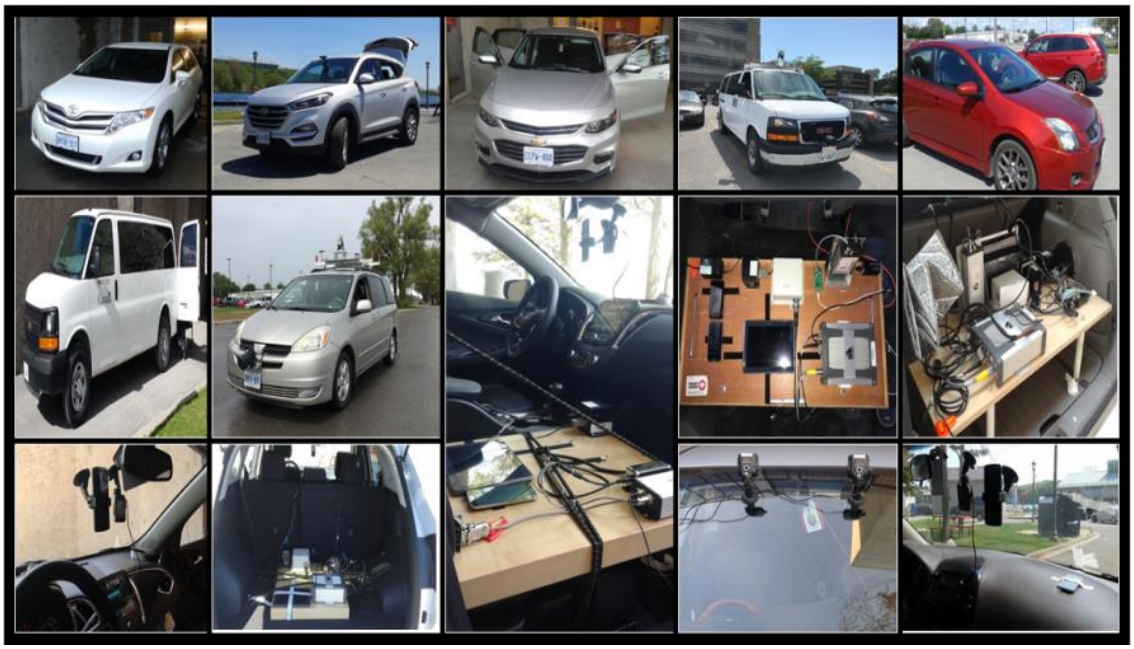

Figure 3-16 Multiple vehicles, testbed, and sensors utilized in the data collection of the road surface conditions

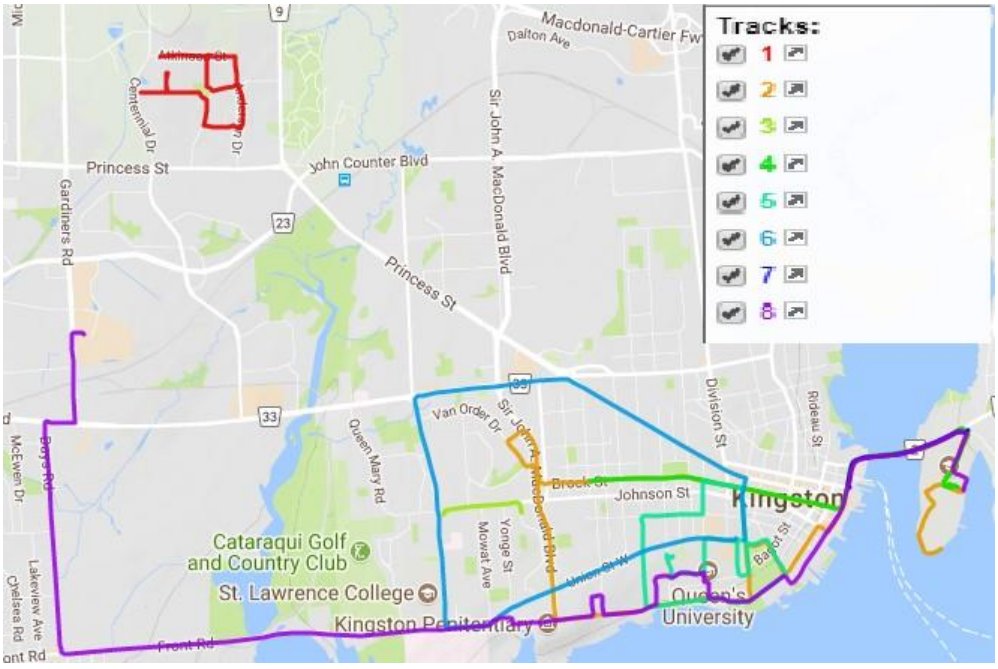

Figure 3-17 Multiple trajectories used for system building, testing, and training

During the trajectories, the attended anomalies were: potholes, manholes, transverse cracks, longitudinal cracks, railroad tracks, speedbumps, deceleration strips, paved roads, and road dents. For every single trajectory, several datasets of road anomalies were built utilizing the measurements of the several sensors that were involved in every trajectory. The road anomalies were labelled in these datasets, while using the recorded videos for guidance. Later the data sets from each trajectory were combined; these datasets were used independently or combined with other data sets from different trajectories. The data sets of varying sizes were arranged for building, training, and testing of classifiers.

For each trajectory, each land vehicle was equipped with various sensors that collected the linear accelerations, angular rotations and GPS measurements. The linear acceleration and the angular rotation measurements are GPS time-stamped. The recorded videos are also GPS time-stamped. In case the linear acceleration or angular rotation measurements have exceeded a predetermined threshold, the recorded video of this trajectory is checked frame by frame to manually and visually identify the road anomaly. As an example, Table 3.2 shows the road anomaly data set for a particular trajectory. Table 3.2 shows an example of the data set created for each trajectory. The example trajectory was held in Kingston, ON, on July 25$^{\text{th}}$ and was held in the downtown area. The data set also included the car model, the sensors used and placement location within the vehicle. For every detected road anomaly in the trajectory, the readings of the linear accelerations and angular rotations are saved and labelled with the type of the anomaly. The sufficient data rate of the inertial sensors was examined in order to guarantee valuable information about the road anomalies that enable better detection and classification.

Table 3-2 Example of a trajectory-based road anomaly data set

Trajectory Name	Car Model	Trajectory Date
Downtown Kingston	 Toyota Venza, 2017	July 25th, 2017

Anomaly Type	Anomaly Location (Lat/Long)	Used Sensor	Sensor Placement	Linear Acceleration	Angular Rotation	GPS Time (Seconds)
"Severe Pothole"	44.223019, -76.493851	 Nexus 5	Windshield	Recorded Measurements	Recorded Measurements	1185023445
"Severe Pothole"	44.223019, -76.493851	 IMU Xbow	Testbed (Driver Chair)	Recorded Measurements	Recorded Measurements	1185023445
"Mild Manhole"	44.222416, -76.501028	 Nexus 5	Windshield	Recorded Measurements	Recorded Measurements	1500989479
"Mild Manhole"	44.222416, -76.501028	 IMU Xbow	Testbed (Driver Chair)	Recorded Measurements	Recorded Measurements	1500989479

As an example, the data were collected using the Samsung Tablet and VTI unit at data rates of 100 Hz and 20 Hz, respectively. The orientation of the sensors of both units was aligned to have the vertical linear acceleration in the +Z direction, the longitudinal and transverse linear accelerations are in the +Y and +X directions, respectively. The Tablet and VTI data were compared at multiple anomalies and road conditions.

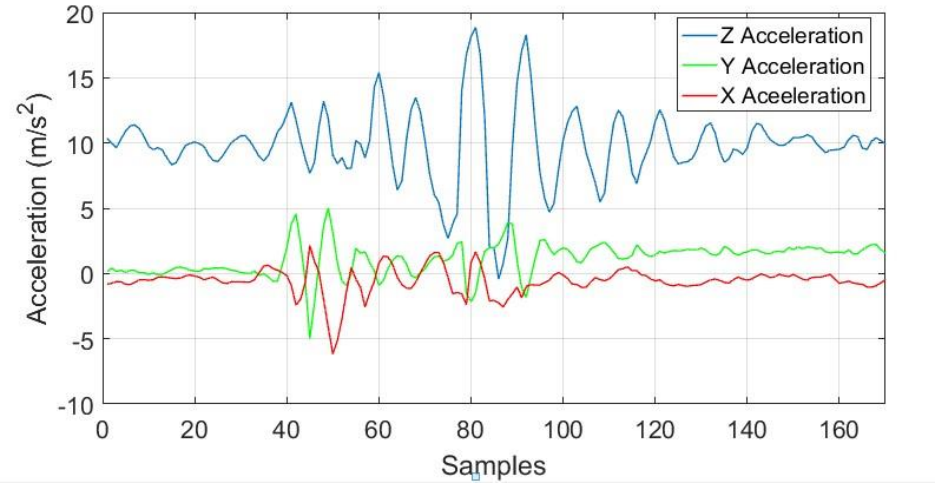

Figure 3-18 Three-axis linear acceleration of the (Tablet) data during a (pothole) driving.

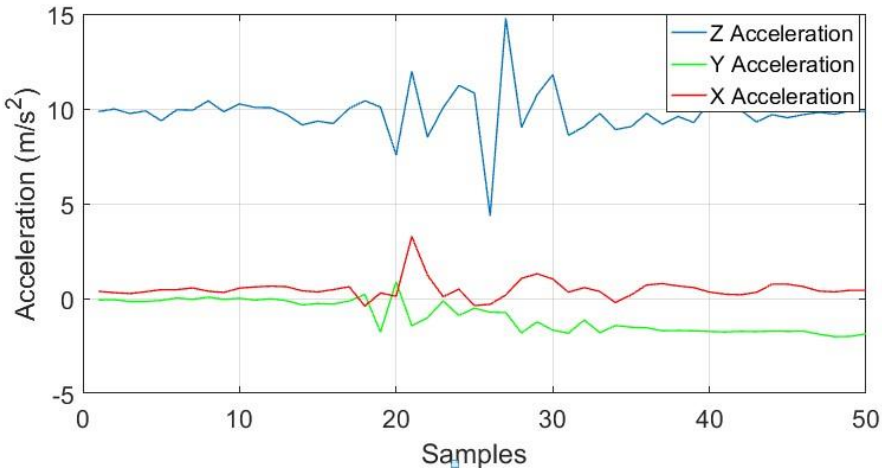

Figure 3-19 Three-axis linear acceleration of the (VTI) data during a (pothole) driving.

The comparison showed that the VTI data logged at 20 Hz, lack rich features that can be efficiently used to identify and classify each event. Figures 3.18 and 3.19 show the three-axis linear acceleration for the Tablet and VTI unit during a severe pothole event. As

depicted from the figures, the data collected at 100 Hz contains more features and better descried the road anomaly than the ones collected at 20 Hz. In order to provide a full signature of the road anomalies on the collected linear accelerations and angular rotations measurements, the data rates were set to 100 Hz in all the inertial sensors, and IMUs utilized in the whole trajectories.

3.4 Data Preprocessing and Sensor De-noising

The acceleration and angular rotation data should have unique features that can distinguish each road anomaly from the other anomalies. Most of the inertial sensors in both vehicles and smart devices are vulnerable to noises, biases and errors, as described in Section 2.2.1. These factors affect the sensor measurement and lead to a change in its real value, which induce faulty and noisy measurements [68]. Erroneous signals can provide misleading features or encounter a feature extraction process. Figure 3.20 shows the difference between noisy and clean vertical acceleration measurements while driving over railroad tracks. The clean signal is definitely enabling more insights on the road anomaly signature on the acceleration data. Principally, the sensed and collected data reflects vehicle motion regular dynamics, road anomalies effects and noise. For IMU's, specifically, there are multifarious sources of noise. Basically, IMU's noise can be branched to long-term errors (ones with low-frequency components) and short-term errors (ones with high-frequency components). Long-term errors could be presented as a result of different causes. For instance, the noise from external or internal heat distribution variations or temperature is represented by exponentially correlated noise.

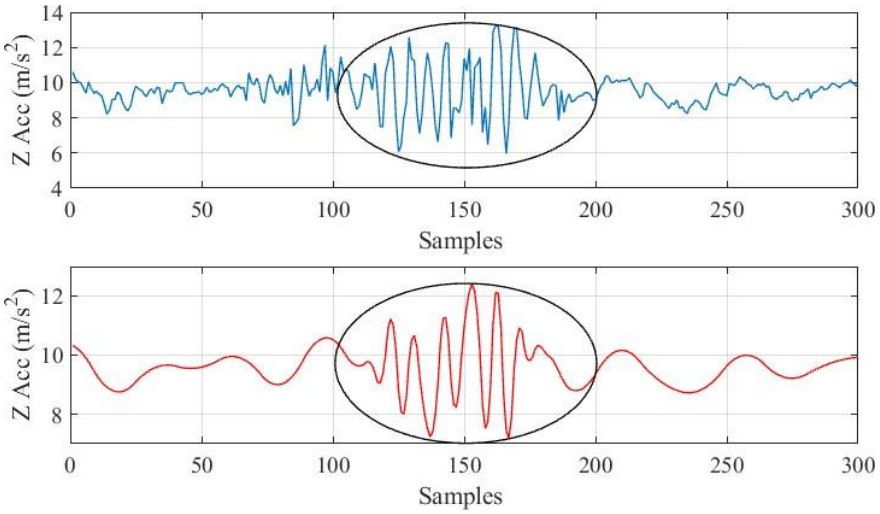

Figure 3-20 Vertical acceleration measurements while driving over railroad tracks, noisy measurements are in (blue), clean ones in (red)

Long term noise appears in low frequencies and is identified as time-varying additive noise. In addition, random walk, another form of the low noise frequency component, could appear as a result of shot or thermal noise in a photodetector of optical gyros [26, 27, and 68]. On the other hand, for short-term errors, they could be presented as a result of different causes. For instance, white sensor noise is distributed in all the frequencies of a sensor according to its bandwidth, this type of noise is a result of electronic instruments such as power supplies, quantization errors during digitization or even through the semiconductor devices intrinsic noise [69, 70]. Clearly, suppressing the noise effects on the sensed data is a challenging process as the long-term errors are mixed with vehicle dynamics low frequencies [71, 72]. Also, removing the effects of the high-frequency noise could eliminate the road anomalies' effects leading to high detection errors.

In order to achieve robust signal de-nosing, the best-case scenario is that full prior information about the signal is available. In such a case, signal and noise joint probabilities are known, and the average estimation error could be minimized [47]. As mentioned in earlier, FT has the main drawback of that once a frequency domain transformation is conducted, any related time domain information is not present. While WDFT was has a drawback of the fixed window width that always raises the time-frequency trade-off. The narrow window, width leads to appropriate time localization but lacks the sufficient frequency resolution. Also, WDFT suffers from the spectral leakage phenomena described in Section 2.2.2.

In wavelet analysis, the process grants the usage of relatively long time windows where low-frequency components are required. Meanwhile, where high-frequency content is needed, shorter intervals are adopted. Consequently, in the WMRA process, as described in section 2.2.2 and appears in Figure 2.3 the signal approximation contains the signal low frequencies. The regular WMRA does not consider the signal details that usually include the effects of the road anomalies mixed with high-frequency noises as well. To bypass the challenges of wavelet de-noising, a wavelet packet de-noising is adopted in our analysis. Wavelet packets, as shown in Figure 3.21, apply an initial decomposition step that separates the signal into approximation, A, and details, D. Furthermore, both of A and D are decomposed for several levels in order to break the signal into fine resolution components [47, 73]. Regarding the de-noising approach, an orthogonal wavelet packet de-noising analysis was utilized.

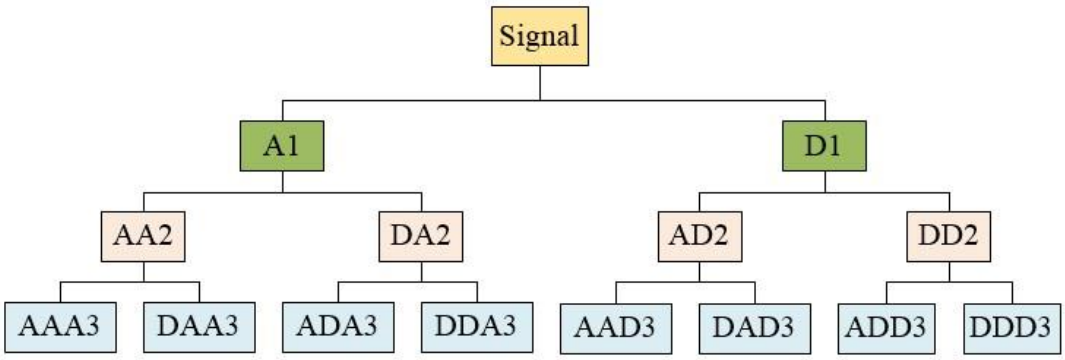

Figure 3-21 Wavelet Packet Analysis

The analysis utilizes wavelet packet bases that can break down the frequency axis into apportioned slots with multiple sizes, and these slots are translated in time to cover the entire time-frequency plane. As any space, V_j, could be split to sub-spaces of approximation, V_{j-1}, and details, W_{j-1}, where:

$$V_j = V_{j-1} + W_{j-1} \tag{3.1}$$

In the case of orthogonal bases, this is done by breaking the orthogonal basis of V_j to orthogonal bases of approximation and details to $\{\phi_{j-1}(t-2^{j-1}n)\}_{n\,\epsilon\mathbb{Z}}$ and $\{\Psi_{j-1}(t-2^{j-1}n)\}_{n\,\epsilon\mathbb{Z}}$, respectively, this split is specified by a pair of conjugate mirror filters $h[n]$ and $g[n] = (-1)^{1-n}\, h[n-1]$. For thresholds, a soft threshold of *Stein unbiased risk estimator* (SURE) that introduced in [75] was used. As mentioned in [47], reducing the thresholding risk could occur by choosing a threshold less than $\sigma\sqrt{2log_e N}$, where σ is the standard deviation and N is the signal length. For the SURE thresholding, T:

$$T = \sqrt{2\, log_e(Nlog_2(N)} \tag{3.2}$$

In order to assess the performance of the discussed wavelet packet de-noising, it was applied to the system inputs that appear in Table 3.3. These inputs are the linear accelerations and the angular rotations gathered by various adopted IMUs. In this work, the wavelet packet of Daubechies family six is used. The input signals were decomposed to the sixth levels of approximations and details. Figures 3.22 and 3.23 show the linear accelerations and angular rotations for the Crossbow IMU, wavelet packet de-noised Crossbow IMU and IMU-CPT during a road anomaly. It was intentionally chosen to show the results of the packet de-noising of the Crossbow IMU, as it has the lowest performance among all the IMUs in our experiments

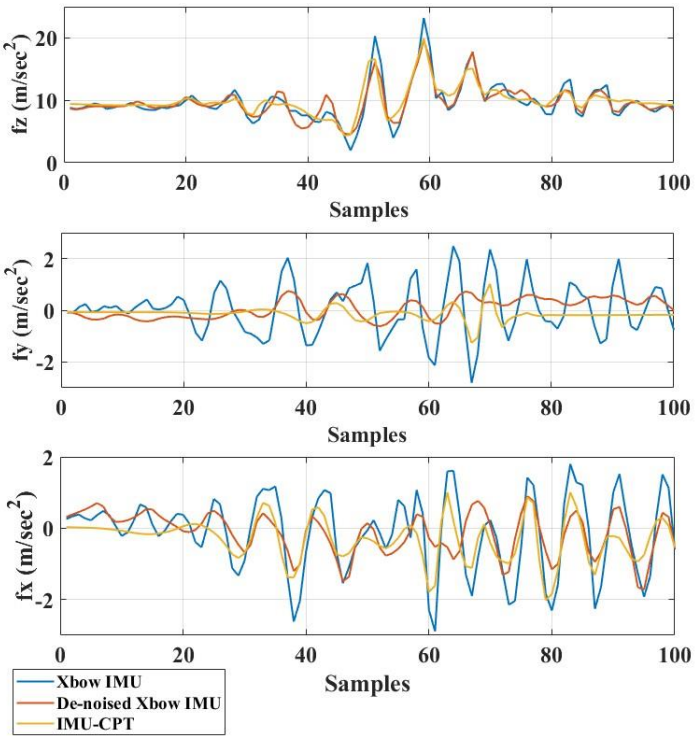

Figure 3-22 Linear accelerations for Xbow IMU, wavelet packet de-noised Xbow IMU, and IMU-CPT during road anomaly

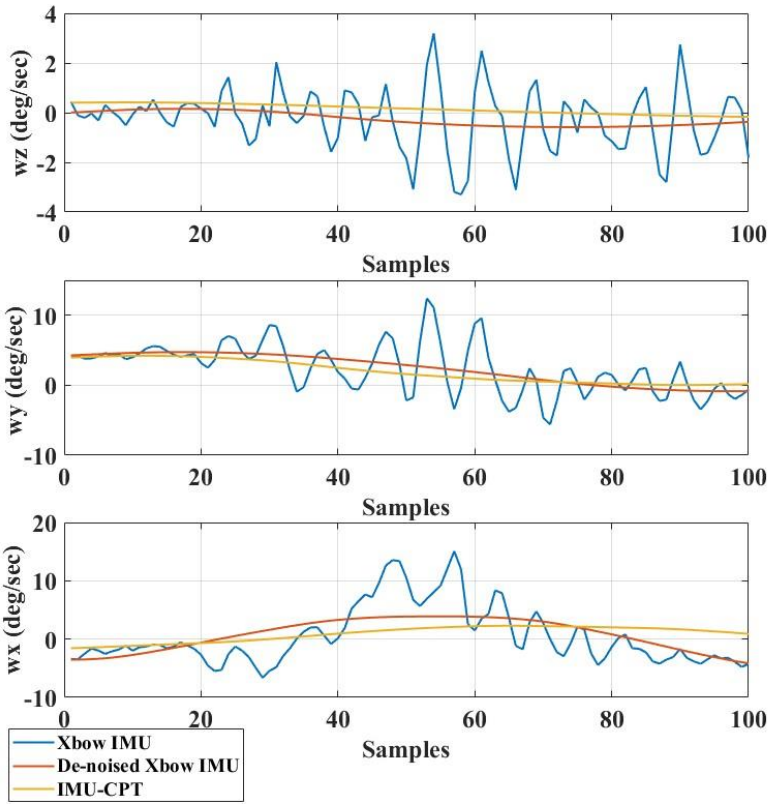

Figure 3-23 Angular rotations for Xbow IMU, wavelet packet de-noised Xbow IMU and IMU-CPT during road anomaly

Table 3-3 Standard Deviations for XBOW IMU, Wavelet Packet De-Noised XBOW IMU, and IMU-CPT

Inertial Sensor Measurement	STD of XBOW	STD of WP De-noised XBOW	STD of IMU-CPT
f_z	3.108	2.528	2.290
f_y	1.006	0.376	0.248
f_x	1.079	0.608	0.596
ω_z	1.239	0.281	0.200
ω_y	3.551	2.110	1.607
ω_z	4.999	2.730	1.274

.In addition, the IMU-CPT was used as a reference IMU due to its higher performance among the others. The standard deviation results displayed in Table 3.3 show that wavelet packet de-noising of the Crossbow IMU has been enhanced on average by approximately 48%.

Furthermore, all the sensed linear accelerations and angular rotations gathered by the whole utilized IMUs are de-noised using the same technique before being applied to the feature extraction process, as shown in the system architecture in Figure 3.1. In addition to the Crossbow IMU results, and in order to examine the impact of the wavelet packet de-noising on the inertial sensors embedded in the smart devices, the results related to the Samsung Tablet was provided in Figures 3.24 and 3.25. They plot the linear accelerations and angular rotations for the accelerometers and gyroscopes sensors of the tablet device, wavelet packet de-noised tablet sensors and IMU-CPT during the same road anomaly shown in Figures 3.22 and 3.23. Consequently, as displayed in Figures 3.24 and 3.25, wavelet packet de-noising enhanced the quality of the tablet accelerometers and gyroscopes.

Table 3.4 shows the standard deviations of the linear accelerations and the angular rotations of the tablet sensors before and after wavelet packet de-noising compared to IMU-CPT as a reference. The wavelet packet de-noising enhanced the tablet sensor measurements by approximately 40 % on average. The enhancement in the collected linear and angular rotation measurement will facilitate the feature extraction process and enable better anomalies detection and categorization rate.

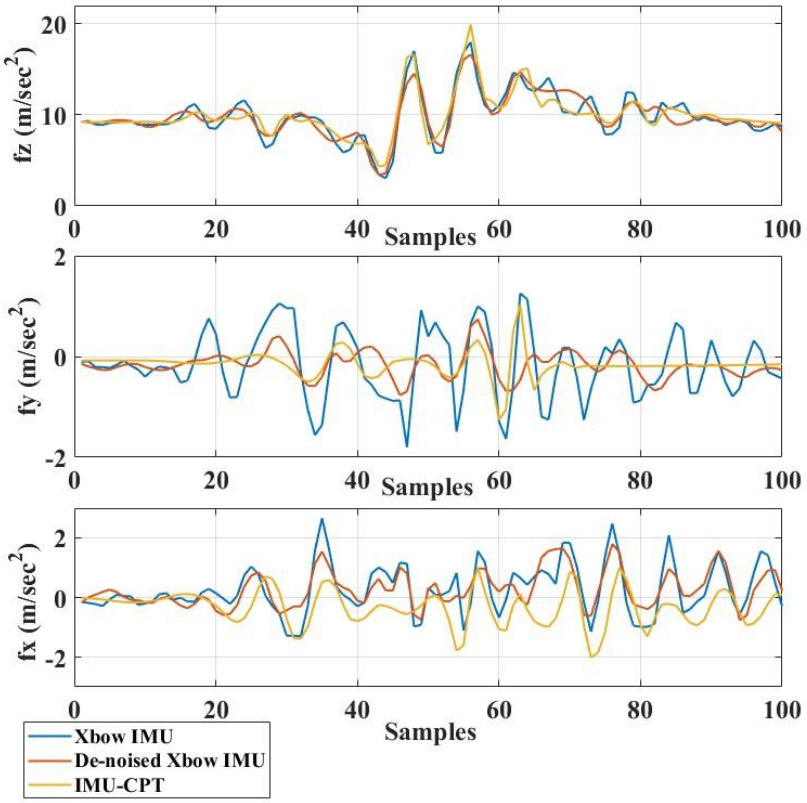

Figure 3-24 Linear accelerations for Samsung Tablet accelerometers, wavelet packet de-noised Samsung Tablet accelerometers, and IMU-CPT during road anomaly

Table 3-4 Standard Deviations for XBOW IMU, Wavelet Packet De-Noised Samsung Tablet, and IMU-CPT

Inertial Sensor Measurement	STD of XBOW	STD of WP De-noised Tablet	STD of IMU-CPT
f_z	2.568	2.300	2.290
f_y	0.667	0.262	0.248
f_x	0.836	0.614	0.596
ω_z	1.575	0.212	0.200
ω_y	3.822	2.308	1.607
ω_z	4.764	2.848	1.274

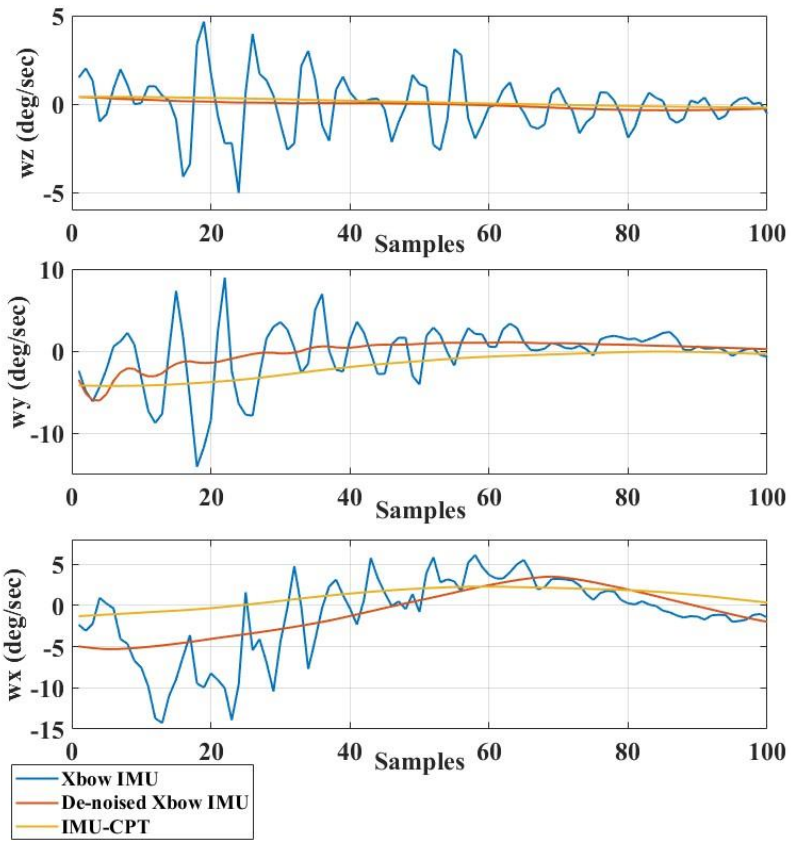

Figure 3-25 Angular rotations for Samsung Tablet Gyroscopes, Wavelet Packet De-noised Samsung Tablet gyroscopes, and IMU-CPT during road anomaly.

3.5 Feature Extraction and Comprehensive Dataset Creation

Highlighting and analyzing the effects of road surface anomalies on the vehicle motion as shown in Figure 3.3, it was noticed that the disturbance of the motion occurs at the sensed transversal and angular rotation of the IMUs. However, considering the data of the angular rotation along the Z-direction could be misleading as it is mainly used in identifying the vehicle heading angle. Accordingly, the other five system inputs were combined, as listed in Tables 3.3 and 3.4.

Based on the nature of the events, the effects of the attended anomaly with single-sided wheels (ex. manhole) appears on the three-axes of the transversal acceleration and on the angular rotation along the X-axis. Meanwhile, the double-sided wheel anomalies (ex. transverse cracks) mainly affect the Z-Y transversal accelerations and the angular rotation around the Y-axis. Additionally, vehicle speed, V, is considered in order to avoid the misleading effects of getting in or out of a parking event.

The sensed linear accelerations and angular rotations are present in all the data sets. For extracting descriptive features of road anomalies, the data sets are "time windowed" at 1 second each. During a time window, a vector of more than 75 features was constructed. In order to construct efficient datasets, the events that were mainly considered were the ones that have their signature on the sensed data to occur in the same time window. However, for some events, where the signature of the anomaly is divided between two successive time windows, an overlap was made between these time windows to assure the best collection of the anomaly signature over the sensed data.

There are multiple feature extraction techniques adopted for road surface condition monitoring [38, 56] and other applications such as motion mode recognition [76]. The main feature extraction techniques can be categorized into Statistical, Time-Domain, Frequency-Domain, and Time-Frequency Domain features. Statistical, time domain, frequency domain, and other features were adopted in the feature extraction work in this thesis. Statistical features are mainly describing typical or central values of a data set and give measures on the data distribution behaviour [76, 77]. Regarding the statistical features used, at each time window, the main statistical features computed are: mean, median,

mode, range, maximum, minimum, root mean square (RMS), peak to RMS range, root sum of the squares, standard deviation, variance, interquartile range, percentile range, cumulative maximum, and minimum.

Some statistical features that combine the effects of more than one acceleration component at the same time epoch were also developed. These combined features help distinguish similar behaviour events as potholes and manholes. Considering time-domain features that describe the signal variation concerning the time domain, multiple zero and threshold crossing rates and also the local maxima and minima points within each time window was also used.

Frequency domain features describe the signals' behaviour in the frequency domain. Frequency domain features were computed such as mean and median frequencies, and also computed the estimated power spectral density within a time window. The other features used include multiple cross-correlations and cross-covariance between transversal and longitudinal accelerations. The main types of used features and their definitions are summarized in Table 3.5. All these computed features were used in constructing a unique feature vector at each time window and for each type of data set to provide a high description level of each labelled road surface anomaly. For every road anomaly, the feature vectors constructed form all the sensors that participated in one trajectory are collected together. These vectors are added to the other feature vectors collected from the other sensors that participated in other trajectories but describing the same road anomaly.

Table 3-5 Example of feature extraction techniques and their definitions

Feature	Domain	Definition
Mean	Statistical	$\text{Mean (s)} = \frac{1}{K}\sum_{m=1}^{K} s[m]$
Mode	Statistical	The most frequent value in a time window
Median	Statistical	The threshold value that separates the higher and lower 50% of samples in a time window
x^{th} Percentile	Statistical	The threshold value that separates the (100% - x %) higher samples from the lower x% of samples in a time window
Interquartile Range	Statistical	The range between (100%-x%) and x% of the samples in time widow
Variance	Statistical	$var(s) = \sigma_s{}^2 = \overline{(s-\bar{s})^2}$
Standard Deviation	Statistical	$std(s) = \sqrt{var(s)} = \sigma_s$
Root Mean Square	Statistical	$RMS(s) = \sqrt{\frac{1}{K}\sum_{m=1}^{k} s[m]^2}$
Local Maxima	Time	The number of maxima points in a time window
Local Minima	Time	The number of minima points in a time window
Threshold Crossing Rate	Time	$tcr(s) = \frac{1}{K-1}\sum_{m=1}^{K} \mathbb{C}\{s[m]s[m-1] < T\}$
Mean Frequency	Frequency	Estimates the mean normalized frequency of the power spectrum of a time window
Median Frequency	Frequency	Estimates the median normalized frequency of the power spectrum of a time window
Cross-Correlation of Linear Accelerations	other	$\frac{\sum_{m=1}^{K}(f_y[m]-\overline{f_y})(f_x[m]-\overline{f_x})}{\sqrt{\sum_{m=1}^{K}(f_y[m]-\overline{f_y})^2\sum_{m=1}^{K}(f_x[m]-\overline{f_x})^2}}$
Cross-Correlation of angular rotations	other	$\frac{\sum_{m=1}^{K}(w_y[m]-\overline{w_y})(w_x[m]-\overline{w_x})}{\sqrt{\sum_{m=1}^{K}(w_y[m]-\overline{w_y})^2\sum_{m=1}^{K}(w_x[m]-\overline{w_x})^2}}$

All these feature vectors are used to build a comprehensive data set that describes ten road anomalies with different levels of severity. This dataset is later used to train and test the system classifier, as shown in Figure 3.1. To show how this data set was constructed, Table 3.6 listed the major components of the dataset.

Table 3-6 Example of a comprehensive road anomaly dataset

Time Window	**Feature 1 (Max. Ver. Acc.)**	**...**	**...**	**Feature 75 (Threshold Crossing)**	**Anomaly Type**	**Sensor Used**	**Land Vehicle**
(i)	17 m/s^2	...	...	15	"Severe Pothole"	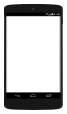 Nexus 5	 Toyota Venza, 2017
(i+1)	19 m/s^2	...	...	14	"Severe Pothole"	 Samsung Tablet	 Nissan Sentra, 2010
...	...	...	...	...	...	...	...
(i+100)	13 m/s^2	...	...	5	"Mild Manhole"	 OBD II	 Hyundai Tucson, 2018
(i+101)	14 m/s^2	...	...	7	"Mild Manhole"	 IMU Xbow	 Chevrolet Van, 2012
...	...	...	...	...	...	...	...

For example, for the "severe pothole" anomaly type, all the feature vectors extracted from all the sensors mounted in all the vehicles that were participated in all the trajectories are summed together in order. These vectors are followed by, for example, the feature vectors that describe "mild manhole" that were also collected from all the trajectories. As mentioned earlier, this dataset was used in the classification component.

3.6 Road Anomaly Classification

The held road experiments led to a comprehensive dataset of more than 1000 road anomaly events, plus data for mild road driving. Through analysis, it was observed that the roads located downtown and receive high traffic and less maintenance have a road anomaly or irregularity on average at every 1 second. Concurrently, the average anomalies go down to reach an average of 1 anomaly per 8 seconds within the relatively new and well-maintained residential neighbourhoods. These numbers show the demand and the challenges of robust anomaly detection systems.

The labelled events in the datasets spanned various anomalies with multiple severity levels. Mainly, and based on their frequent presence and their significant effects on vehicle motion, it was chosen to build the system to monitor potholes, manholes, transverse cracks, longitudinal cracks, road dents, railway tracks crossings, speed bumps, deceleration strips and paved stone road. Some anomalies such as railway track crossings, speed bumps, and deceleration strips have well-known locations to authorities and road operators. However, these could be harmful to the vehicles if they are improperly installed or not well-maintained, hence it was decided to detect and classify their level of severity as well. On

the other hand, there are some road types such as paved stone roads, which can be wrongly detected as longitudinal cracks; therefore, they were also detected and classified.

As the first step in building the classifier, various classification techniques were adopted, such as decision trees [78], support vector machine [79], k-nearest neighbour [80] and ensemble Meta classifiers [81]. Additionally, the dataset built for each trajectory was used to train each type of classifier with the labelled feature vector constructed from each event. The results showed a higher average performance within multiple classification techniques achieved by the support vector machine and bagged trees.

Training sets could be present at any distribution rather than spherical, and a kernel function could substitute the feature vectors' inner product. Kernel functions [79] span linear, polynomial, and radial basis function kernels. On the other hand, ensemble Meta classifiers [81] adopt classification techniques where multiple classifiers of a different or similar type are being trained over the same or subsets of a training set. Specifically, in bagging, a classifier is being trained in leveraging subsets of training sets. The construction of the subsets is a result of random selection from the main training set. Accordingly, almost 75% of the comprehensive dataset was used in building and training the SVM module as well as bagging classifiers. The remaining 25 % was used for the performance assessment.

For the SVM, a cubic kernel function was used to build a multi-level classifier with an automatic kernel scale. In the training process, all 75 features were used in order to achieve better results. For the ensemble Meta classifier, a bagged trees classifier was built and trained. Hence, in the early stages of training, both classifiers were observed to have a

better performance of the multi-level SVM over the Bagged trees. As a result, the performance of the SVM classifier was assessed with the comprehensive dataset. Table 3.7 presents various types of road types or anomalies with their corresponding number of occurrences. The datasets for the anomalies presented in Table 3.7 are used for testing the classifier. Furthermore, a confusion matrix that presents the results for eight various road types and anomalies with different levels of severity was adopted. Additionally, in Table 3.8, the SVM multi-level classifier showed an average performance of approximately 90% True Positive Rate (TPR) while achieving approximately 10 % of the average False Negative Rate (FNR).

Table 3-7 Various road types and anomalies and their number of occurrences used for the SVM-based classifier testing

Road Type or Anomaly	Number Of Occurrences
Mild Road	60
Mild Pothole	30
Severe Pothole	20
Mild Manhole	40
Severe Manhole	25
Transverse Crack	50
Longitudinal Crack	40
Mild Dent	20
Severe Dent	10
Deceleration Strips	10
Speedbumps	20
Mild Railway Crossing	20
Severe Railway Crossing	10
Paved Stone Road	50

The highest TPR of approximately 95% was present in predicting two different kinds of road types and anomalies (mild road driving and longitudinal cracks). On the other hand, the highest FNR of approximately 20% was achieved while detecting deceleration strips. On many occasions, when attending the deceleration strips, they were being detected as transverse cracks (20%) because of improper construction or less maintenance.

Moreover, to assess the analysis of the extracted features in building the classifier, the average FNR of single-sided events (ones attended with one side of the wheels) and double-sided events were assessed to check how often a miss-detected event is being predicted within the same general class. Consequently, the single-sided events (mild potholes, severe potholes, mild manholes, and severe manholes) achieved an average FNR of approximately 11%. It was found that approximately 91% of the miss-detected single-sided events were detected as other single-sided events at different types and multiple severity levels. On the other hand, the double-sided events (ones attended with both sides of the wheels) of the same general class (transverse cracks, deceleration strips, mild railway crossing, and severe railway crossing) achieved an average FNR of 13% while 83% of the miss-detected double-sided events were being predicted as single-sided events.

Regarding the False Positive Rate (FPR), the average FPR for the whole anomalies and types is 9.7%. As the highest FPR is achieved in the case of deceleration strips with 40%, while the lowest is obtained in the case of speedbumps with 0%. For single-sided events, the case of severe manhole experienced the highest FPR with 16.6%. On the other hand, for double-sided events, deceleration strips experienced the highest FPR with 40%.

It was predicted that the main reasons for the miss-predicted events occur as different levels of severity might have the same features when sensed with different car models. For example, the mild pothole sensed by a sedan or hatchback car with a relatively old year makes and low suspension performance might have the same features as a severe pothole being sensed by a Van with large tire sizes and good suspension performance. Additionally, when sensing an event with equivalent car models, the features of the same anomaly may vary based on the driver's behaviour, way of attendance, and the velocity during the attendance. Even with high quality of detection, a dynamic road monitoring system is essential to avoid the miss-detection that could occur because of different car models and the further deterioration of roads due to high-traffic, less frequent maintenance, and weather conditions.

To assure efficient road conditions monitoring, accurate geo-location is required. Otherwise, the reporting could be misleading and lead to a double effort form the municipalities in re-surveying the assessed roads. Considering the GPS challenges, the integrated navigation systems show a high potential in geo-locating the detected irregularities. The proposed positioning system is discussed in the following Chapter.

Table 3-8 Confusion Matrix for road surface anomalies detection

	Predicted Road Anomaly																
Actual Road Anomaly	*MR*	*MP*	*SP*	*MM*	*SM*	*TC*	*LC*	*MRD*	*SRD*	*DS*	*SB*	*MRC*	*SRC*	*PSR*	**TP**	**FN**	**FP**
MR	95%									5%					95%	5%	6.6%
MP		90 %	3.3%	3.3%				3.3%							90%	10%	16.6 %
SP			85%	5%	5%		5%								85%	15%	2%
MM		5%		90%				5%							90%	10%	10%
SM			4%		92%				4%						92%	8%	8%
TC	4%					94%				2%					94%	6%	10%
LC	2.5 %			2.5%			95%								95%	5%	1.25 %
MRD		10 %						90%							90%	10%	15%
SRD					10%				90%						90%	10%	10%
DS						20%				80%					80%	20%	40%
SB											90 %		5%	5%	90%	10%	0%
MRC		5%				10%						85%			85%	15%	5%
SRC												10%	90%		90%	10%	10%
PSR	2%			2%		2%								94%	94%	6%	2%
Average															90%	10%	9.7%

Mild Road: **MR**, Mild Pothole: **MP**, Severe Pothole: **SP**, Mild Manhole: **MM**, Severe Manhole: **SM**, Transverse Cracks: **TC**, Longitudinal Cracks: **LC**, Mild Road Dent: **MRD**, Severe Road Dent: **SRD**, Deceleration Strips: **DS**, Speedbumps: **SB**, Mild Railway Crossing: **MRC**, Severe Railway Crossing: **SRC**, Paved Stone Road: **PSR**

3.7 Summary

In this chapter, a framework for a road surface condition monitoring and route quality assessment was proposed and discussed briefly. Common road anomalies and irregularities identification were crucial aspects of the competent performance that is required such systems. Multiple road trajectories and surveys were conducted, leveraging eight land vehicles that were equipped with various sensors. These road trajectories were successfully identified ten types of road anomalies and analyzed their effects on the sensed linear accelerations and angular rotations. The collected data are preprocessed and de-noised utilizing wavelet packet-based signal de-noising techniques. The example results show an enhancement in the measurement quality of both IMUs and smart devices of approximately 44%. The signal de-noising enabled an efficient feature extraction process that distinguishes every road anomaly based on their signatures on the sensed data. The feature vectors constructed from the whole trajectories are combined and used in building a comprehensive dataset of different road types and anomalies of different severity levels. This dataset was used to train a multi-level machine learning-based SVM classifier to detect and categorize the monitored road anomalies. The classifier showed a performance of TPR of 90 %.

Chapter 4

Integrated Geo-referencing for the Detected Road Anomalies

4.1 Framework for Integrated Geo-referencing System with Adaptive Resolution

In Chapter 3, road surface anomalies detection and categorization were discussed and presented. Accurate geo-location is highly required to enable reasonable reporting for the detected anomalies to the municipalities and road operators. GNSS commercial receivers have two major drawbacks when they are adopted in geo-locating the monitored anomalies. The first drawback is that these receivers are not available most of the time, especially in the downtown core and urban canyons. The second challenge for the GNSS commercial receivers that they operate at 1 Hz, which does not imply a good resolution specifically at high driving speeds.

To overcome GNSS positioning systems challenges, INS, when integrated with GNSS receivers, provides accurate and continuous positioning [26]. Low-cost MEMS-based inertial sensors (accelerometers and gyroscopes) that are embedded in INS systems in land-vehicles and ubiquitous smart devices are not susceptible to the same challenges of GNSS. However, stand-alone INS solutions are prone to long-term position drifts and errors [82]. To avoid positioning errors in INS solutions, inertial sensors' biases and different sources of noises were analyzed and assessed. In particular, inertial sensors noises were categorized

into short and long-term errors [68, 83]. The short-term errors are dominated by high-frequency components, while low-frequency components present long-term errors. Short term errors are a result of electronic equipment and power supplies. Also, a random angle walk is considered short-term noise due to its high-frequency nature [83].

On the contrary, exponentially correlated noise that results from internal or external temperature variations is considered as long-term errors [68]. Bias instability from electronic components appear in low-frequency components and is also regarded as long-term errors [83]. To suppress inertial sensor noises, in [71], a Wavelet Multi-Resolution Analysis (WMRA) was proposed to eliminate the long-term errors of INS that are mixed with low frequencies, to describe the vehicle motion. WMRA adopted a wavelet function of the Daubechies family together with a soft thresholding technique. However, the lack of sufficient experimental results that span different and complicated real driving scenarios limit the reliability of the proposed method.

Authors in [84], applied a Daubechies wavelet-based de-noising technique to eliminate inertial sensor noise before integrating INS with GNSS in a combined solution. The proposed method used soft thresholding for noise-suppressing, and the authors compared their integration system after de-noising with low pass filtering (LPF) - based system integration. The results did not show significant enhancement regarding root mean square error, as the wavelet-based integrated system outperforms the LPF by approximately 20%. Also, the major limitation of the authors' proposed scheme is that they only considered GNSS without INS. In [85], a de-noising technique that combines wavelet de-noising and Allan Variance (AV) analysis were proposed to suppress both short and long-term noises.

The authors utilized road test experiments to assess the proposed de-noising technique on the performance of loosely coupled INS/GNSS integration. In their results, the combined de-noising method achieved a maximum error of 53.61 m compared to 92.51 m obtained by AV de-nosing only. The major drawback is that AV needs big data sets to produce consistent AV curves, which introduces additional complexity to the proposed solution. Also, the lack of experimental validation with extended and multiple GPS outages made the assessment of the positioning error enhancement not sufficient enough.

Considering INS/GNSS integrated positioning systems, there are various integration approaches that entirely or partially utilize the IMUs as embedded accelerometers and gyroscopes [27, 82, 86]. Applying the Kalman Filter (KF) in the integration of GNSS and INS was the most utilized integration methodology [14, 26]. On the other hand, the Particle Filter (PF) was proposed as a competitive alternative for integrated positioning [27, 28]. Consequently, the major challenge of the linearized KF is that the stochastic sensor errors and navigation error states are linearly modelled. Such linearized modelling leads to solution divergence, especially during GNSS outages [29].

On the other hand, PF techniques such as Sampling/Importance Re-sampling (SIR), Mixture PF (MPF) and Parallel Cascade Identification PF (PCI PF) have the capabilities of nonlinear modelling [82, 87, 88]; that allow the PF to model high order motion dynamics and noise characteristics [82]. The major challenge in adopting PF techniques for INS/GNSS integration is their high computational complexity compared to the linearized KF and extended Kalman filter (EKF) [26].

Also, during extended GNSS outages, the integration solutions mainly rely on the full inertial measurement units (IMUs), which have limitations due to the uncompensated biases [14]. The integration filters are operated in prediction mode when the GNSS updates are not available. The predicted INS errors are being considered in the mechanization solution to enhance its performance. However, the compensation is not always efficient, and there are notable residual errors remaining [26, 82]. RISS [26] is utilized to overcome the INS biases and noise errors. In RISS, only two accelerometers, one gyroscope and a wheel odometer are used instead of full IMUs. The odometer speed is considered in RISS to avoid the errors of the accelerometer biases. On the other hand, the pitch and roll angles are computed through combining accelerometers and odometer measurements, thus to prevent the horizontal gyroscope errors and biases [26]. Nevertheless, noise from inertial sensors and errors need to be eliminated to enhance the performance of the RISS in extended GNSS outages.

Other positioning technologies such as vision, LiDARs and radars may suffer from environmental aspects such as fog, rain and snow that limit their performance. Also, some of these sensors, such as LiDARs, are not affordable yet in terms of cost and the high computational capabilities that are, in some cases, beyond the requirements of ubiquitous vehicular services [89]. Thus an integrated geo-location system that addresses the mentioned challenges and also provides adaptive position and resolution is required.

In this work, an adaptive data rate geo-referencing framework is provided. The system first augments the GNSS by fusing its corresponding location measurements with a de-noised RISS at 1 Hz. The obtained accurate position is then fed to a RISS or a full

mechanization module when triggered by a road event that requires a higher resolution geo-referencing or positioning. Accordingly, the mechanization module or RISS utilizes the output of the RISS/GNSS module along with the inertial sensor measurements to provide high-resolution position information regarding the detected events. The monitored events and their corresponding location information update a database for reporting or further analysis purposes.

The adaptive resolution geo-referencing framework structure and components are presented in this section and discussed in detail in the following two sections. Also, a description of the conducted processes and the information flow is provided. Accordingly, as shown in Figure 4.1, the framework uses the inertial sensors and GNSS receivers within the land vehicles or the ones embedded in the smartphones. The inertial sensors are used to collect information that describes the vehicle motion dynamics that can be used in both navigating the vehicles and in extracting information for the road surface condition. In addition, GNSS receivers are utilized to collect location measurements (position, velocity). The details are in the following sections.

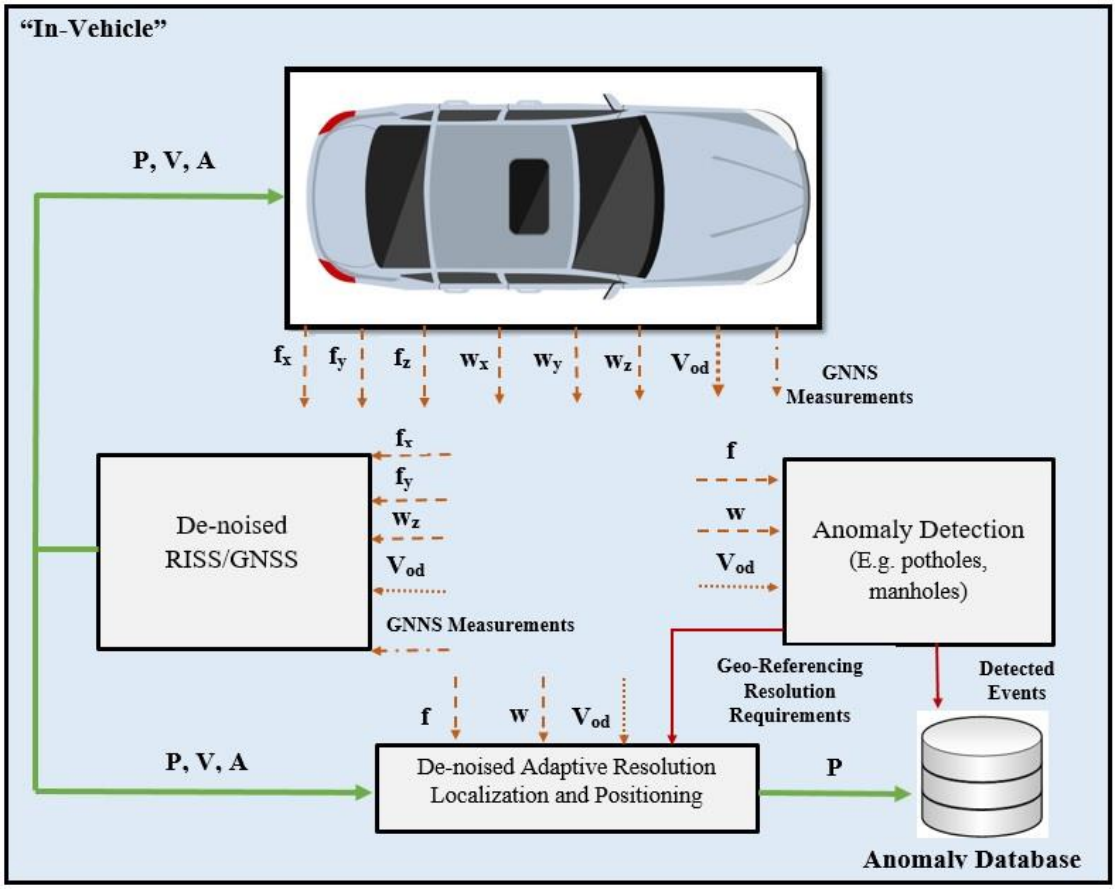

Figure 4-1 Framework for adaptive resolution integrated geo-referencing

4.2 De-noised RISS/GNSS integrated Geo-referencing

4.2.1 Wavelet Packet-based EKF RISS/GNSS Integration

In this section, the de-noised-based RISS/GNSS component is presented and discussed. For the INS/GNSS integration, INS increasingly drifts with time due to the implicit mathematical combination within the mechanization process, which causes the bias errors of both accelerometers and gyroscopes to be accumulated [85]. KF can be utilized in INS to optimally estimate the error-state, including position errors, velocity errors and

orientation errors. In general, KF is an algorithm for optimally estimating the error state of a system from measurements corrupted by noise. The KF algorithm is a sequential recursive algorithm for optimal least-mean variance estimation of the error states. In addition to its benefits as an optimal estimator, the KF provides real-time statistical data related to the estimation accuracy of the error states, which is very useful for quantitative error analysis [26]. In Figure 4.2, the system model used for INS/GNSS integration is illustrated.

In this work, a closed-loop de-noised 3D RISS/GNSS loosely coupled integration is used because it is robust and simple to implement compared to the other integration forms [26]. As shown in Figure 4.3, a wavelet packet-based signal de-noised 3D RISS/GNSS positioning system is presented thoroughly. As discussed aftermentioned, the inertial sensors measurements contain frequencies that describe the vehicle motion dynamics, effects of road anomalies, noises and errors. In positioning, the frequency components describe the regular vehicle motion is required, and the other components should be omitted; otherwise, they influence the accuracy of the INS solution and drifts in a short time.

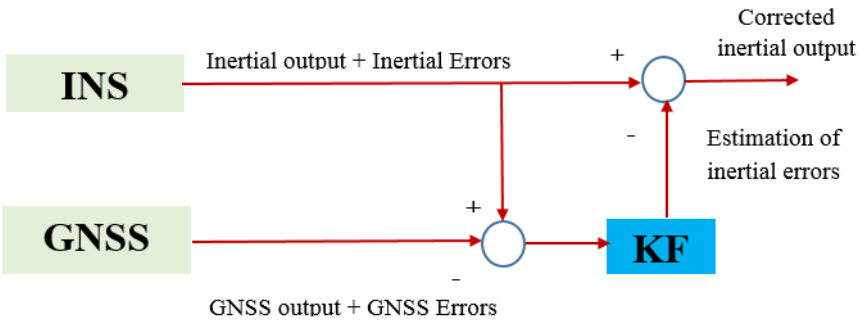

Figure 4-2 System model for KF-based INS/GNSS integration

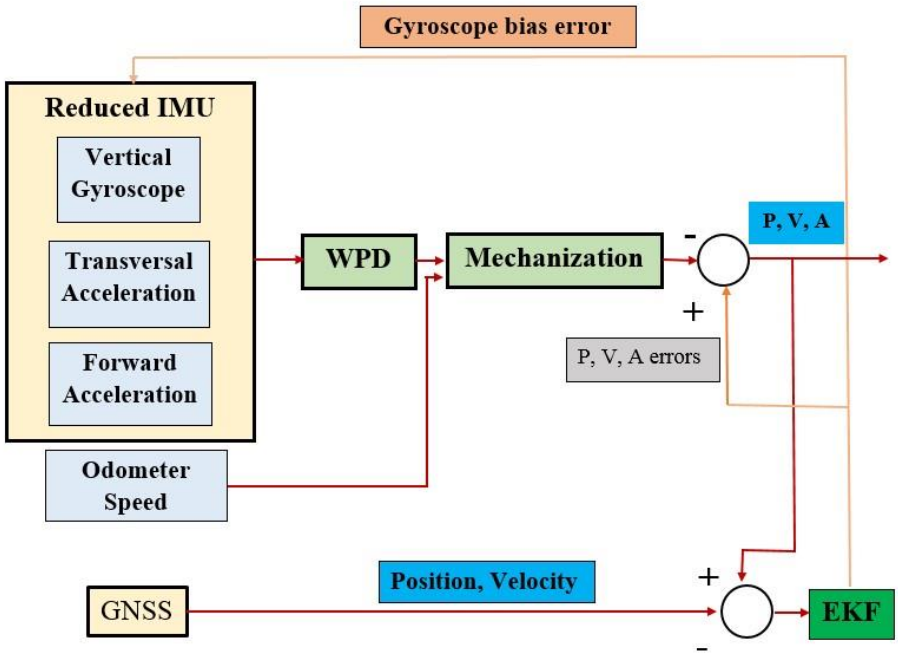

Figure 4-3 EKF-Based wavelet packet-3D RISS/GNSS closed-loop loosely coupled integrated positioning system, where P, V and A are the position velocity and Attitude, respectively

Low frequencies mainly describe the vehicle motion up to 10 Hz. However, regular filtering, FFT, WDFT and even WMRA may eliminate some high frequencies that represent some vehicle motions and thus introduce error in position. As discussed in the previous chapters, wavelet-packet de-noising (WPD) can decompose the signal into a multilevel of approximations and details and applying thresholds that are used to reconstruct the signal with the appropriate combination of approximations and details. For this work, the Daubechies wavelet family of order 8 and 5 levels of signal decomposition is applied. These selections assure the best performance while de-noising the inertial sensors.

As shown in Figure 4.3, the readings of one gyroscope and two accelerometers of the RISS system are the input of the WPD stage. In this stage, WPD is applied to de-noise the gyroscope and accelerometers data to suppress both short and long-term errors and noises. The continuously de-noised linear accelerations and angular rotations will enhance the results of the mechanization process and improve the accuracy of the computed position updates through the RISS/GNSS integration module described in the following parts of the section. As aftermentioned and shown in Figure 4.3, 3D RISS that utilize one gyroscope, two accelerometers and an odometer were adopted.

The main advantage of using the 3D RISS rather than full IMU is when the pitch and roll angles are calculated using accelerometers. The biases or noises of the two omitted gyroscopes are avoided. Also, calculating the velocity using the forward speed gathered by the odometer allows bypassing any uncompensated noises or biases of two accelerometers [27, 87, 90]. Accordingly, the de-noised sensor signals, along with the odometer measurements, are the input for the mechanization process. Basically, the navigation state vector of 3D RISS is given by $x = [\varphi, \lambda, \Omega, v_e, v_n, v_u, r, p, A\ ]^T$ where φ is the latitude, λ is the longitude, Ω is the altitude, v_e is the velocity towards east, v_n is the velocity towards north, v_u is the up velocity, r is the roll angle, p is the pitch angle, and A is the azimuth. Consequently, the pitch angle is given by:

$$p = sin^{-1}\left(\frac{f_y - a_{od}}{g}\right) \tag{4.1}$$

where f_y is the forward acceleration, a_{od} is the vehicle acceleration calculated using the vehicle acceleration recorded by the odometer, and g is the gravitational acceleration. The roll angle is obtained as follows:

$$r = -\sin^{-1}\left(\frac{f_x + v_{od}\omega_z}{g\cos p}\right) \tag{4.2}$$

The transversal acceleration is f_x, the vehicle speed extracted from the odometer measurement is v_{od}, the angular rotation around the vertical Z-axis is ω_z. Besides, considering relatively low values of pitch and roll, the azimuth angle is calculated as follows:

$$\dot{A} = -\left(\omega_z - \omega_e \sin\varphi - \frac{v_e \tan\varphi}{R_N + \Omega}\right) \tag{4.3}$$

R_N is the normal radius of the Earth curvature and h is the altitude. All the linear acceleration and angular rotation values are compensated for their biases and de-noised. Moreover, the three velocities can be transformed from the forward velocity and computed as follow:

$$v_e = v_{od} \sin A \cos p \tag{4.4}$$

$$v_n = v_{od} \cos A \cos p \tag{4.5}$$

$$v_u = v_{od} \sin p \tag{4.6}$$

Considering R_M as the meridian radius of curvature, the latitude φ, the longitude λ, the altitude Ω, can be calculated as follow:

$$\dot{\varphi} = \frac{v_n}{(R_m + \Omega)} \tag{4.7}$$

$$\dot{\lambda} = \frac{v_e}{(R_N + \Omega)\cos\varphi} \tag{4.8}$$

$$\dot{\Omega} = v_u \tag{4.9}$$

Note that the gyroscope measurement error is the primary source of error in the 3D RISS [26]. Gyroscope measurement errors introduce errors in horizontal velocity and positions. Compared to the gyroscopes measurement errors, the accelerometers measurement errors have less influence on the errors in the horizontal velocity and positions.

There are various techniques used in integrating the INS and GNSS. Considering the open-loop KF, in some cases, the dynamic error model is linearized around a nominal navigation state while neglecting some representative terms [27]. Also, the absence of the feedback from the KF to the INS dynamic model leads to imprecise prediction in the presence of extended GNSS outages [91].

On the other hand, the PF general INS/GNSS integration is suitable for nonlinear-based dynamic systems [92]. In the PF filtering technique, extensive computational processes are held as conditional probability functions are adopted for state representation. Accordingly, particles that are weighted samples are used to approximate the probability

density functions along with the prediction, update and re-sampling held at each iteration [93].

The EKF closed-loop process, as shown in Figure 4.2, surpasses the KF as the linearization is carried out on the corrected RISS outputs. This is besides the bias compensation of the gyroscope measurements achieved by the EKF. Thus, reliable and accurate navigation can be obtained while bypassing expensive computational processes of PF [92]. In the following paragraphs, the EKF 3D RISS/GNSS integration model is presented.

For the EKF, the discrete-time domain is given by:

$$\delta x_{k+1} = \boldsymbol{\Phi}_{k,k+1}\delta x_k + \ \boldsymbol{G}_k w_k \Delta t \tag{4.10}$$

where the state transition matrix is $\boldsymbol{\Phi}_{k,k+1}$, the error state vector is given by δx_k, the noise parameter matrix is $\boldsymbol{G}_k$, w_k is a Gaussian noise vector with a zero mean and $\boldsymbol{\Delta t}$ is the time interval. The system dynamic matrix $\boldsymbol{F}$ can be downsized to provide the state transition matrix $\boldsymbol{\Phi}_k$ .Given that the measurement model of the discrete KF is presented by [94]. The 3D RISS error state vector is given by:

$$\delta x = [\delta\varphi, \delta\lambda, \delta\ \Omega, \delta v_e, \delta v_n, \delta v_u, \delta A, \delta a_{od}, \delta b_z\ ]^T \tag{4.11}$$

where $\delta\varphi$ is latitude error, $\delta\lambda$ is longitude error, $\delta\Omega$ is altitude error, δv_e is east velocity error, δv_n is north velocity error, δv_u is upward velocity error, δA is azimuth error, δa_{od} is

the error in acceleration extracted from odometer measurements, and δb_z is the gyroscope bias error. The mentioned motion equations are linearized to obtain an error model of the closed-loop EKF used for INS/GNSS integration in this work. This linearization process is performed by keeping only the first term of Taylor's series expansion. Accordingly, these linearized equations are used to build the $\boldsymbol{F}$ matrix, and the position of each term can be indicated by F_{mn}, where m is for the row and n is for the column. These equations are given by:

$$\delta\dot{\varphi} = \underbrace{\frac{\delta v_n}{(R_M+h)}}_{F_{15}} \tag{4.12}$$

$$\delta\dot{\lambda} = \underbrace{\frac{\delta v_e}{(R_N+\Omega)\cos\varphi}}_{F_{24}} + \underbrace{\frac{\mathrm{v_e}\ \tan\varphi}{(R_N+\Omega)\cos\varphi}}_{F_{21}} \tag{4.13}$$

$$\delta\ \dot{\Omega} = \underbrace{\delta v_u}_{F_{36}} \tag{4.14}$$

$$\delta\dot{v_e} = \underbrace{\sin A\cos p}_{F_{48}}\,\delta a_{od} + \underbrace{a_{od}\ \cos A\cos P}_{F_{47}} - \underbrace{\left(\omega_z - b_z - \ \omega_e\sin\varphi - \frac{v_e\tan\varphi}{R_N+\Omega}\right)}_{F_{45}}\delta v_n +$$

$$\underbrace{v_n}_{F_{45}}\,\delta b_z + \underbrace{v_n\left(\omega_e\cos\varphi + \frac{v_e\ sec^2\varphi}{R_N+\Omega}\right)}_{F_{41}}\ \delta\varphi + \underbrace{\frac{v_n\tan\varphi}{R_N+\Omega}}_{F_{44}}\ \delta v_e \tag{4.15}$$

$$\dot{\delta v_n} = \underbrace{\cos A \cos p}_{F_{58}} \delta a_{od} + \underbrace{a_{od} \ \sin A \cos P}_{F_{57}} \ \delta A -$$

$$\underbrace{\left(\omega_z - b_z - \ \omega_e \sin\varphi - \frac{2v_e \tan\varphi}{R_N + \Omega}\right)}_{F_{54}} \delta v_e + \underbrace{v_e}_{F_{45}} \delta b_z + \underbrace{v_e \left(\omega_e \cos\varphi + \frac{v_e \ sec^2\varphi}{R_N + \Omega}\right)}_{F_{51}} \delta\varphi \qquad (4.16)$$

$$\dot{\delta v_u} = \underbrace{\sin p}_{F_{68}} \ \delta a_{od} \qquad (4.17)$$

$$\dot{\delta A} = \underbrace{\delta b_z}_{F_{79}} + \underbrace{\left(\omega_e \cos\varphi + \frac{v_e \ sec^2\varphi}{R_N + \Omega}\right)}_{F_{71}} \delta\varphi + \underbrace{\frac{\tan\varphi}{R_N + \Omega}}_{F_{74}} \ \delta v_e \qquad (4.18)$$

The odometer and gyroscope errors are modelled as a Gauss-Markov process of the first order and given by:

$$\dot{\delta a_{od}} = \underbrace{\beta_{od}}_{F_{88}} \ \delta a_{od} + \ \sqrt{2\beta_{od}{\sigma_{od}}^2}\omega(t) \qquad (4.19)$$

$$\dot{\delta b_z} = \underbrace{-\beta_z}_{F_{99}} \ \delta b_z + \ \sqrt{2\beta_z{\sigma_z}^2}\omega(t) \qquad (4.20)$$

where β_{od} and σ_{od} are the Gauss-Markov process parameters for δa_{od}, while β_z and σ_z are for δb_z. Thus, the full dynamic, $\boldsymbol{F}$, matrix can be constructed given the terms denoted at each corresponding place, and the rest of the terms are set to zero. Consequently, the

measurement model for the loosely coupled integration of INS/GNSS gives the difference between the GNSS position/velocity and INS position/velocity as:

$$\delta z = \boldsymbol{D}\ \delta x + v \tag{4.21}$$

where the measurements vector $\boldsymbol{\delta z}$ is given by:

$$\delta z = \begin{bmatrix} \varphi_{GNSS} - \varphi_{INS} \\ \lambda_{GNSS} - \lambda_{INS} \\ h_{GNSS} - h_{INS} \\ v_{e_{GNSS}} - v_{e_{INS}} \\ v_{n_{GNSS}} - v_{n_{INS}} \\ v_{u_{GNSS}} - v_{u_{INS}} \end{bmatrix} \tag{4.22}$$

Moreover, the design matrix $\boldsymbol{D}$ is given as:

$$\boldsymbol{D} = \begin{bmatrix} 1 & 0 & 0 & 0 & 0 & 0 & 0 & 0 & 0 \\ 0 & 1 & 0 & 0 & 0 & 0 & 0 & 0 & 0 \\ 0 & 0 & 1 & 0 & 0 & 0 & 0 & 0 & 0 \\ 0 & 0 & 0 & 1 & 0 & 0 & 0 & 0 & 0 \\ 0 & 0 & 0 & 0 & 1 & 0 & 0 & 0 & 0 \\ 0 & 0 & 0 & 0 & 0 & 1 & 0 & 0 & 0 \end{bmatrix} \tag{4.23}$$

where the term $\boldsymbol{v}$ is a Gaussian noise vector with zero mean with covariance matrix $\boldsymbol{R} = \langle vv^T \rangle$.

The EKF algorithm is divided into two stages; the prediction is given by [26]:

$$\Phi_{k,k+1} = \boldsymbol{I} + \ \boldsymbol{F}_k \Delta t \tag{4.24}$$

$$\boldsymbol{P}_{k+1}^{-} = \ \Phi_{k,k+1} \boldsymbol{P}_k^{+} \Phi_{k,k+1}^{T} + \ \boldsymbol{Q}_k \tag{4.25}$$

As $\boldsymbol{I}$ is the identity matrix, $\boldsymbol{P}_{k+1}^{-}$ is the prior estimate of error state covariance matrix and $\boldsymbol{Q}_k$ is the system noise matrix. While the update stage is given by [26]:

$$\boldsymbol{K}_{k+1} = \ \boldsymbol{P}_{k+1}^{-} \boldsymbol{D}^T \ [\boldsymbol{D} \boldsymbol{P}_{k+1}^{-} \boldsymbol{D}^T + \boldsymbol{R}_k]^{-1} \tag{4.26}$$

$$\delta x_{k+1}^{+} = \ \boldsymbol{K}_{k+1} \ \delta z_{k+1} \tag{4.27}$$

$$\boldsymbol{P}_{k+1}^{+} = \ (\boldsymbol{I} - \boldsymbol{K}_{k+1}) \ \boldsymbol{P}_{k+1}^{-} \tag{4.28}$$

Given that, δx_{k+1}^{+} is the estimation of the error state and $\boldsymbol{P}_{k+1}^{+}$ is the posterior error covariance matrix estimation.

In the following subsection section, the capabilities of the proposed WPD 3D RISS/GNSS in providing continuous and accurate navigation solutions during different outage periods is provided. The potential of the WPD appears in bringing up the performance of the low-cost IMUs to the high-end versions regarding the measurement

quality. Also, the de-noised inertial measurements lead to accurate position computation in the mechanization process.

Furthermore, the EKF-based integration accurately predicts the navigation solution during various and extended GNSS outages that outperform the traditional KF and PF navigation solutions. The impact of the proposed WPD based de-noising appears during GNSS outages where the positioning resolution relies totally on inertial sensors. Several controlled experiments were conducted where a reference solution from a high-end navigation system is available. As is described in detail in the following subsection, the tests involve introducing various types of GNSS outages in terms of the motion dynamics and the periods of the interruptions. During these different GNSS outage types, the performance of the WPD based de-noising method was assessed, and how it improved the positioning accuracy in challenging GNSS environment was validated.

4.2.2 Experimental Activities, Results and Discussion on WPD 3D RISS/GNSS

To assess the capabilities of the proposed INS/GNSS integration system, three road experiments held in Kingston, Ontario and Montreal, Quebec, spanning multiple driving scenarios and areas were undertaken. During these experiments, there were periods of straight driving, taking sharp turns, driving at various speeds, and full stops. The trajectories contained downtown scenarios where the GNSS receiver experienced multipath and successive outages as well as urban roadways, highway sections, driving through a tunnel, and driving where a complete and continuous outage of GNSS was present.

The first trajectory is in downtown Kingston which includes narrow urban streets with rough road surfaces. It also involves driving at relatively low speeds. The second trajectory is in downtown Montreal which contains a dense metropolitan area with heavy traffic that requires multiple stops and starts. This trajectory has a drive in a long tunnel, which implies 220 seconds of natural GNSS outage. The third trajectory experiences highway driving at relatively high speeds between Napanee and Kingston.

In all three trajectories, the MEMS-grade IMU provided by Crossbow (model IMU300CC-100) was used as the RISS component in the proposed system. While the land vehicle forward speed was collected from the on-board diagnostics (OBD) interface using the CarChip device at a data rate of 1 Hz. The proposed system results were evaluated and compared to high-end reference solutions. In the first trajectory, the reference solution was obtained by NovAtel Span integrated solution. This solution is conducted by the integration of an OEM4 GNSS receiver with IMU-CPT logged at 100 Hz. However, the integrated solution is provided at 1 Hz. Regarding the second and third trajectories, the reference solution is supplied by the NovAtel G2 Pro-Pack SPAN unit that integrates a Honeywell HG1700 tactical-grade IMU logged at 100 Hz with an OEM4 GNSS receiver. The positioning accuracy of the two references (ground truth) is within 1.8 meters. Also, the references azimuth angle accuracy is 0.05 degrees. Further details on the specifications of the reference can be found in [41]. Regarding the specifications of the multiple IMUs used for the three trajectories, Table 4.1 summarizes their main features and specifications.

Table 4-1 Specifications of the Utilized IMUs

Specifications	**IMU300CC-100 (Trajectory 1,2,3)**	**IMU- CPT (Trajectory 1)**	**IMU HG1700 (Trajectory 2,3)**
Update Rate	>100 Hz	100 Hz	100 Hz
Gyroscopes			
Bias	$\pm 2\ deg/s$	$\pm 20\ deg/hr$	$One\ deg/hr$
Scale Factor	<1%	<0.15%	150 ppm
Random Walk	2.22 $deg/\sqrt{hr}$	0.0667 $deg/\sqrt{hr}$	0.125 $deg/\sqrt{hr}$
Accelerometers			
Bias	$< \pm 30\ mg$	$< \pm 50\ mg$	$1\ mg$
Scale Factor	<1%	<0.4%	$300\ ppm$
Range	$\pm 2g$	$\pm 10g$	$\pm 50g$

4.2.2.1 First Trajectory

In this trajectory, the setup was mounted on a van as shown in Figure 4.4. The experiment was held in Kingston. Furthermore, as shown in Figure 4.5, this trajectory spans the downtown core and urban roads with different driving scenarios, including left and right turns with different angles, straight driving, multiple stops and various traffic conditions. The distance covered was approximately 14 kilometres, and the duration of the trajectory was approximately 35 minutes, including times when the van was stationary. To assess the performance of the proposed system under GNSS complete outages, eight simulated total outages in the post-processing process were introduced. The duration of each outage is 60 seconds during various driving scenarios, speeds, and roads, as shown in Figure 4.5.

Figure 4-4 Testbed Mounted in a land vehicle (Van) utilized for the First Trajectory

Figure 4-5 Road test trajectory in Kingston with multiple GNSS outages (in black)

The system performance is evaluated in Tables 4.2 and 4.3 providing the root means square (RMS) and Maximum 2D positioning error, respectively. In the two tables, the errors for the 3D RISS/ GNSS and the WPD-3D RISS/GNSS systems were presented. The WPD-3D RISS/GNSS presents better performance than 3D RISS/GNSS in terms of lower 2D positioning errors during the eight simulated outages. In conclusion, the WPD-3D RISS/GNSS enhances the average 2D RMS error of the 3D RISS/GNSS by approximately 69%. To provide a comparison of the performance of the proposed method, the position solution of the WPD system, along with the 3D RISS/GNSS and the NovAtel reference solutions, is provided. During the fourth outage, the land vehicle turned three times, two stop signs, and one yield sign. This route had scenarios of driving with variable speed during complete GNSS outage. The geo-referencing solutions of the two systems and the reference solution are shown in Figure 4.6.

Table 4-2 2D RMS Horizontal Position Error in Meters during Outages, First Trajectory

Outage No.	Outage Duration (seconds)	3D RISS/GNSS	WPD-3D RISS/GNSS
1	60	4.29	1.71
2	60	5.00	1.36
3	60	10.63	4.56
4	60	12.53	2.79
5	60	4.17	0.97
6	60	5.87	1.47
7	60	9.80	2.07
8	60	4.75	2.90
Average	60	7.13	**2.22**

Table 4-3 2D Maximum Horizontal Position Error in Meters during Outages, First Trajectory

Outage No.	Outage Duration (seconds)	3D RISS/GNSS	WPD-3D RISS/GNSS
1	60	10.75	5.53
2	60	9.23	2.52
3	60	17.68	11.59
4	60	12.53	5.77
5	60	8.08	2.92
6	60	6.48	3.96
7	60	23.13	6.86
8	60	9.43	5.26
Average	60	12.16	**5.51**

Figure 4-6 Positioning Solution during the GNSS forth outage of the first Trajectory

In addition, Figure 4.7 illustrates a comparison between the azimuth angles calculated by WPD-3D RISS/GNSS system and the azimuth angle extracted from NovAtel reference. The graph shows the proposed solution and how the reference coincide. The performance of the systems during the seventh outage was provided. Figure 4.8 presents the navigation solution of the 3D RISS/GNSS, WPD-3D RISS/GNSS and the reference solution. The figure shows that the WPD-3D RISS/GNSS outperforms the conventional RISS/GNSS. During the seventh outage, WPD-3D RISS/GNSS has better performance than the 3D RISS/GNSS system.

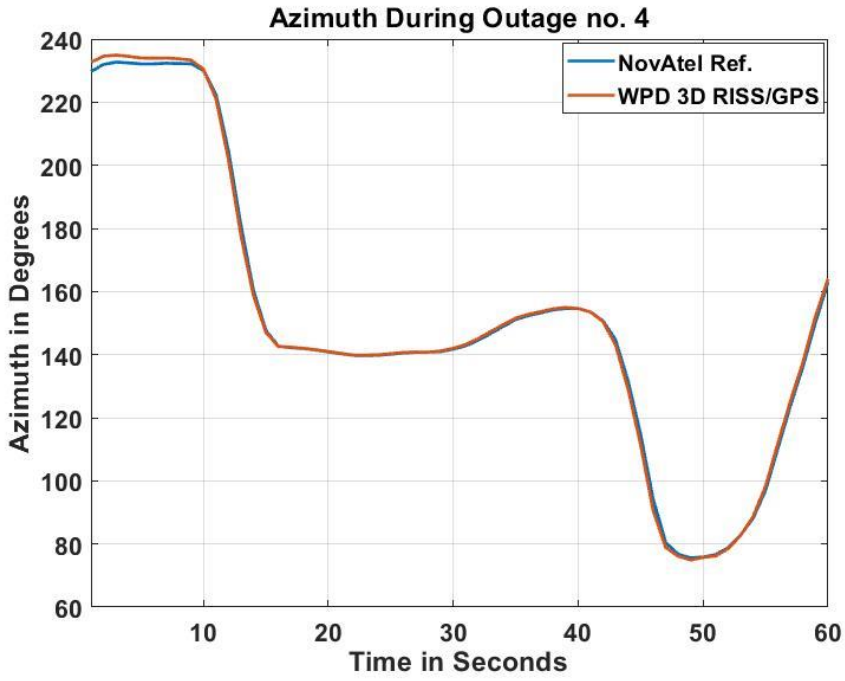

Figure 4-7 The azimuth of WPD-3D RISS and NovAtel reference during the fourth outage of the first trajectory

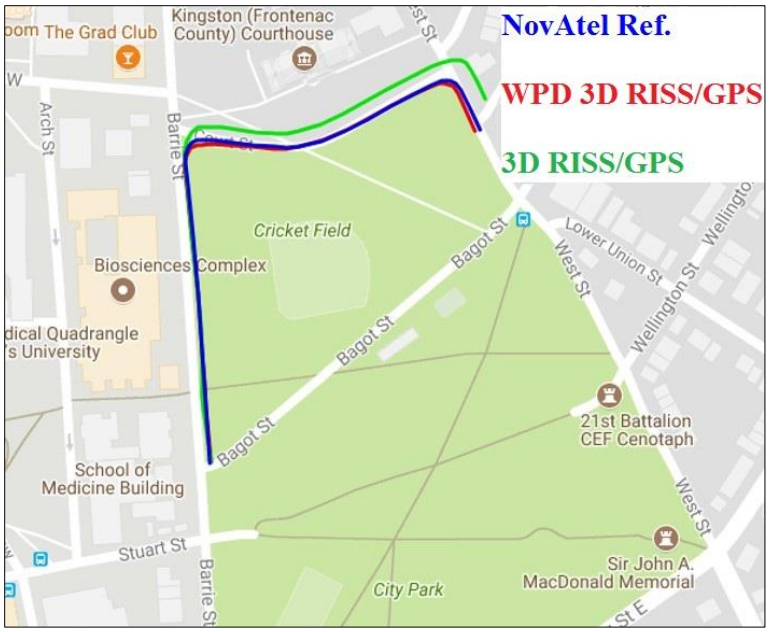

Figure 4-8 Positioning solution during the GNSS seventh outage of the first trajectory

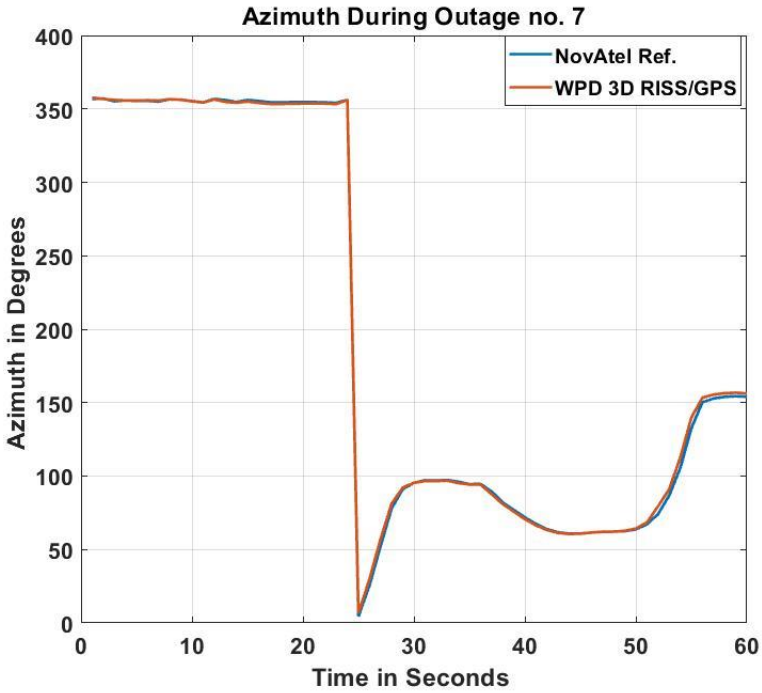

Figure 4-9 The azimuth of WPD-3D RISS and NovAtel reference during the seventh outage of the first trajectory

In Figure 4.9, the consistency of the azimuth calculations during outage number seven extracted from WPD-3D RISS/GNSS when compared to the NovAtel reference is highlighted.

4.2.2.2 Second Trajectory

For this trajectory, a van was utilized for the road experiment in Montreal. During this trajectory, a distance of approximately 100 km was covered in 85 minutes of continuous driving. As shown in Figure 4.10, this road test had urban roadways where some roads were straight, and some had more significant slopes, right and left turns with various angles, multiple stops at stop signs and traffic lights, and numerous speeds according to the road nature and traffic. Eight simulated outages, and one real outage that occurred while driving in the tunnel crossing the St. Lawrence River was assessed to appraise the performance of the proposed system during GNSS complete outages.

Accordingly, Tables 4.4 and 4.5 present the RMS and Maximum 2D horizontal position errors for 3D RISS/ GNSS, and WPD-3D RISS/ GNSS, concerning the same reference provided by NovAtel G2 Pro-Pack SPAN unit The RMS and maximum error results show a significantly better performance of the proposed system when compared to 3D RISS/GNSS as WPD-3D RISS/GNSS enhanced the average 2D horizontal RMS position errors by 49%. Also, enhancement of approximately 45% is achieved for the average 2D positioning maximum error.

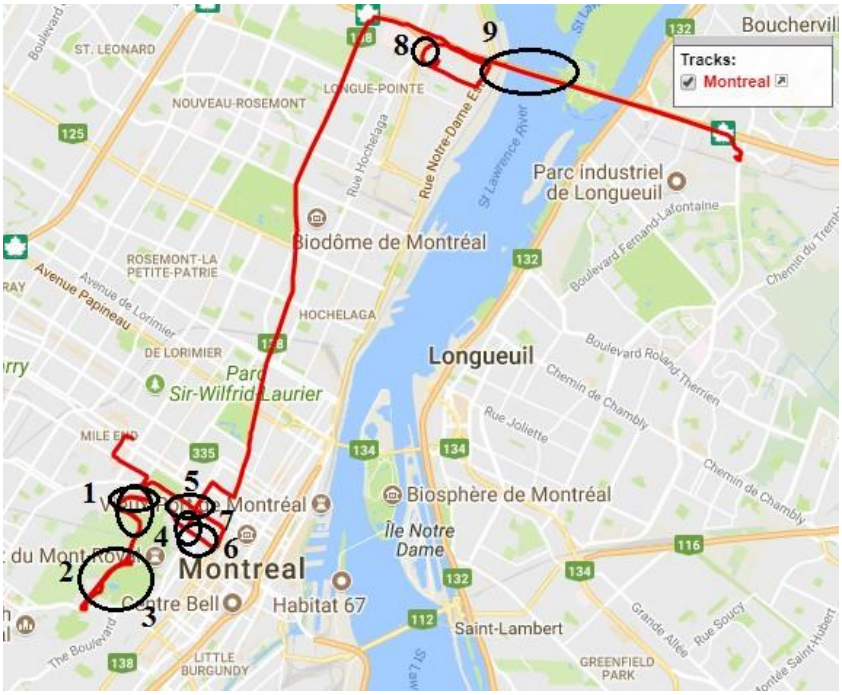

Figure 4-10 Road Test Trajectory in Montreal with Multiple GNSS Outages (in black)

Table 4-4 2D RMS Horizontal Position Error in Meters during Outages, Second Trajectory

Outage No.	Outage Duration (seconds)	3D RISS/GNSS	WPD-3D RISS/GNSS
1	30	9.09	4.26
2	80	15.36	4.99
3	80	14.55	6.43
4	80	15.57	5.92
5	60	14.65	8.95
6	90	13.82	5.33
7	70	13.53	6.81
8	120	10.35	8.88
9	220	17.98	12.54
Average	92	13.87	**7.12**

The results show the significance of adopting WPD de-nosing in the closed-loop loosely coupled integration of the GNSS and INS through EKF. The positioning solutions are shown and compared to the 3D RISS/GNSS concerning the NovAtel reference solution during selected outages to give an overview of the performance of the WPD-3D RISS/GNSS system. In these chosen outages, various driving scenarios were considered to span multiple dynamics and areas. For the third outage, in particular, Figure 4.11 provides the 2D positioning solution of the WPD system compared to 3D RISS/GNSS while considering a ground truth solution by the NovAtel reference. Figure 4.11 and Table 4.4 shows the performance of WPD-3D RISS/GNSS regarding the average 2D position-errors. However, towards the end of the outage, the proposed system drifts, achieving a higher maximum 2D position error compared to 3D RISS/GNSS. This drift affects the azimuth angle of the proposed system, as shown in Figure 4.12.

Table 4-5 2D Maximum Horizontal Position Error in Meters during Outages, Second Trajectory

Outage No.	Outage Duration (seconds)	3D RISS/GNSS	WPD-3D RISS/GNSS
1	30	15.34	7.44
2	80	25.80	10.83
3	80	22.31	25.26
4	80	29.84	10.25
5	60	27.29	11.89
6	90	23.76	8.41
7	70	24.16	11.86
8	120	17.02	15.65
9	220	35.56	20.85
Average	92	24.56	**13.60**

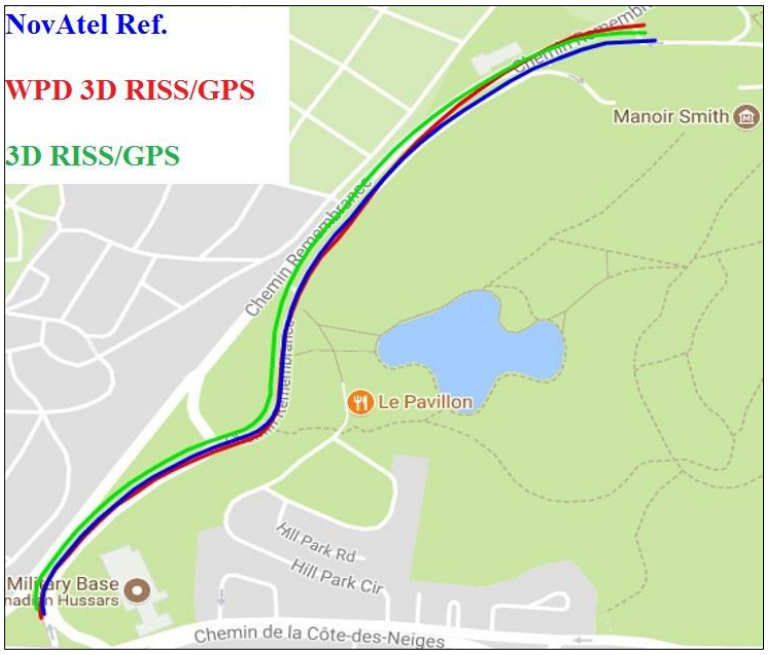

Figure 4-11 Positioning solution during the GNSS third outage of the second trajectory

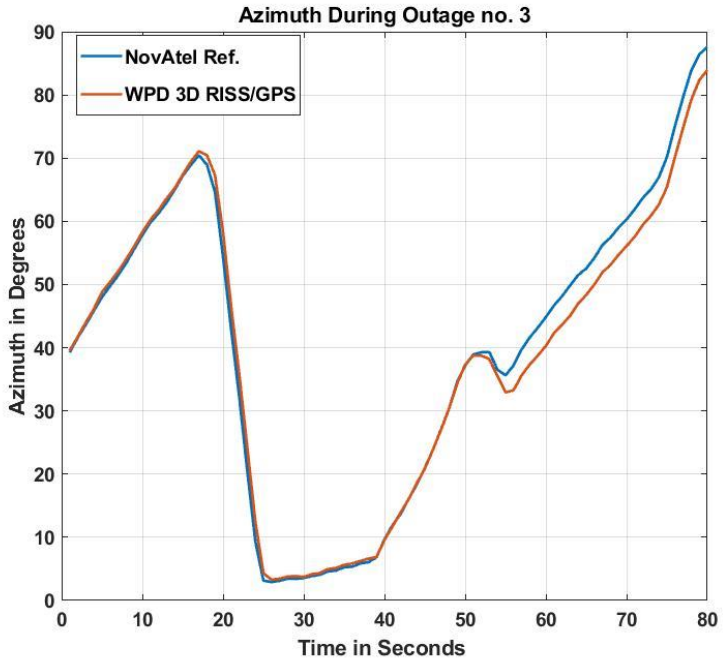

Figure 4-12 The azimuth of WPD-3D RISS and NovAtel reference during the third outage of the second trajectory

Furthermore, the performance of the proposed method is illustrated during the fourth outage in Figure 4.13 to examine the performance in the presence of different dynamics. Accordingly, WPD 3D RISS/GNSS grants a better positioning solution than 3D RISS/GNSS concerning the NovAtel reference solution. Moreover, the system performance was assessed during the fourth outage by comparing the azimuth angle calculated by WPD-3D RISS/GNSS with the reference, as shown in Figure 4.14. The azimuth of the proposed system followed the same behaviour of the azimuth extracted from the reference and provided a consistent performance through the full length of the outage.

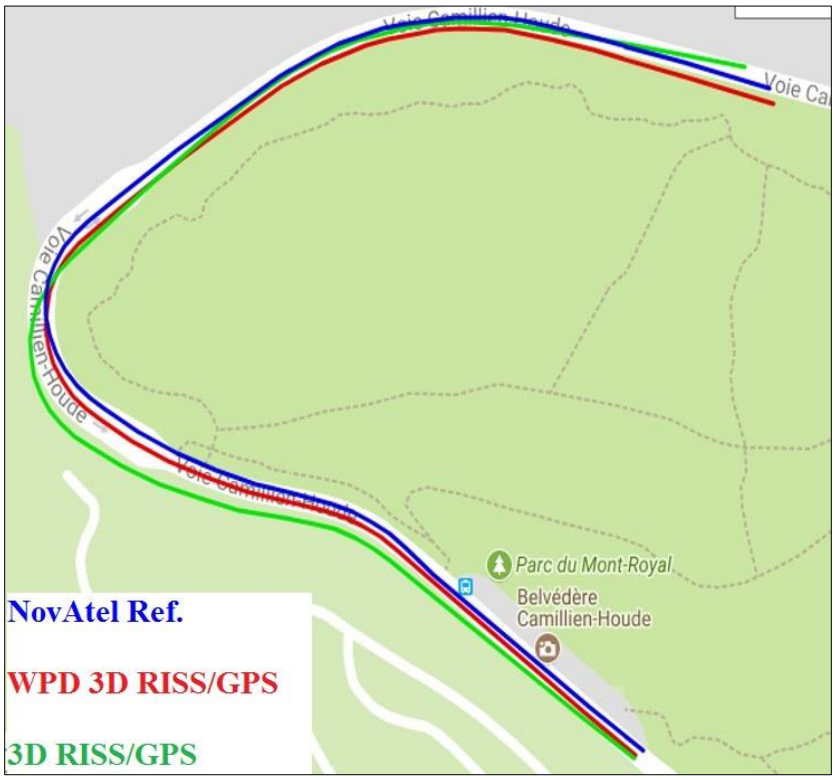

Figure 4-13 Positioning solution during the GNSS forth outage of the second trajectory

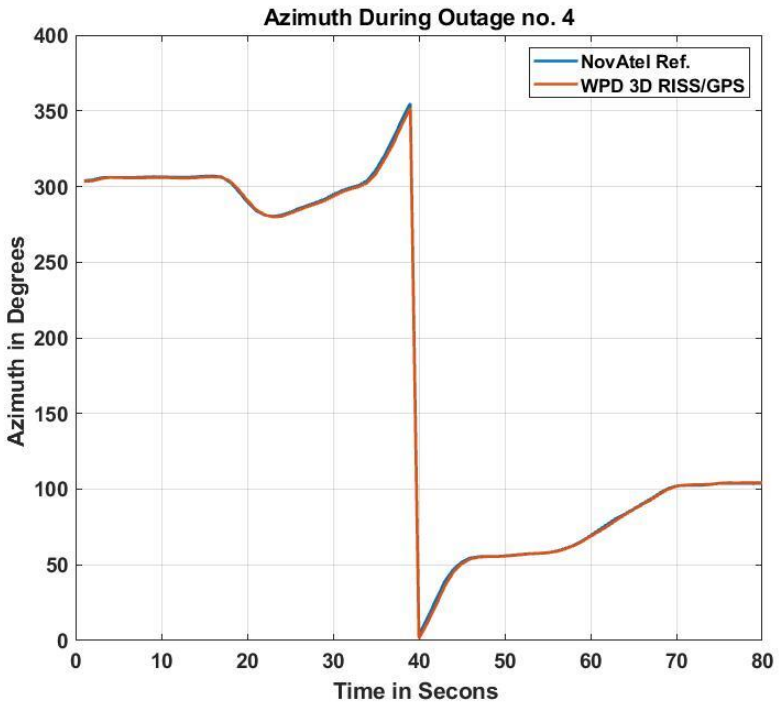

Figure 4-14 The azimuth of WPD-3D RISS and NovAtel reference during the fourth outage of the second trajectory

In Figure 4.15, the performance of the WPD-3D RISS/GNSS system was evaluated during natural and complete outages. The positioning solution is provided for the proposed method with the 3D RISS/GNSS. Both systems are compared with the reference during the ninth outage. In this outage, a complete and natural GNSS Outage occurred and lasted for 220 seconds while driving in a tunnel crossing the St. Lawrence River. The new system achieved an RMS 2D position error of 12.45 m and a maximum 2D position error of 13.60 m. These results enhanced the maximum 2D position error of 3D RISS/GNSS by 41 %. Figure 4.16 shows a consistent azimuth angle performance of the proposed system compared to the azimuth of the ground truth.

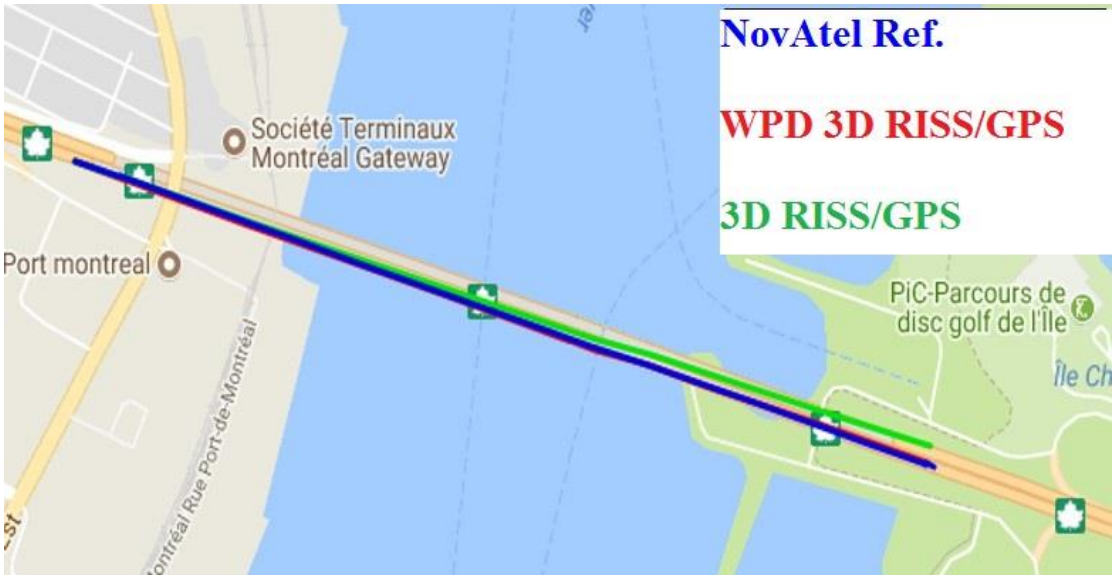

Figure 4-15 Positioning solution during the GNSS ninth outage of the second trajectory

Figure 4-16 The azimuth of WPD-3D RISS and NovAtel reference during the ninth outage of the second trajectory

4.2.2.3 Third Trajectory

The third road experiment was carried out around Kingston. The path had extended highway portions between Kingston and Napanee as well as multiple urban roadways driving. As shown in Figure 4.17, the experiment included various driving dynamics and areas. For analyzing the performance of the system, ten simulated GNSS outages were introduced. These outages included different driving scenarios, speeds, and areas.

In Table 4.6, the maximum 2D position errors are presented during the ten outages for the WPD-3D GNSS, and 3D RISS/GNSS concerning a positioning solution reference provided by NovAtel G2 Pro-Pack SPAN unit. The proposed system continues to have better performance compared to 3D RISS/GNSS. The WPD-3D RISS/GNSS provides a better average 2D maximum position error than the 3D RISS/GNSS by 62 %.

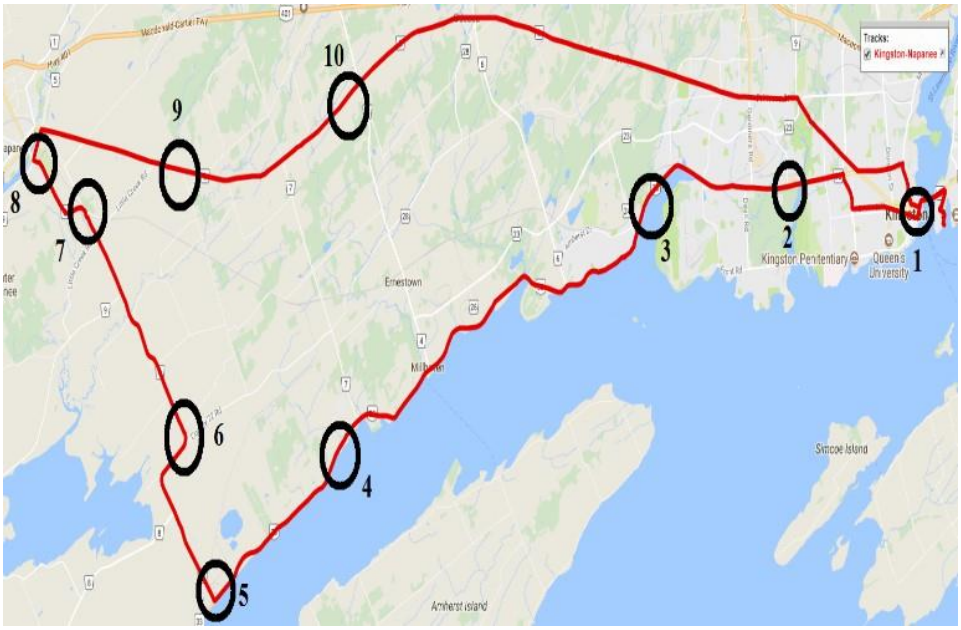

Figure 4-17 Road Test Trajectory between Kingston and Napanee with Multiple GNSS Outages (in black)

Table 4-6 2D Maximum Horizontal Position Error in Meters during Outages, Third Trajectory

Outage No.	Outage Duration (seconds)	3D RISS/GNSS	WPD-3D RISS/GNSS
1	60	9.69	5.94
2	60	10.55	0.99
3	60	10.87	5.27
4	60	25.33	10.09
5	60	21.63	5.36
6	60	14.04	7.8
7	60	15.81	8.88
8	60	25.04	6.02
9	60	7.82	2.29
10	60	12.17	5.53
Average	60	15.29	**5.81**

To demonstrate the capabilities of the proposed system, as an example, the duration of the fifth outage was extended to four minutes as shown in Figure 4.18. Concerning the 2D maximum positioning errors, WPD-3D RISS/GNSS achieves a maximum error of 9.63m. While the 3D RISS/GNSS mostly drifts to accomplish a 2D maximum position error of 64.70 m. Accordingly, Figure 4.19 shows the azimuth angle calculated by the proposed system and compares it to the azimuth angle obtained by the reference. The figure shows an accurate performance of WPD 3D RISS/GNSS regarding consistent azimuth angle results during complete and extended outages of GNSS. It also illustrates and proves the capabilities and reliability of the proposed method of providing accurate and continuous positioning during GNSS outages under various driving scenarios and areas

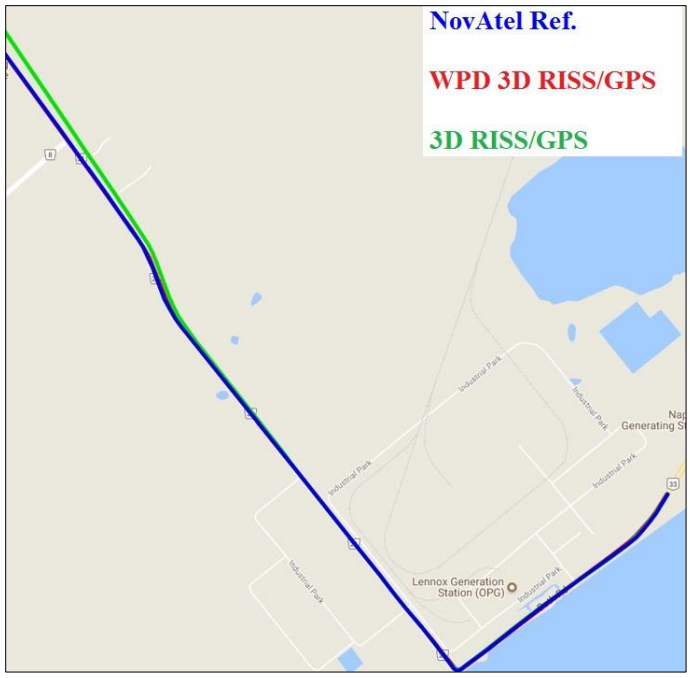

Figure 4-18 Positioning solution during the extended fifth GNSS outage of the third trajectory

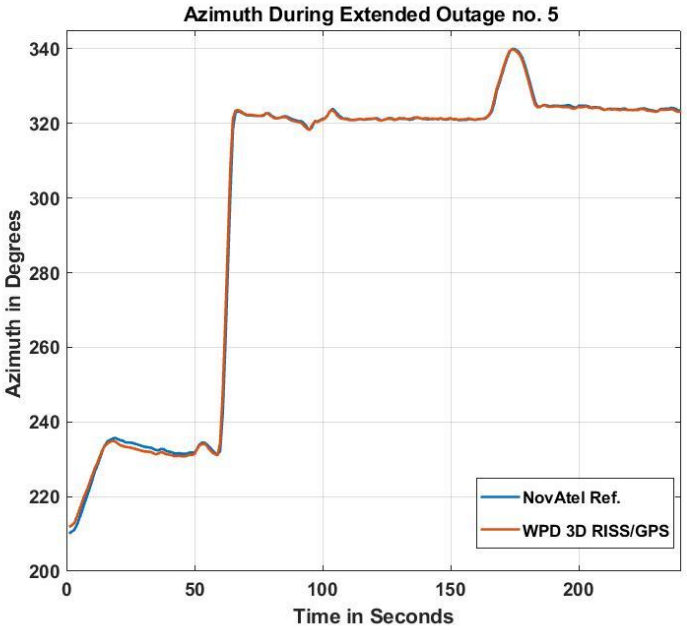

Figure 4-19 The azimuth of WPD-3D RISS and NovAtel reference during the fifth extended outage of the third trajectory

4.3 Case Study on the Adaptive Resolution Anomalies' Geo-referencing

In general, and as mentioned earlier in this chapter, the typical low-resolution location updates provided by the GPS commercial receivers are not useful in Geo-locating the road anomalies. At high speeds, for example, for a highway with a speed limit of 100 km/h, the vehicles travel around 28 m/s. With the GPS update of 1 Hz, a location stamp can be achieved with a resolution of 28 meters. Geo-referencing the road anomalies or ice accumulation requires a higher resolution localization in order to precisely report these events.

In the proposed system, as shown in Figure 4.1, the event detection component collects the inertial sensor linear accelerations and angular rotations measurements at a data rate of 100 Hz, and the vehicle speed at 1 Hz. With the aid of predetermined measurement thresholds, the event detection module is informed of a road anomaly or irregular driving event. For a consecutive time windows of one second each, the inertial measurements are de-noised using the wavelet packet decomposition process. Afterwards, the SVM-multi level classifier is used to detect and categorize the type of occurred road anomaly.

For efficient reporting and further analysis, detected road events, specifically, the ones that occurred at high speeds, may need additional location information. Regarding the road hazards, the event detection module can decide the exact time instant the road event has started. Also, the vehicle speed is monitored to guide with the position resolution requirement. For instance, a position update with a resolution of approximately 1m is

required in most of the cases. Then, a time-stamped request is sent to the adaptive positioning and localization module along with the required rate to request the required position information.

Once a road event is detected, the detecting module sends a detailed request of the required positioning or localization resolution. The details include the time window or windows that a higher position resolution is required. Also, the event detection component clarifies the nature of the required location information. For road anomalies, the event detection module sends the exact time instant where the event has started and requests a high-resolution geo-location for the monitored event while also considering the vehicle speed. The adaptive rate geo-referencing then requests the (P, V, A) information of the time window or windows that need additional location information. The adaptive geo-referencing module can utilize a RISS or full mechanization procedures to provide a higher resolution position. In the case that the RISS used in the higher resolution positioning module, the WPD RISS/GNSS provides the module with (P, V, A) of a specific time window to be used in initializing the RISS module. Afterwards, the RISS utilizes the inertial measurements with the upsampled odometer speed to predict the high-resolution position requested by the event detection module.

The detected event and its location information are updating the database, as shown in Figure 4.1. A case study is used to illustrate the methodology of the adaptive resolution geolocation framework. The experiment was held in Kingston, ON. In this scenario, the vehicle was travelling at a speed of 50 km/hr. This speed indicates that the RISS/GPS module can provide a position resolution of 15 m/sec. During the driving experiment, the

event detection module, with the aid of the inertial sensors, was able to detect a severe manhole that disturbed the vehicle motions, as shown in the accelerometers measurements in Figure 4.20. The integrated RISS/GPS module has determined the position of the monitored manhole at points 1 and 2 in Figure 4.21. Accordingly, the low-resolution position of 1 Hz has led to a misleading geo-location for the monitored event. As shown in Figure 4.20, the inertial sensors were logged at 100 Hz. Using pre-set measurement thresholds, the event started at the sample no.30.

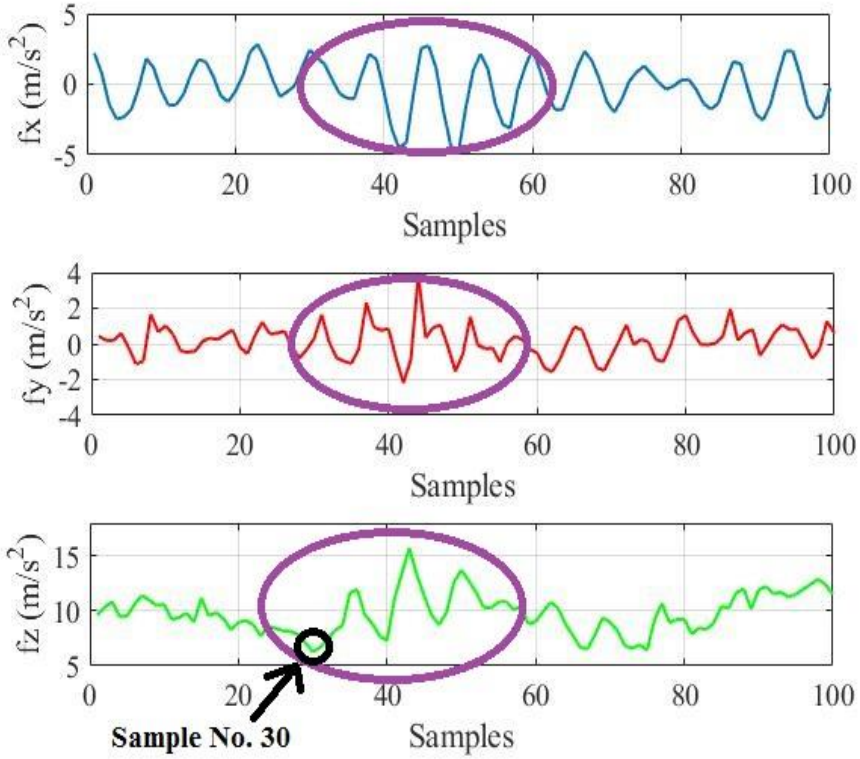

Figure 4-20 Three-axis accelerometer measurements for a detected road anomaly (Manhole)

Figure 4-21 Adaptive resolution geo-referencing of a road anomaly (Manhole)

Thus when a significant change of the vertical acceleration measurements was detected. This implies that the event approximately occurred at one-third of the time window of one second. Taking into consideration that the vehicle was travelling at 50 km/hr, the event detection module requests a higher resolution point position at 10 Hz. Moreover, it specifies that the requested point position is the one corresponding to the sample no.30. The adaptive resolution positioning component then requests the (P, V, A) information at the time window number 1 that is shown in Figure 4.1.

In addition, the odometer measurement at the time windows numbers 1 and 2 are used in an upsampling process to get a speed update of 10 Hz. The (P, V, A) of time window no. 1 is used to initialize the RISS module and leveraging the Equations 4.1-4.9 that are

used to predict the point position corresponds to the sample no. 30, where the manhole was detected. As shown in Figure 4.21, the predicted high data rate manhole position is more accurate than the position of the time window no.1 and no.2 that are shown in Figure 4.21. The presented case study shows the significance of the proposed framework for geo-referencing the monitored road conditions.

4.4 Summary

In this chapter, a framework for the adaptive resolution geo-referencing system was presented. Present road conditions monitoring systems are relying on commercial GNSS receivers to localize the monitored road anomalies. However, GNSS signals suffer from partial and complete outages and multipath propagation in downtown cores and urban canyons. Also, most of these commercial receivers are operated at 1 Hz, which implies low-resolution geo-referencing, specifically when vehicles are travelling at high speeds. The absence of accurate localization for the monitored anomalies will lead to a misleading assessment of the road conditions and may induce additional efforts to the municipalities in re-checking the monitored roads. INS, when integrated with the GNSS, bridge the position outages occur during GNSS outages. In long outages, INS position solution drifts due to the initial sensor errors and noises. The proposed framework leveraged the WPD to de-noise the inertial sensors and remove the high-frequency components that describe the effects of the road anomalies while maintaining the frequencies that only describes the vehicle motion dynamics. The denoised sensors are then integrated into the form of RISS/GNSS in a closed-loop form utilizing EKF. The geolocation update is 1 Hz because of the GNSS updates limitations. When the system detects a road anomaly, it requests the

desired resolution of the position updates. The de-noised sensors enable efficient standalone RISS operation to provide a high-resolution geo-location for the monitored road anomaly.

Chapter 5

Vehicle Route Planning Involving Road Quality

The privilege of monitoring road surface conditions along with the corresponding accurate location opened the door towards a dynamic and frequent assessment of the road segments' conditions. This assessment can benefit route planning when the drivers request to navigate smooth roads to their destinations while having a safe and comfortable drive.

In this chapter, a framework for route suggestions that involve road quality is presented. As described in section 3.1, a cloud-based system leverages the corwdsensed-based datasets of the monitored anomalies with their accurate location to provide route assessment and suggestions for the drivers. This system consists of two major components, the first is to assess the average road segments quality and the second component is used to evaluate the potential routes based on the average route quality while considering the route time and length.

5.1 Road segments Quality Assessment

In this section, the road segment quality assessment component is presented and discussed. As shown in Figure 5.1, the road anomalies database collected by each crowdsensing node (vehicle) is communicated to the cloud, as shown in Figure 3.1. Accordingly, the detected irregularities A^j and their corresponding locations l^j are used to update a bigger database that contains the inter-vehicle cross-referenced crowdsensed road anomalies. In order to accurately assess the road segment quality, the location stamped road anomalies need to

be matched to the correct road segment. For instance, in Canada, the road information database shown in Figure 5.1 is built through accessing the National Road Network (NRN) Canada, which includes road segment information such as location, name, type, direction, address range, rank and class [95].

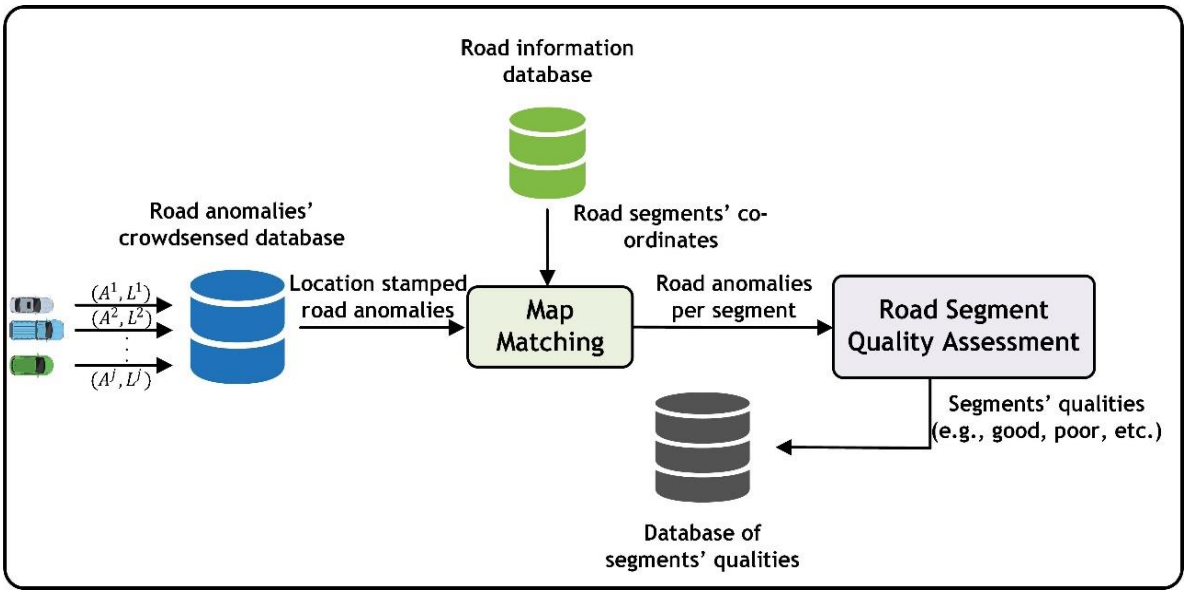

Figure 5-1 On-Cloud Road Segment Quality Assessment

The realization of this road segment assessment component is held using a machine intelligence-based fuzzy inference system (FIS). Basically, fuzzy logic is intended to deal with real-world applications through a framework able to deal with ambiguity and inaccuracy [96]. In fuzzy logic, quantified rules or statements are adopted to avoid firm true or false decisions. Accordingly, fuzzy logic sets grant objects values that range from 0 to 1 through graded memberships. Therefore, FIS maps sets of given inputs to outputs with the aid of fuzzy logic.

In addition, FIS dynamic performance is modelled by sets of descriptive linguistic rules that are set according to the system designer's prior knowledge [96]. For example, the fuzzy rules of a multiple-input-single-output (MISO) fuzzy system are given by :

R1: if (a) is X1 and (b) is Y1, then (c) is Z1;

R2: if (a) is X2 and (b) is Y2, then (c) is Z2; (5.1)

.....

Rn: if (a) is Xn and (b) is Yn, then (c) is Zn;

As *a, b* and *c* are linguistic variables representing two inputs process state variables and one output variable. While Xi and Yi are linguistic values of the linguistic *a, b* in the universe of discourse U and V with $i = 1, 2, \ldots, n$. The linguistics values Zi of the linguistic variable c in the universe of discourse W in the case of Mamdani FIS [97].

Fundamentally, as shown in Figure 5.2, four components together represent the FIS. The fuzzy rules which can be called "IF-THEN" are built according to the prior knowledge of the required system. Also, the input domain crisp values, U, are outlined with fuzzy sets defined in the same universe of disclosure by the aid of the fuzzification stage. On the other hand, an inverted operation is carried by the defuzzification stage to map the crisp values of the output domain V with the predefined fuzzy sets. Further details on FIS structure and derivations can be found in [98]. For road segment assessments, inputs from the road surface types and conditions data sets are used to compute three inputs for the FIS.

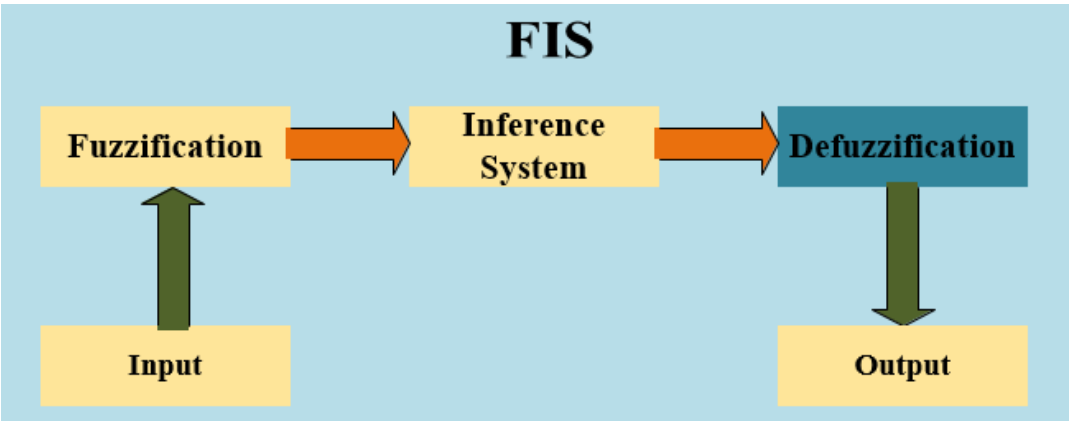

Figure 5-2 FIS system Structure

The first input is related to the total number of road anomalies in a given road segment, S. For each segment, a normalized percentage of road anomalies, RA, is computed simply through dividing the total number of anomalies over, S, to reflect the density of the anomalies in a particular segment. Thus this input is mapped to three membership functions, which are defined as low, moderate and high. As shown in Figure 5.3, a *sigmoidal* membership function was adopted for both low and high functions. The second input is representing the effect of the anomalies severity level on the assessment of a road segment. Different road segments can be equal in lengths and have the same density of anomalies. However, these segments should not receive the same assessment decision if they experience different types of anomalies of different levels of severity. Accordingly, the average percentage of anomalies severity level in each segment is calculated and normalized concerning the segment length and presented by mild and severe *sigmoid* membership functions.

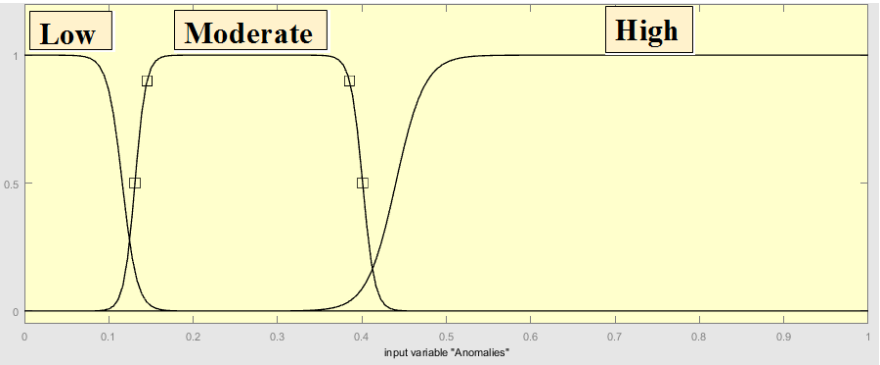

(a)

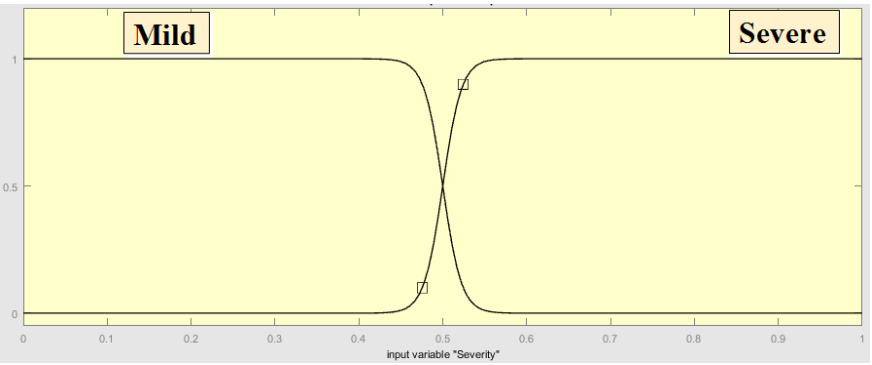

(b)

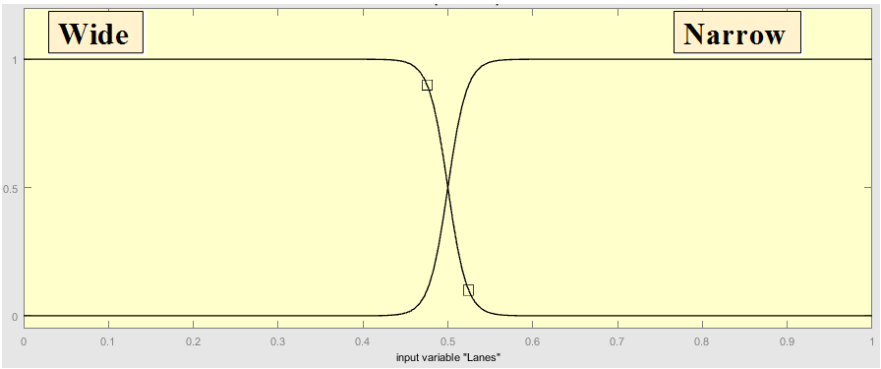

(c)

Figure 5-3 Membership functions utilized in road segments assessment: a) percentage of anomalies (low, moderate, and high), b) average level of severity (low and high) and c) lanes (narrow and wide)

Lastly, the third input is to distinguish road segments of single and double lanes. This input was chosen to represent the significance of the road segment wideness on its quality assessment. The road segments with multi-lanes allow the driver to maneuver before the anomalies easily while this is difficult to occur in single road segments and it can lead to dangerous scenarios within the two ways road segments. The third input is also mapped through two *sigmoid* wide and narrow membership functions. In this FIS, the fuzzification of the inputs is mapped by 11 Mamdani fuzzy rules. The road assessment FIS is then defuzzified to enable three output levels of road segment quality. They are classified into Good, Moderate and poor segments.

5.2 Vehicle Route Recommendation

In this section, the potential route assessments and suggestions based on the average road quality are presented. As shown in Figure 5.4, a driver of SV requests a route plan form a service provider. Accordingly, most of the route planning service providers suggest potential routes based on both the trip time and route length. Road segments of each potential route are identified with the aid of the NRN database. The average segments' qualities of each potential route are then pulled from the road segments quality constructed in Section 5.1. The average segments qualities are used as an input for route assessment-FIS based component. In this component, there are three inputs adopted to asses the potential routes and decide on the route recommendation. The first input is the average quality of the segments in a potential route. The first input is controlled by three

membership functions, namely poor, moderate and good which reflects one aspect of the route evaluation as shown in Figure 5.5.

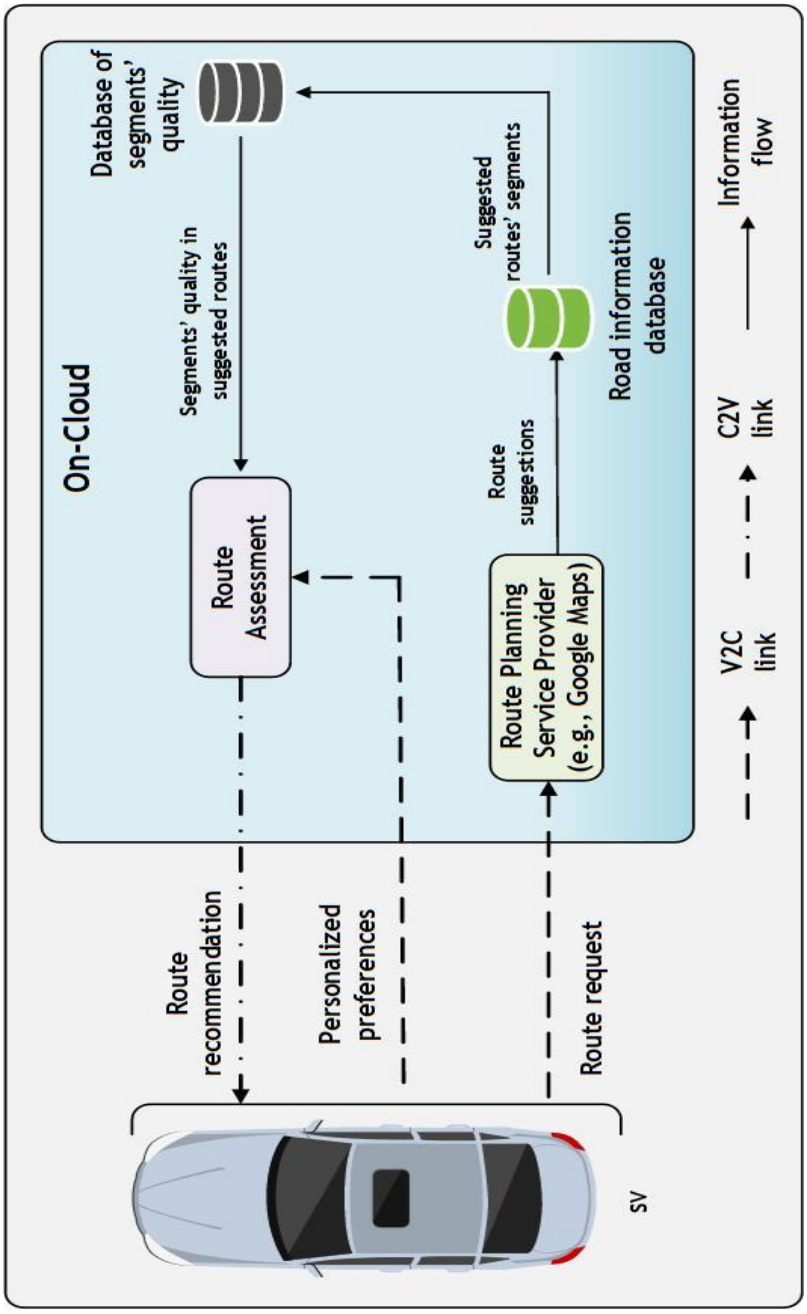

Figure 5-4 Route planning system based on driver preferences and average road quality

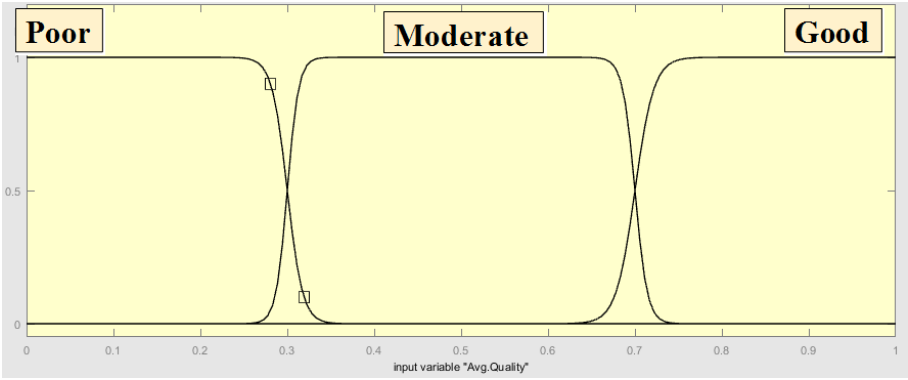

(a)

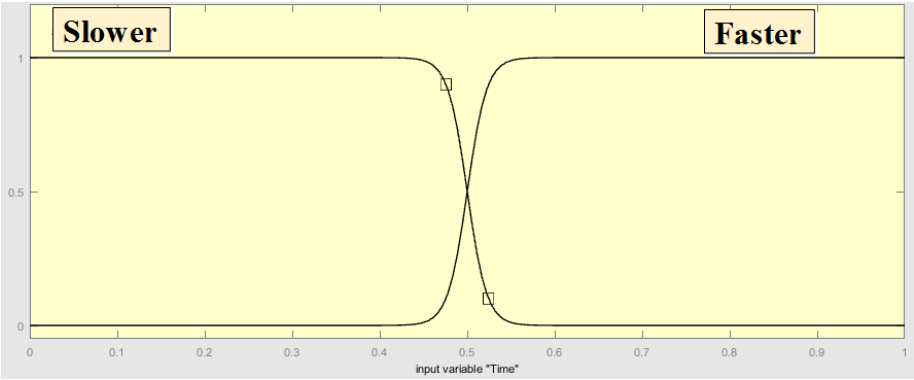

(b)

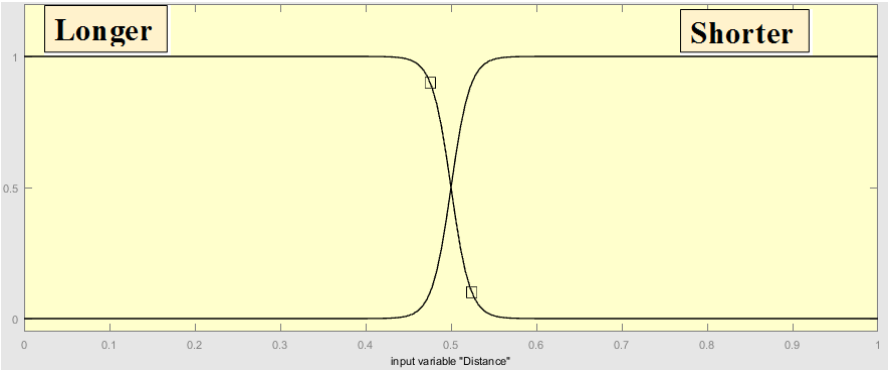

(c)

Figure 5-5 Membership functions utilized in route suggestion: a) average segments quality (poor, moderate, and good), b) route time (slow and fast) and c) route length (long and short)

Two *sigmoid* functions were adopted for the poor and good membership functions, while the product of two *sigmoidal* functions was used for the moderate one. Note that the primary concern in the proposed route planning is in providing high road quality routes. However, high traffic routes and long paths should be avoided as well whenever is possible. Therefore, the second and third inputs are described by the route travel time and route distance, respectively. The second one is divided into two sigmoid membership functions named slower and faster. On the other hand, the third input is also described by two sigmoid membership functions called longer and shorter. In the route recommendation FIS, the fuzzification of the three inputs is controlled by 12 fuzzy rules. While the defuzzification of this cascaded FIS provides three output levels of route recommendations, they are divided into (not suggested, marginally suggested and suggested). The system capabilities are assessed using real-road test cases in the following sections.

5.3 Road Test Cases

In this section, two real-road test cases are used to show the system performance. These cases were held in Kingston, ON. For the first road test case, a real trip request as shown in figure 5.6. In this trip, the driver requires route planning to travel from point A to point B while requesting a stable and safe drive as the highest priority. According to Google maps, as shown in Figure 5.7, there are two suggested routes. The first one reaches point B in 5 minutes, and it is 1.3 Km regarding route distance. On the other hand, the second recommended route travel time is 7 minutes, with a distance of 1.4 Km. Thus

according to Google maps suggestions, which are mainly provided based on less trip time and shortest route distances, Route 1 is recommended, as shown in Figure 5.7.

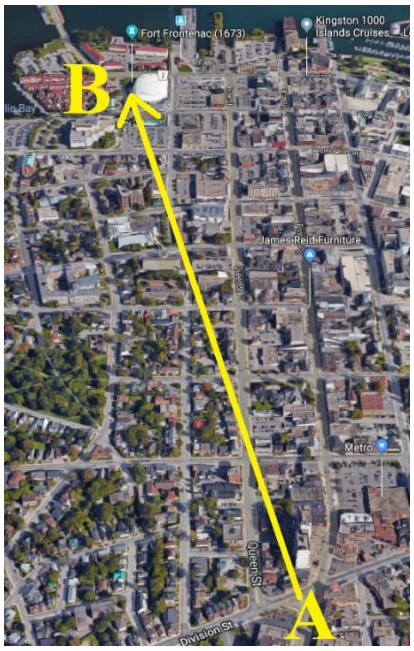

Figure 5-6 Route planning request from point A to point B (top view)

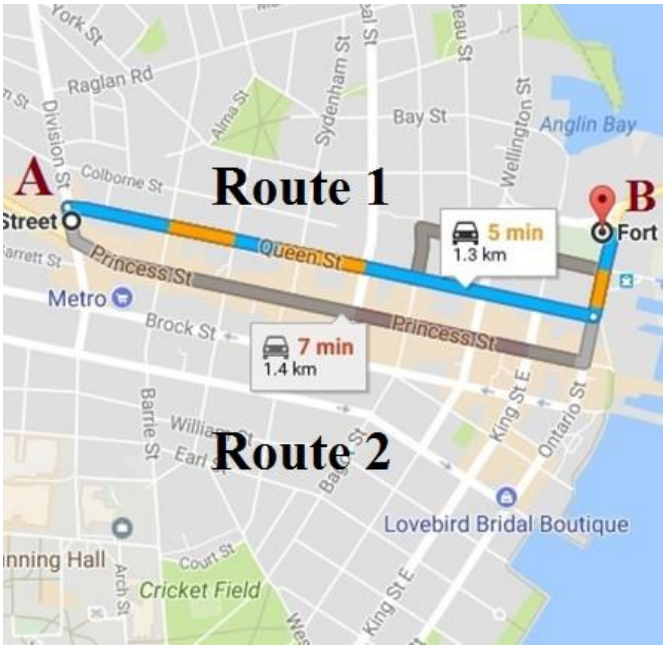

Figure 5-7 Route suggestions provided by Google Maps, first road test case

Consequently, as requested by the driver, the safe and high road quality has the highest priority in the trip satisfaction. In this regard, the system extracted the quality of the road segments in the potential routes, as listed in Table 5.1 and shown in Figure 5.8. The road segments' qualities information on Route 1 and Route 2 were assessed. The first route (suggested by Google Maps) has nine road segments.

In this route, there are eight segments assessed as poor quality ones, and there is only one segment assessed as a moderate one. On the other hand, the second recommended route (Route 2) consists of 10 segments. Utilizing the first FIS, five of the road segments within this route are evaluated as good ones, and there were other four assessed as moderate while only one is considered a poor road segment. As per Figure. 5.8, the assessed road segments of Route 1 and Route 2 are highlighted with different colours to indicate different levels of quality.

Table 5-1 Road Segment Assessment for Route 1 and Route 2

Road Segments Number	Route 1	Route 2
1	Poor	Moderate
2	Poor	Moderate
3	Poor	Good
4	Poor	Good
5	Poor	Good
6	Poor	Good
7	Poor	Good
8	Moderate	Moderate
9	Poor	Moderate
10	NA	Poor

Afterwards, the route suggestion FIS was adopted to recommend the route with the higher average road segments quality. In this FIS, the output of the road segments quality database along with the trip time and route distance in each route is used to set the routes recommendation levels. Given the predefined fuzzy rules, the three inputs and the required priority to the route with high road segments quality, the proposed route planning system, contrary to Google Maps suggestions, recommended Route 2, as shown in Figure 5.9. For the second road test case that was held in Kingston ON, the driver requested a route plan to travel from point A to point B. According to Google Maps, there were three suggested routes of different lengths and trip time.

Figure 5-8 Road segments assessment for the two routes suggested by Google Maps

Figure 5-9 Route recommendation according to the average route's road quality

As depicted from Figure 5.10, Google Maps outweighed Route 1 over the other two routes because it provides the shortest path and travel time. However, for a driver who set the average route's road quality as the highest priority, the potential route may change. The system utilized the RNN to determine the road segments of each potential route. The RNN indicated that Route one, tow and three consists of 26, 20 and 24 road segments, respectively. Consequently, the road segments' quality information is retrieved from the database, as shown in Figure 5.4. The data. The average road qualities defined by a metric named quality indicator (QI) indicated that Route one and three have poor average road quality. While the average road quality in route two is moderate, as shown in Figure 5.10. Considering the trip time, route lengths' and the average route's road quality, the route assessment component of the system suggested Route two as the best-recommended route.

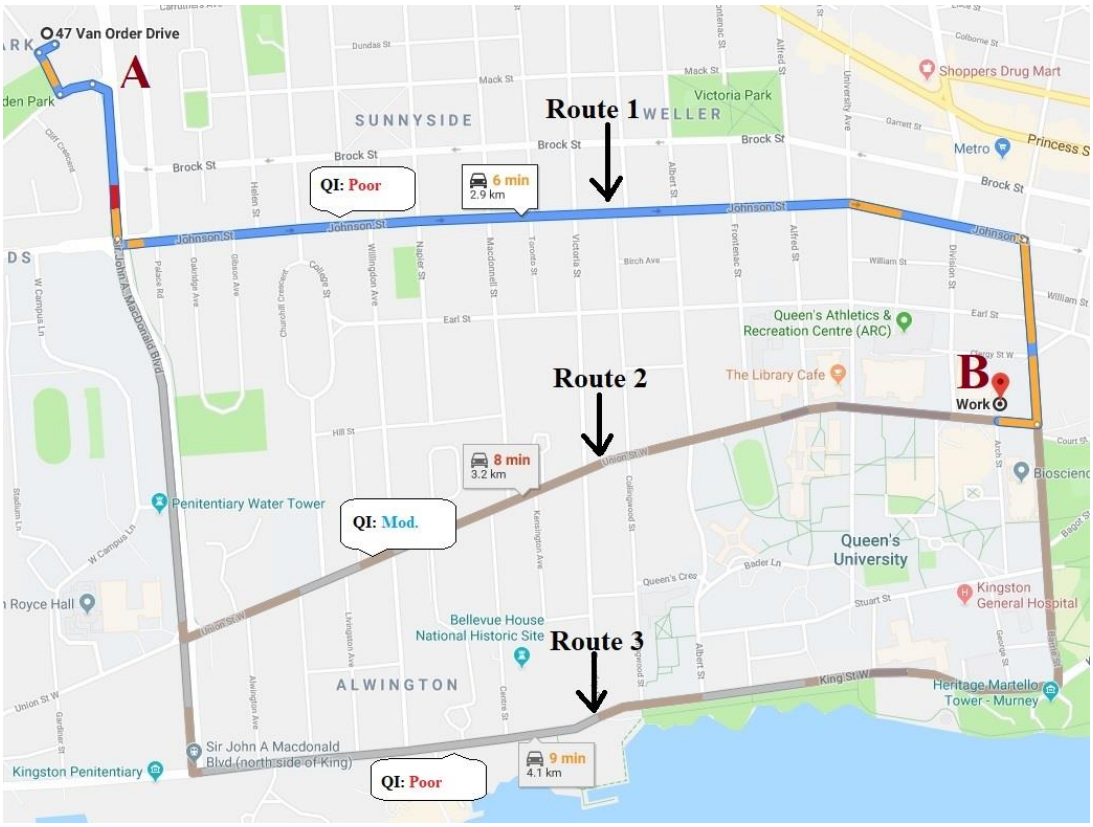

Figure 5-10 Route suggestions provided by Google Maps, second road test case

In general, the route suggestions are always limited to the ones provided by the route trip-planning provider. For example, in the second road test case, Google Maps suggested three potential routes, with two of them, have a poor road quality while the third one has a moderate road quality. With access to the road network and road segments qualities database, additional potential routes were found with better road quality and reasonable trip time and distance. In Figure 5.11, a new suggested route is provided with a good road quality on average. In conclusion, monitoring road surface conditions opened the door towards new metrics for safe and comfortable route planning.

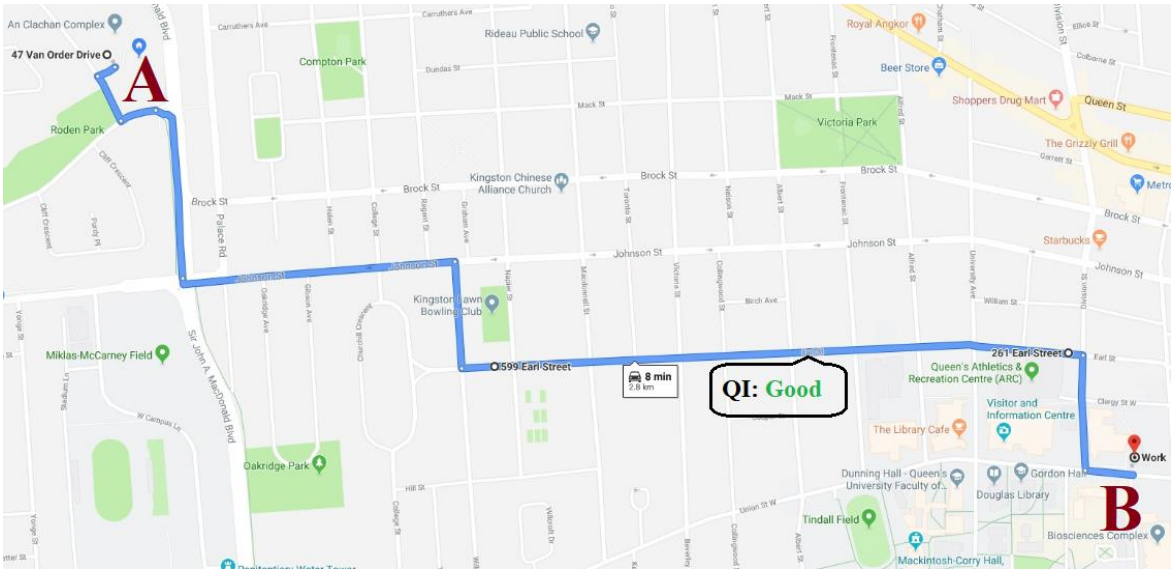

Figure 5-11 New suggested route with average road quality of (Good), second road test case

5.4 Summary

In this chapter, a framework for dynamic route planning that involves the average route's road quality as a new metric was presented. In this framework, a cloud-based system was proposed to utilize the information of the monitored road anomalies and their locations to asses the road segments' average quality. A FIS-based component leveraged the anomalies density, anomalies average severity level and the road segment wideness and decided on average road segment quality. For trip planning, the system used RNN to assign the road segments of the potential routes suggested by route planning providers such as Google Maps. The road segment quality database was used to retrieve the information regarding the road segment qualities in the potential route. Afterwards, the FIS-based route assessment utilized the segments' quality information while considering the route time and

length and enabled route suggestions while maximizing the importance of the average route quality as a driver's preference. Accessing the road network information and road segments quality database introduced new potential routes with better road quality and reasonable trip time and distance. This framework highlighted the importance of including more personalized metrics for dynamic route planning that lead to driver safety and comfort while travelling to their destinations.

Chapter 6

Conclusions and Future Directions

This thesis addressed a vital component of future intelligent transportation systems and road information services (RIS). The deployment of inertial sensors and GNSS receivers in land vehicles and smart devices (i.e. smartphones, tablets, etc.) has opened the door for monitoring road surface conditions to enable better and safe operation of our daily traffic. In addition, the notable growth of the in-vehicle storage and computational capabilities has helped in the efficient delivery of the road and vehicular services. Road health conditions are dramatically affecting the whole traffic systems management and operation. The deteriorated road conditions lead to vehicle damage, induce driver discomfort and even injuries and cause traffic jams that disturb the traffic management system. Road surface anomalies may exhaust the municipality resources in the required road surveying and potential repairs and reconstructions. Most of the road surface conditions monitoring systems lack the required functionality that provides timely and accurate reporting of the damaged roads as well as providing helpful feedback to the road drivers.

6.1 Summary and Conclusions

The research work in this thesis provided a framework that tackled the significant drawbacks of the present RIS systems that monitor the road health conditions. Existing systems that are developed or adopted by the municipalities and traffic operators rank the roads according to the defects in the road infrastructure condition regardless of their effects

on the vehicle operation. Moreover, traditional road inspection is usually held manually through what is called eye inspection, and it has two significant drawbacks. The first is that road inspections are normally held every two years, which is a long period where the road condition may deteriorate quickly, specifically in countries that experience harsh weather conditions. The other aspect is surveying the roads is an exhausting process for the municipalities if it is required frequently. The other systems owned by third parties lack the sufficient categorization of the road anomalies and the different levels of severity.

In this regard, this thesis, in chapter 3, provided detailed road surveys to identify the common road anomalies, their effects on vehicle operation, and it has successfully identified ten road anomaly types with different levels of severity. The surveys utilized different types of land vehicles that have different years of making, suspension system quality, and tire size. The road anomalies have been attended in different driving styles and speeds; thus, an adequate analysis of their effects on the vehicle movement is guaranteed. In addition, the road anomalies were classified into two major categories of single-sided road anomalies that disturb either side of the vehicle, and double-sided that transverse the vehicle movement and affect both sides of the vehicle.

One another aspect that influences the performance of the road conditions monitoring systems is the data quality. Many factors, such as rich data collection, sensor measurement quality, and data rate, either individually or combined, affect the data quality. Rich data collection is a critical aspect that present systems do not adequately consider. In this work, eight land vehicles of different make, size and year of make were utilized in data collection.

These vehicles were operated by voluntary drivers of different gender, age and driving styles to make sure that comprehensive data collection is gathered.

An additional important metric is the utilized sensors and their quality. In the existing systems, many factors were not profoundly considered, such as the appropriate sensor usage, measurement quality, and data rate as well as sensors and testbed placement within the vehicles. In this work, these factors were carefully considered. In the data collection phase, both accelerometers and gyroscopes embedded in the IMUs and smart devices were used. It has been found that linear accelerations monitored by the accelerometers capture features of the double-sided anomalies. The angular rotations monitored by the gyroscopes are useful in detecting the single-sided ones. Inertial sensors can collect data at different rates, but to capture sufficient features of the road anomalies, the sensors measurements were acquired at 100 Hz. However, low-cost commercial inertial sensors used in land vehicles and smart devices suffer from noises and biases. In Chapter 3, the utilized WPD-based denoising has enhanced the quality of the commercial inertial sensors' measurements by approximately 44 %. To guarantee a comprehensive data collection, IMUs, smart devices and testbeds were placed in different spots within the land vehicles, including windshield, dashboard, armrest, cup holder, passenger's seat, back seats and the vehicle trunk. Our comprehensive data collection resulted in building road surface conditions monitoring systems.

Furthermore, statistical, time, frequency, time-frequency domain, wavelet-based features were used to enable accurate detection and categorization of the road anomalies and their levels of severity. In this thesis, a combination of 75 features was used to distinguish the

road anomalies. A machine learning-based SVM classifier was successfully able to detect ten road anomalies with different severity by TPR of 90%.

Nevertheless, sufficient reporting for the monitored road anomalies requires adequate geolocation; otherwise, the reported information will be misleading, and the road operators and the municipalities will end up by resurveying the road anomalies. The existing systems utilize the commercial GNSS receivers to localize the road anomalies. However, GNSS suffers from partial or complete outages on many occasions such as downtown cores, urban canyons, tunnels, ...etc. At high speeds, the typical GNSS update of 1 Hz provides low-resolution location information, which is not suitable in geo-locating the road irregularities. Integrated navigation systems are promising solutions for geo-locating the road anomalies. The inertial sensors utilized for monitoring road irregularities can also be utilized for integrated geolocation with the GNSS receivers. In chapter 4, a framework of adaptive resolution positioning is proposed. This system utilized WPD to enhance the quality of the inertial sensors measurements and extract the vehicle motion dynamics form the monitored road surface anomalies and other sensors' noises and disturbances. The proposed loosely-coupled WPD-based 3D RISS/GNSS has outperformed the conventional loosely-coupled 3D RISS/GNSS in terms of the average 2D position accuracy during extended periods of GNSS outages by 56%. Also, an adaptive resolution geo-referencing up to 10 Hz is provided to enable better positioning accuracy of the road anomalies.

In addition, the road anomalies and their corresponding levels of severity have provided the opportunity to evaluate the average conditions of the road segments. This information is not only valuable for municipalities while setting their plans and priorities for road

repairs and reconstruction, but also benefit the city drivers and helps in having safe and comfortable trips. In Chapter 5, a FIS is introduced to consider the average route quality as a new metric in the route planning process. This two-stage FIS system was able to evaluate the average quality of the road segments. The proposed FIS utilized the average route quality and other metrics while ranking the potential routes and providing the suggested route with better road quality. The proposed FIS-based system was evaluated in three test cases. Our results showed that the fastest and shortest routes are not necessarily always the best choice for specific drivers. Our solution showed that a new route planning attribute based on road surface conditions could result in route recommendations that are more appropriate to some drivers based on their preference, possibly related to trip comfort.

6.2 Future Directions

1- Although the solution offered in this thesis was based on collecting large data sets, adding more road test data would definitely benefit the performance of the proposed system in monitoring road surface conditions. More experiments may involve more types of vehicles and also may consider Concrete roads as the presented work only considered asphalt and paved stone roads. These experiments will result in detecting additional types of road anomalies and will enable a better understanding of the road quality and its effect on the vehicle and the driver. With massive data collection, deep learning and reinforcement learning-based classifiers, the anomalies detection and categorization rates can be increased. A cloud-based

service, together with a mobile application (operating in both iOS and Android platforms) would be an important extension of this work and shall benefit RIS in the future.

2- Furthermore, with the gradual growth of the vehicle computational capabilities, adopting additional sensors such as vision Cameras and LIDARs will provide more insights into the categorization of the road anomalies and implicitly enhance the road quality assessment. These additional sensors can also enable better and high data rate geolocation accuracy of the monitored road irregularities. Different modes of INS/GNSS of integration, such as tightly coupled and ultra-tightly coupled, could enhance the geo-referencing accuracy, but a computational complexity trade-off should be addressed.

3- Finally, involving the road quality while routing the vehicles open the door towards more personalized route planning. A combination of the fast route, shortest path, and good road quality can be further addressed along with other metrics such as driver behaviour and competence level, road curvature and environmental attributes. Personalized and safe route planning will help the city operators in better understanding its needs and set better management, operation and spending.

Bibliography

1- D. Minoli, K. Sohraby and B. Occhiogrosso, "IoT Considerations, Requirements, and Architectures for Smart Buildings—Energy Optimization and Next-Generation Building Management Systems," *IEEE Internet Things J.*, vol. 4, no. 1, pp. 269-283, Feb. 2017.

2- Gartner Says 8.4 Billion Connected 'Things' Will Be in Use in 2017, Up 31 Percent from 2016," *Gartner*. [Online].
Available: https://www.gartner.com/en/newsroom/press-releases/2017-02-07-gartner-says-8-billion-connected-things-will-be-in-use-in-2017-up-31-percent-from-2016. [Accessed: Nov-2019].

3- A. Kamilaris and A. Pitsillides, "Mobile Phone Computing and the Internet of Things: A Survey," *IEEE Internet Things J.*, vol. 3, no. 6, pp. 885-898, Dec. 2016.

4- S. M. A. Oteafy and H. S. Hassanein, "Resilient IoT Architectures Over Dynamic Sensor Networks With Adaptive Components," *IEEE Internet Things J.*, vol. 4, no. 2, pp. 474-483, Apr. 2017.

5- A. Gharaibeh, M. A. Salahuddin, S. J. Hussini, A. Khreishah, I. Khalil, M. Guizani and A. Al-Fuqaha, "Smart Cities: A Survey on Data Management, Security and Enabling Technologies," *IEEE Commun. Surveys Tuts.*, vol. 19, no. 4, pp. 2456-2501, 2017.

6- M. Handte, S. Foell, S. Wagner, G. Kortuem and P. J. Marrón, "An Internet-of-Things Enabled Connected Navigation System for Urban Bus Riders," *IEEE Internet Things J.*, vol. 3, no. 5, pp. 735-744, Oct. 2016.

7- M. A. Rahman and M. S. Hossain, "A Location-Based Mobile Crowdsensing Framework Supporting a Massive Ad Hoc Social Network Environment," *IEEE Comm. Mag.*, vol. 55, no. 3, pp. 76-85, Mar. 2017.

8- X. Wang, X. Zheng, Q. Zhang, T. Wang and D. Shen, "Crowdsourcing in ITS: The State of the Work and the Networking," *IEEE Trans. Intell. Transp. Syst.*, vol. 17, no. 6, pp. 1596-1605, Jun. 2016.

9- J. Wahlström, I. Skog; P. Händel, "Smartphone-Based Vehicle Telematics: A Ten-Year Anniversary," *IEEE Trans. Intell. Transp. Syst.*, vol. 18, no. 10, pp. 2802-2825, Oct. 2017.

10- Intelligent Transportation Systems Society of Canada (ITS Canada), Overview, 2016. [Online].

Available: https://www.itscanada.ca/education/overview/overview/. [Accessed: Nov-2019].

11- "Intelligent Transportation System Market Size & Share | ITS Report 2024." [Online].

Available: https://www.grandviewresearch.com/industry-analysis/intelligent-transportation-systems-industry. [Accessed: Nov-2019].

12- "Integrated Traffic Systems Market worth $37.5 billion by 2025." [Online]. Available: https://www.marketsandmarkets.com/PressReleases/integrated-traffic-system.asp.

[Accessed: Nov-2019].

13- "Pothole Damage Costs Drivers $3 Billion Annually Nationwide | AAA SoCal." [Online].

Available: http://news.aaa-calif.com/news/pothole-damage-costs-drivers-3-billion-annually-nationwide. [Accessed: Nov-2019].

14- Road Safety Canada Consulting, Canada, and Transport Canada, *Road safety in Canada*. Ottawa, Ont.: Transport Canada, 2012.

15- "Intelligent Transportation Systems - ITS Strategic Plan 2015-2019." [Online]. Available: https://www.its.dot.gov/factsheets/itsjpo_stratplan.htm. [Accessed: Nov-2019].

16- "ITS Canada 2015-2019 Strategic Plan" [Online]. Available: https://www.itscanada.ca/it/strategy/index.html. [Accessed: Nov-2019].

17- "Intelligent Transportation Systems ICT Infrastructure", [Online] Available: https://ec.europa.eu/transport/themes/its/road/application_areas/ict_infrastructure_en. [Accessed: Nov-2019].

18- "Smart Transport for Australia", [Online] Available: https://www.its-australia.com.au/wp-content/uploads/Smart-Transport-for-Australia.pdf. [Accessed: Nov-2019].

19- H. M. Amar and O. A. Basir, "A Solution to the Congestion Problem: Profiles Driven Trip Planning," in *2016 IEEE 84th Vehicular Technology Conference (VTC-Fall)*, pp. 1-6, Montreal, QC, 2016.

20- H. M. Amar, N. M. Drawil and O. A. Basir, "Traveler Centric Trip Planning: A Behavioral-Driven System," *IEEE Trans. on Intell. Transp. Syst.*, vol. 17, no. 6, pp. 1521-1537, June 2016.

21- WAZE Mobile. "WAZE Outsmarting Traffic, Together." [Online] Available: http://www.waze.com/. [Accessed: Nov-2019].

22- A. E. M. Taha, "Facilitating safe vehicle routing in smart cities," in *2017 IEEE International Conference on Communications (ICC)*, Paris, FR, pp. 1-5 2017.

23- F. Harrison, and H-A. Park. "Comparative performance measurement: Pavement smoothness"
[Online] Available: http://onlinepubs.trb.org/onlinepubs/archive/notesdocs/20-24(37)b_fr.pdf. [Accessed: Nov-2019]

24- P. Mohan, V. Padmanabhan and R. Ramjee, "Nericell: Rich Monitoring of Road and Traffic Conditions using Mobile Smartphones," *ACM SenSys*, pp. 323–336, NY, 2008.

25- A. Mednis, G. Strazdins, R. Zviedris, G. Kanonirs and L. Selavo, "Real-time pothole detection using Android smartphones with accelerometers," in *2011 International*

Conference on Distributed Computing in Sensor Systems and Workshops (DCOSS), Barcelona, Spain, pp- 27-29, 2011.

26- A. Noureldin, T. B. Karamat, and J. Georgy, Fundamentals of Inertial Navigation, Satellite-based Positioning and their Integration. Springer-Verlag Berlin Heidelberg, 2013.

27- A. Noureldin, T. B. Karamat, M. D. Eberts, and A. El-Shafie, "Performance enhancement of MEMS-based INS/GPS integration for lowcost navigation applications," *IEEE Trans. Veh. Technol.*, vol. 58, no. 3, pp. 1077–1096, 2009.

28- "Asphalt PASER Manual – Transportation Information Center." [Online]. Available: https://epd.wisc.edu/tic/publication/asphalt-paser-manual/. [Accessed: Nov-2019].

29- P. D. Groves, Principles of GNSS, Inertial, and Multisensor Integrated Navigation Systems, Second Edition, 2 edition. Boston: Artech House, 2013.

30- J. Eriksson, L. Girod, B. Hull, R. Newton, S. Madden and H. Balakrishnan, "The pothole patrol: using a mobile sensor network for road surface monitoring," in *Proc. Of the 6th Int. Conf. on Mobile Systems, Applications, and Services*, Breckenridge, CO, USA, 2008.

31- J. Jang, A. W. Smyth, Y. Yang, and D. Cavalcanti, "Road surface condition monitoring via multiple sensor-equipped vehicles," *IEEE INFOCOM,* Hong Kong, pp. 43–44., Apr. 2015.

32- J. Celaya-Padilla *et al.*, "Speed Bump Detection Using Accelerometric Features: A Genetic Algorithm Approach," *Sensors*, vol. 18, no. 2, p. 443, Feb. 2018.

33- "Assessment of Roadway surface conditions Using Onboard Vehicle Sensors: Final Report" [Online]. Available: https://rosap.ntl.bts.gov/view/dot/32155. [Accessed: Nov-2019].

34- A. Fox, B. V. K. V. Kumar, J. Chen, and F. Bai, "Multi-Lane Pothole Detection from Crowdsourced Undersampled Vehicle Sensor Data," *IEEE Trans. Mobile Comput.*, vol. 16, no. 12, pp. 3417–3430, Dec. 2017.

35- D. K. Jackson, "Systems and methods for monitoring and reporting road quality," US9108640B2, 18-Aug-2015.

36- F. Cong, H. Hautakangas, J. Nieminen, O. Mazhelis, M. Perttunen, J. Riekki and T. Ristaniemi, "Applying Wavelet Packet Decomposition and One-Class Support Vector Machine on Vehicle Acceleration Traces for Road Anomaly Detection," *Advances in Neural Networks* – ISNN, Volume 7951, pp 291-299, 2013.

37- P. M. Harikrishnan and V. P. Gopi, "Vehicle Vibration Signal Processing for Road Surface Monitoring," *IEEE Sensors J.*, vol. 17, no. 16, pp. 5192–5197, Aug. 2017.

38- G. Xue, H. Zhu, Z. Hu, J. Yu, Y. Zhu, and Y. Luo, "Pothole in the Dark: Perceiving Pothole Profiles with Participatory Urban Vehicles," *IEEE Trans. Mobile Comput.*, vol. 16, no. 5, pp. 1408–1419, May 2017.

39- F. Seraj, B. J. van der Zwaag, A. Dilo, T. Luarasi, and P. J. M. Havinga, "Roads: A road pavement monitoring system for anomaly detection using smart phones," in *Proc. of the 1st Int. Workshop on Machine Learning for Urban Sensor Data*, SenseML 2014, Nancy, France, ser. *Lecture Notes in Computer Science*, pp. 1–16, 2014.

40- A. Allouch, A. Koubaa, T. Abbes, and A. Ammar, "RoadSense: Smartphone Application to Estimate Road Conditions Using Accelerometer and Gyroscope," *IEEE Sensors J.*, vol. 17, no. 13, pp. 4231–4238, Jul. 2017.

41- A. S. El-Wakeel, J. Li, A. Noureldin, H. S. Hassanein, and N. Zorba, "Towards a Practical Crowdsensing System for Road Surface Conditions Monitoring," *IEEE Internet Things J.*, pp. 1–14, 2018.

42- P. Aggarwal, Z. Syed, A. Noureldin, and N. El-Sheimy, MEMS-Based Integrated Navigation. Boston: Artech House, 2010.

43- I. Skog, P. Handel, J. Nilsson, and J. Rantakokko, "Zero-Velocity Detection—An Algorithm Evaluation," *IEEE Trans. Biomed. Eng.*, vol. 57, no. 11, pp. 2657–2666, Nov. 2010.

44- D. Freedman, R. Pisani, and R. Purves, *Statistics*, 4th Edition. New York, NY, USA: W. W. Norton & Company, 2007.

45- A. N. Akasnsu and R. A. Haddad, Multiresolution Signal Decomposition, 2nd ed. Academic Press, 2001.

46- S. Mitra, Digital signal Processing —A computer based approach. 4th ed. New York: McGraw–Hill, 2011.

47- S. Mallat, A Wavelet Tour of Signal Processing: The Sparse Way. 3rd ed. New York: Academic Press, 2008.

48- M. Perttunen *et al.*, "Distributed Road Surface Condition Monitoring Using Mobile Phones," in *Ubiquitous Intelligence and Computing*, vol. 6905, C.-H. Hsu, L. T. Yang, J. Ma, and C. Zhu, Eds. Berlin, Heidelberg: Springer Berlin Heidelberg, 2011, pp. 64–78.

49- A. Géron, Hands-On Machine Learning with Scikit-Learn and TensorFlow. 1st ed. O'Reilly Media, 2017.

50- C. Bishop, Pattern Recognition and Machine Learning. New York: Springer-Verlag, 2006.

51- D. M. J. Tax and R. P. W. Duin, "Support Vector Domain Description," *Pattern Recognition Letters*, vol. 20, no. 11, pp. 1191–1199, Nov. 1999.

52- L. Rokach and O. Maimon, Data Mining With Decision Trees: Theory and Applications, 2nd ed. River Edge, NJ, USA: World Scientific Publishing Co., Inc., 2014.

53- I. Witten and E. Frank, Data Mining: Practical Machine Learning Tools and Techniques. San Francisco, CA, USA: Morgan Kaufmann Publishers Inc., 2005.

54- T. Hastie, R. Tibshirani, and J. Friedman, The Elements of Statistical Learning: Data Mining, Inference, and Prediction, 2nd ed. New York, NY, USA: Springer, 2009.

55- R. Y. Wang, Y. T. Chuang and C. W. Yi, "A crowdsourcing-based road anomaly classification system," in *2016 18th Asia-Pacific Network Operations and Management Symposium (APNOMS)*, Kanazawa, JP, pp. 1-4, 2016.

56- T. S. Brisimi, C. G. Cassandras, C. Osgood, I. C. Paschalidis, and Y. Zhang, "Sensing and Classifying Roadway Obstacles in Smart Cities: The Street Bump System," *IEEE Access*, vol. 4, pp. 1301–1312, 2016.

57- M. S. Grewal *et al.*, Global Positioning Systems, Inertial Navigation, and Integration, 2nd ed. New York: Wiley, 2007.

58- J. Eriksson, L. Girod, B. Hull, R. Newton, S. Madden and H. Balakrishnan, "The pothole patrol: using a mobile sensor network for road surface monitoring," in *Proc. Of the 6th Int. Conf. on Mobile Systems, Applications, and Services*, Breckenridge, CO, USA, 2008.

59- E. M. Pont, J. Provost and C. Kuenzel, "Development of a methodology for monitoring and prediction of road surface conditions in highly automated driving," in *2017 22nd IEEE International Conference on Emerging Technologies and Factory Automation (ETFA)*, Limassol, Cy, pp. 1-7, 2017.

60- P. Misra and P. Enge, Global Positioning System: Signals, Measurements, and Performance, 2nd Editio. Lincoln, Massachusetts, USA: Ganga-Jamuna Press, 2010.

61- S. Djahel, R. Doolan, G. M. Muntean and J. Murphy, "A Communications-Oriented Perspective on Traffic Management Systems for Smart Cities: Challenges and Innovative Approaches," in *IEEE Commun. Surveys Tuts.*, vol. 17, no. 1, pp. 125-151, First quarter 2015.

62- F. R. Soriano, J. J. Samper-Zapater, J. J. Martinez-Dura, R. V. Cirilo-Gimeno and J. Martinez Plume, "Smart Mobility Trends: Open Data and Other Tools," in *IEEE Trans. Intell. Transp. Syst*, vol. 10, no. 2, pp. 6-16, Summer 2018.

63- A. T. Akabane, R. L. Gomes, R. W. Pazzi, E. R. M. Madeira and L. A. Villas, "APOLO: A Mobility Pattern Analysis Approach to Improve Urban Mobility," *GLOBECOM 2017 - 2017 IEEE Global Communications Conference*, Singapore, 2017, pp. 1-6.

64- L. Xiao and H. K. Lo, "Adaptive vehicle navigation with en route stochastic traffic information," *IEEE Trans. Intell. Transp. Syst.*, vol. 15, no. 5, pp. 1900–1912, Oct. 2014.

65- T. Liebig, N. Piatkowski, C. Bockermann and K. Morik, "Dynamic Route Planning with Real-Time Traffic Predicitions," *Information Systems*, vol. 64, pp. 258-265, 2017.

66- C. Chen *et al.*, "MA-SSR: A Memetic Algorithm for Skyline Scenic Routes Planning Leveraging Heterogeneous User-Generated Digital Footprints," *IEEE Trans. on Veh. Technol.*, vol. 66, no. 7, pp. 5723-5736, July 2017.

67- E. Galburn, K. Pelechrinis, and E. Terzi, " Urban navigation beyond shortest route: The case of safe paths," *Information Systems*, vol. 57, pp. 160-171, 2016.

68- N. El-Sheimy, S. Nassar and A. Noureldin, "Wavelet de-noising for IMU alignment," *IEEE Aerosp. Electron. Syst. Mag.*, vol. 19, no. 10, pp. 32-39, Oct. 2004.

69- J. Skaloud, A. M. Bruton, and K. P. Schwarz, "Detection and filtering of short-term (1/f) noise in inertial sensors," *Navigation*, vol. 46, no. 2, pp. 97–107, 1999.

70- M. Jafari, T. A. Najafabadi, B. Moshiri, S. S. Tabatabaei and M. Sahebjameyan, "PEM Stochastic Modeling for MEMS Inertial Sensors in Conventional and Redundant IMUs," *IEEE Sensors J.*, vol. 14, no. 6, pp. 2019-2027, Jun. 2014.

71- W. Abd-Elhamid, A. Osman, and A. Noureldin, "Wavelet Multi-resolution analysis for enhancing the performance of integrated GPS and MEMS-based navigation system," *Geomatica*, vol. 59, no. 1, pp. 61-72, Mar. 2005.

72- E. I. Laftchiev, C. M. Lagoa and S. N. Brennan, "Vehicle Localization Using In-Vehicle Pitch Data and Dynamical Models," *IEEE Trans. Intell. Transp. Syst.*, vol. 16, no. 1, pp. 206-220, Feb. 2015.

73- L. Lau, "Wavelet packets based denoising method for measurement domain repeat-time multipath filtering in GPS static high-precision positioning applications", *GPS Solut.*, vol. 21, no. 2, pp 461–474, Apr. 2017.

74- C. K. Chui, An Introduction to Wavelets: Wavelet Analysis and Its Applications. Boston, MA: Academic, 1992.

75- C. M. Stein, "Estimation of the mean of a multivariate normal distribution," *Ann. Statist.*, vol. 9, no. 6, pp. 1135–1151, 1981.

76- M. Elhoushi, J. Georgy, A. Noureldin and M. J. Korenberg, "Motion Mode Recognition for Indoor Pedestrian Navigation Using Portable Devices," *IEEE Trans. Instrum. Meas.*, vol. 65, no. 1, pp. 208-221, Jan. 2016.

77- M. Elhoushi, J. Georgy, A. Noureldin and M. J. Korenberg, "A Survey on Approaches of Motion Mode Recognition Using Sensors," *IEEE Trans. Intell. Transp. Syst.*, vol. 18, no. 7, pp. 1662-1686, Jul. 2017.

78- M. Jaworski, P. Duda and L. Rutkowski, "New Splitting Criteria for Decision Trees in Stationary Data Streams," *IEEE Trans. Neural Netw. Learn. Syst.*, no. 99, pp. 1-14. 2017.

79- C. Cortes and V. Vapnik, "Support-vector networks," *Mach. Learn.*, vol. 20, no. 3, pp. 273–297, Sep. 1995.

80- Y. Ying and P. Li, “Distance metric learning with eigenvalue optimization,” *J. Mach. Learn. Res.*, vol. 13, pp. 1–26, 2012.

81- T. Hastie, R. Tibshirani, and J. Friedman, *The Elements of Statistical Learning: Data Mining, Inference, and Prediction*, 2nd ed. New York, NY, USA: Springer, 2009.

82- S. Zhao, Y. Chen and J. A. Farrell, "High-Precision Vehicle Navigation in Urban Environments Using a MEM's IMU and Single-Frequency GPS Receiver," *IEEE Trans. on Intell. Transp. Syst.*, vol. 17, no. 10, pp. 2854-2867, Oct. 2016.

83- N. El-Sheimy, H. Hou and X. Niu, "Analysis and Modeling of Inertial Sensors Using Allan Variance," *IEEE Trans. Instrum. Meas.*, vol. 57, no. 1, pp. 140-149, Jan. 2008.

84- C.W. Kang, C.H. Kang, and C.G. Park, “Wavelet De-Noising Technique for Improvement of the Low Cost MEMS-GPS Integrated System”. in *Proceedings of International Symposium on GPS/GNSS*, Taipei, Taiwan, 26–28 Oct. 2010.

85- A.G. Quinchia, G. Falco, E. Falletti, F. Dovis, C.A. Ferrer, “Comparison between Different Error Modeling of MEMS Applied to GPS/INS Integrated Systems,” *Sensors*, vol. 13, no. 8, pp. 9549-9588, Jul. 2013.

86- J.H. Han, C.H. Park, C.K. Hong, and J.H. Kwon, “Performance Analysis of Two-Dimensional Dead Reckoning Based on Vehicle Dynamic Sensors during GNSS Outages,” *J. of Sens.*, vol. (2017), pp. 1-13, Sept. 2017.

87- J. Georgy, A. Noureldin, M. J. Korenberg and M. M. Bayoumi, "Low-Cost Three-Dimensional Navigation Solution for RISS/GPS Integration Using Mixture Particle Filter," *IEEE Trans. on Veh. Technol.*, vol. 59, no. 2, pp. 599-615, Feb. 2010.

88- P. Aggarwal, Z. Syed, and N. El-Sheimy, “Hybrid extended particle filter (HEPF) for integrated civilian navigation system,” in *Proc. IEEE/ION PLANS*, Monterey, CA, pp. 984–992 May 2008.

89- A. Taha and N. AbuAli, "Route Planning Considerations for Autonomous Vehicles," *IEEE Com. Mag.*, vol. 56, no. 10, pp. 78-84, Oct. 2018.

90- U. Iqbal, J. Georgy, W. F. Abdelfatah, M. Korenberg and A. Noureldin, “Enhancing Kalman Filtering-Based Tightly Coupled Navigation Solution Through Remedial Estimates for Pseudo-range Measurement using Parallel Cascade Identification,” *Instrument. Sci. & Tech.*, vol. 40, pp. 530–566, Jul. 2012.

91- T. B. Karamat, M. M. Atia, and A. Noureldin, “An enhanced error model for EKF-based tightly-coupled integration of GPS and land vehicle’s motion sensors,” *Sensors*, vol. 15, no. 9, p. 24269, 2015.

92- J. Georgy, A. Noureldin, M. J. Korenberg and M. M. Bayoumi, "Low-Cost Three-Dimensional Navigation Solution for RISS/GPS Integration Using Mixture Particle Filter," *IEEE Trans. on Veh. Technol.*, vol. 59, no. 2, pp. 599-615, Feb. 2010.

93- P. Aggarwal, Z. Syed, and N. El-Sheimy, “Hybrid extended particle filter (HEPF) for integrated civilian navigation system,” in *Proc. IEEE/ION PLANS*, Monterey, CA, pp. 984–992 May 2008.

94- T. B. Karamat, R. G. Lins, S. N. Givigi and A. Noureldin, "Novel EKF-Based Vision/Inertial System Integration for Improved Navigation," *IEEE Trans. Instrum. Meas.*, vol. PP, no. 99, pp. 1-10, Oct. 2017.

95- “Road Network File, Reference Guide, 2018,” in *Statistics Canada Catalogue no. 92-500-G.*

96- W. Abdel-Hamid, A. Noureldin and N. El-Sheimy, "Adaptive Fuzzy Prediction of Low-Cost Inertial-Based Positioning Errors," in *IEEE Trans. Fuzzy Syst.*, vol. 15, no. 3, pp. 519-529, June 2007.

97- M. Mamdani, "Application of fuzzy algorithm for control of simple dynamic plant," Proc. Inst. Elect. Eng., vol. 121, pp. 1585–1588, 1974

98- R. Babuška and H. B. Verbruggen, "Fuzzy set methods for local modelling and identification," in Multiple Model Approaches to Nonlinear Modelling and Control New York, NY, USA: Taylor & Francis, pp. 75–100, 1997.